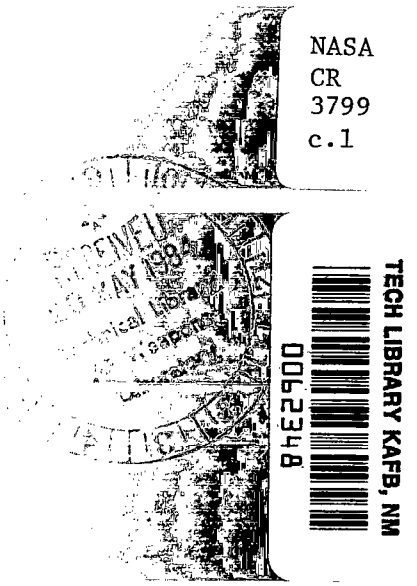

NASA Contractor Report 3799

A SEASAT SASS Simulation Experiment To Quantify the Errors Related to a ±3-Hour Intermittent Assimilation Technique

Winfield B. Sylvester

GRANT NAGW-266
MAY 1984

NASA

NASA Contractor Report 3799

A SEASAT SASS Simulation Experiment To Quantify the Errors Related to a ±3-Hour Intermittent Assimilation Technique

Winfield B. Sylvester
CUNY Institute of Marine and Atmospheric Sciences at The City College
New York, New York

Prepared for
NASA Office of Space Science and Applications
under Grant NAGW-266

NASA
National Aeronautics
and Space Administration
Scientific and Technical Information Branch

1984

TABLE OF CONTENTS

LIST OF FIGURES

LIST OF TABLES

INTRODUCTION

Among the many prominent features on a surface weather map is the cyclone or low. This is an area of relatively low pressure that is usually surrounded by concentric closed isobars. In the Northern Hemisphere the feature is associated with a counterclockwise vortex of air which extends up into an upper level trough. Especially in the middle latitudes, the meteorologist focuses on its detection and the serveillance of its life cycle. The cyclone is a surface event that is believed to have had its beginning in an upper air disturbance that has propagated downward. It forms in the westerly wind current and is characterized by variability in its movement. Climatologically, cyclones travel faster in winter than in summer. Their general west to east motion can be detected in series of consecutive synoptic maps. The weatherman's target is to be able to predict the cyclone - that is, cyclogenesis, movement and filling. Will the cyclone fill or intensify? Where will the center of the low be in t hours, say? These are some of the questions that the meteorologist is aiming to answer satisfactorily.

There is a promise on the horizon that weather and wave forecasting are to see better days. One manifestation of this hope will be realized in much improved forecasts. The new era of advanced satellite technology which has already begun will be partly responsible for these improvements. The efforts of revising and expanding the present data base into enhanced global networks have been instituted. The results of SEASAT can contribute immensely in this regard. The desire to obtain extensive data networks has been expressed by both research scientists and the operational forecaster alike. Knowledge gained in the past has led us to realize that via the non-interactive approach, a course resolution model can be run over a global domain to achieve a weather forecast over an hemispheric area. Sylvester (1978) has noted that in terms of ocean wave forecasting, an attempt at a solution of the ocean-related problem depends on the global interaction of data.

The SEASAT-A satellite was dedicated to the task of providing data on a global, real-time basis. Based on its performance, world-wide coverage has been demonstrated to be practical, useful, and attainable.

Forecasts are futuristic phenomena. Unlike the methods practiced by gazers into crystal balls, the physical scientist adheres to the rule that the subsequent state of the atmosphere evolves from the preceeding one according to physical laws.

To form a well-posed problem for a solution integrated forward in time, a sufficiently accurate knowledge of the state of the atmosphere at the initial time is a necessary condition. Prescribing the initial state has been an area of uncertainty in our endeavors to predict the future state. Thus we fail sometimes because we are unaware of the present atmospheric conditions. Modern scientists have been becoming increasingly aware of this deficiency. The position has been well stated by Ghil, et al. (1979), who asserted that we cannot predict tomorrow's weather because we do not know the weather today. In part, to answer to this challenge, a bold and revolutionary step has been made by Pierson (1983) in his paper "The Measurement of the Synoptic Scale Wind Over the Ocean". His contribution is aimed at showing us how to measure the surface wind correctly.

We have started to identify some of the major problems and should be willing to work towards their solutions. Provided with the assurance that a global network of data points can be provided, the question as to how we can use the information to create the maximum positive impact on our forecasts becomes very important. Unfortunately, the present means for procuring global coverage (the asynoptic nature of satellites) has created another difficulty in our assessment of real-time synoptic situations. New algorithms must be sought to handle the additional data collected by our most modern types of instrumentation more efficiently.

Instead of crystal balls prognosticators have computers to aid them in their quest. All such prognostications depend on computer-based models. The forecast cycle starts after the initial state has been prescribed. Working with real-time data from spacecraft has thus enlarged the area of uncertainty. This incertitude is of primary concern among physical scientists today. One such concern has been expressed in the following quote from Pierson (1979). "There always remains the nagging doubt that improper insertion of asynoptic data, at a particular synoptic time, may do more harm than good towards the goal of improving a numerical weather prediction model".

The object of this report is to investigate one of the ways to assimilate the SEASAT SASS data, as for example, at the National Meteorological Center (NMC). The first guess field at NMC is provided from the "operational" anaysis performed 3 hr. 25 min. after the synoptic observation time. These initial data comprise all observations taken within ± 3-hours of the synoptic time. The practice is that all good asynoptic data are processed as if they belong to the synoptic time. While this ± 3-hour window seems appropriate for winds for constant pressure surfaces above 500 mb., it is not sound for the transient cyclones that move across the surfaces of the earth in the lower atmosphere. The current practice using an intermittent assimilation method (to be described in the paper) for dealing with the SASS data is therefore questionable.

A series of SEASAT orbits over a sequence of "best" low center positions is simulated, using a device provided by the Jet Propulsion Laboratory for studying SEASAT data. These low centers are, upon appropriate interpolation to hourly positions, located at various times during the ± 3-hour data assimilation cycle. At times, the low center is picked up well in advance of the synoptic map time and put in one position. At other times, it is picked up at the last part of the six-hour cycle and put in a second position. The apparent velocities of the low along its track are a strong function of when the spacecraft passed over the low. Large errors in speed are demonstrated by processing two months of simulated SEASAT passes, incorporating a method of repeat orbits, over low centers in the North Pacific and Atlantic oceans during December 1980 and January 1981.

This paper will demonstrate that the data assimilation techniques that use the assumption of a six (± 3)-hour window produce gross errors in the motion of a low center from one synoptic map update time to another. These are some of the errors that are found in the initial specification field that would propagate into very gross errors in a computer based numerical weather forecast.

It has been generally recognized that low centers over the oceans are not correctly located on synoptic maps owing to the sparseness and inaccuracies of the observational data. Added to this are those systematic errors that are observed in the forecast of surface cyclones. These errors have been documented. For example, from an historical perspective, Leary (1971) found systematic underprediction of the depth of maritime cyclones by the (6-L)PE. Druyan (1974) found the GISS model to be similarly deficient in forecasting deeping cyclones. And recently Sanders and Gyakum (1980) showed that both the (6-L)PE and the (7-L)PE underforecast cyclogenesis.

Improperly located low centers displaced one way or another relative to their true positions at a particular moment produce analyses of the fields of motion and mass in the planetary boundary layer that are incorrect over the large area influenced by a scatterometer swath. A preceding and subsequent revolution will produce wind data to each side of a low center such that, for a deeping low, for example, with increasing gradients, the eastern side of the low will be too weak and the western side will be too strong, thus producing an unrealistic assymetric analysis. With an incorrect specification of the lowest level of a computer model with errors in both the surface atmospheric pressure and the field of mass, the integration of the hydrostatic equation so as to define the constant pressure surfaces for the higher levels will project the errors of the lower layers throughout the entire model.

Two other difficulties arise with the ± 3h assimilation. An orbit segment that is over an ocean at, say, 0900 GMT will have part of its data assigned to 0600 GMT and the rest, with an instantaneous discontuity, to 1200 GMT. Also for far north and far south orbits, the same low center and the winds around it can be sighted several different times during the ± 3h window. If all such data are used indiscriminantly, the result will be a blurred surface wind field and a poor analysis. If only the data nearest a synoptic time are used, information is lost.

All of the undesirable consequences of this assimilation method can be illustrated by studying how extratropical cyclone centers are incorrectly located as they travel across the ocean. The analysis errors described above will be well correlated with the mis-location of the cyclones centers.

All these factors have been, in part, a problem of the initial value specification, due to the limitation of the availability of data over the oceans. Meteorological satellites have seemed to have solved the problem of scarcity. But an apparent "catch - 22" situation has surfaced in the area of assimilating the data. In looking ahead to the future, we must be prepared to utilize the SASS data product effectively if ever another spacecraft with this instrumentation is launched. The value of the SASS data should remain great even from the point of view of having positive impacts on weather forecast.

A. SEASAT-A MISSION OVERVIEW

NASA's SEASAT-A can be described as the revolutionary geophysical satellite of all times. The SEASAT experiment had the properties of an operation that had been carefully planned and executed. And in analogy to most revolutionary happenings, it was short-lived and thus all of its ambitious goals were not realized. However, its impact on the scientific community has been tremendous. In fact, after almost five years of its staging, scientists have acquired an appreciation for that polar-orbiting satellite. In some cases, a harvesting of new found knowledge has begun. As its amassed data are being sorted and analysed daily, these many new experiences and insights may surely help to bring about a renaissance in the fields of synoptic oceanography and marine meteorology.

SEASAT-A has played the role of a forerunner in observing the world's ocean. During its some 100 days in orbit, the scientific community has been provided with a wealth of information which should be put to careful study for scientific advancement.

Launched on June 1978, the satellite pioneered new microwave and remote sensing instrumentation for oceanography. The application satellite was dedicated to the measurements of ocean dynamics and geodesy. About once every 36 hours, SEASAT scanned about 95% of the globe and provided high-resolution geophysical data in continuous real-time for ocean surface winds and temperature, wave height, ice condition, ocean topography, and coastal and mid-ocean storms.

There exist many replete reports describing the technologies, capabilities and objectives of the SEASAT mission. These reports have been authored by the sponsors (NASA), the management groups for the project (the Jet Propulsion Laboratory (JPL)) and the scientists who worked on the program. For a more up-to-date inventory of the SEASAT-A mission and results, the reader is referred to the many articles featured in the following special issues of scientific publications:

(1) Science, 29 June 1979, Vol. 204, No. 4400.
(2) IEEE Journal of Ocean Engineering, April 1980, Vol. OE-5 No. 2.
(3) Journal of Astronautical Sciences, Oct-Dec. 1980. Vol. 27, No.4.
(4) Oceanography from Space, 1981, Plenum, New York. J.F.R. Gower, ED.
(5) Journal of Geophysical Research, April 30, 1982 Vol. 87, No. C5.
(6) Journal of Geophysical Research, April 28, 1983, Vol. 88, No. C3.

B. SEASAT-A SCATTEROMETER SYSTEM (SASS)

The SASS was one of the five microwave sensors on SEASAT. This instrument was to provide global surface vector wind stress and surface vector wind under neutral stability at a height of 19.5 m. The specifications for the SASS system aimed for an accuracy of ± 2 m/s in wind speed or 10% in magnitude (whichever was greater), and ± 20° in direction.

The transmitted microwave radiation (at 14.6 GHz) arrived at the sea surface via four narrow fan-shaped beams (two of which were orthogonal), each about 500 km. long, on either side of the subsatellite track. The returned backscattered signal was doppler filtered into cells and a spatial resolution of 50 km resulted.

The radar backscatter measured indirectly the wind speed of a point in or near footprints of approximately 1000 km^2 in area (Brown, et al. 1982). The small-amplitude capillary waves provide the theoretical link between the wind velocity and the radar backscatter, σ^o. As is explained in the technique of Bragg scattering (see Moore and Fung 1979), the strength of σ^o is proportional to the capillary wave amplitude, which in turn is assumed to be in equilibrium with the wind velocity. The wind direction can be derived from radar measurements at different azimuths as the backscatter is anisotropic.

Notwithstanding the strong coupling of the backscatter to the local wind, σ^o is modulated by sea state, and in particular, rainfall rate and air-sea temperature difference, especially when the sign of the difference is changing rapidly (Ross, 1981).

The SASS provided from one to three "aliases" with every correct value of the vector wind. The unsuitable value or values had to be excluded. In order to recover the "true vector wind", three geophysical algorithms (see Schroeder, et al. 1982), which relate the normalized backscatter to wind speed, were developed. These were accomplished via an empirical model function of the form $\sigma^o = \sigma^o$ (V, χ, θ) where V is the neutral stability wind speed in m/s at a height of 19.5 m., χ is the wind direction relative to the pointing direction of the radar beam, and θ is the incidence angle of the radar at sea surface.

Evaluation of the SASS data has been performed by comparison with other independent data sets. These data collected conventionally from research ships, buoys, etc., were utilized in the Gulf of Alaska Seasat Experiment (GOASEX I, Born, et al. Eds. 1979, and GOASEX II, Barrick, et al. 1979) and in the Joint Air Sea Interaction (JASIN, Businger, et al. 1980) program.

Additional comparative data were provided from the SEASAT Storms data set, which included the QE-II storm and hurricanes Fico and Ella (see Jones, et al. 1982).

Data from prelaunch aircraft experiments and the GOASEX I and II workshops were used to develop model functions for the SASS-I algorithm. These model functions, known as W7 and CWK (Schroeder, et al. 1982) were evaluated by using the withheld JASIN surface observations. In this way an independent assessment of the SASS wind vector measuring capabilities could be ascertained.

Comparisons of SASS derived wind (using two-candidate model functions) with high quality withheld surface truth at the JASIN workshop showed better agreement than the SASS specification of ± 2 m/s wind speed and ± 20° wind direction (Jones, et al. 1982).

It should be emphasized that an exact form of the model function is still to be decided upon. Some authors (see Jones, et al. 1982, Pierson, 1982) are of the opinion that other parameters and a number of yet undiscovered geophysical anomalies (e.g., thunderstorm activity) ought to be considered.

An obvious short-coming exists in the assessment of the SEASAT winds. The comparison results were based on measurements obtained over a limited range of wind speeds measured in the mid-latitudes of the northern hemisphere. A true global comparison in a statistical sense would have provided a better comparison set.

From all appearances, it seems that the SASS had been successful in measuring the surface wind at the 19.5 m height. This points to a step in the right direction. Obtaining high-quality surface winds on a global scale is an important ingredient in the advancement of numerical weather and wave forecasting.

C. ASSIMILATION OF DATA IN NUMERICAL MODELS

Initial Value Specification

Nearly all modern weather services base their forecasts on numerical weather prediction models. An initial value specification of all atmospheric variables for these models is required. Analysis, extrapolation and interpolation procedures that convert the measured atmospheric variables at particular times and irregularly spaced locations into numerical values of variables at the regular grid point of the model are carried out. This initial value specification should simulate as accurately as possible the state of the present atmosphere. Once the required measurements are inserted and assimilated, forecasts in the 12-, 24-, 48- and 72-hour time frame and also in the 5-to 10-day range are produced.

An assessment of the output with respect to the impact of the assimilated data should be performed only after considering the nuances of the assimilation procedure employed (Tracton, et al. 1981). Models are far from perfect. They can start up with errors because these errors exist in the actual measurements for initial value specification, or data holes are filled incorrectly. Errors may also result from the way data are inserted into the model. The consensus is that poor forecasts are, at least, in part, attributable to errors in the initial value specification of the synoptic fields.

Most operational models are based on the primitive equations (PE). In this case, the fast moving inertia-gravity waves are retained (until finally damped out) and "noise" is introduced into the solution. These gravity-inertia waves have abnormally large amplitudes compared to their counterparts in the atmosphere. According to Dey (1978), predictions by PE models routinely contain noise over a wide range of scales, some of which are similar to the meteorologically important motions in both wavelength and frequency.

The systematic errors of the model due to physical and numerical deficiencies are a combination of analysis errors due mainly to errors in observing instruments, fluctuations of atmospheric variables on a spatial scale too small to be resolved, interpolation and extrapolation. This combination of errors leads inevitably to uncertainty in the proper determination of the initial state. Numerical dispersion errors arising from limited horizontal resolution grow with time due to dynamic instability (Lorenz 1963); they also contribute to incorrect solutions.

Historical Perspective

In the history of synoptic meteorology, there has always been a lack of sufficient data for synoptic analysis. This insufficiency is compounded with the uneven distribution of the data at hand. Analysts are generally happy to supplement hand-drawn charts with most non-synoptic information. There has been no established rule of thumb for the insertion of past data and the analyst's own personal experience has always been the guiding factor.

The advent of meteorological satellites and the steady improvement of the resolution and physics of computer based numerical forescast. Despite this effective data supplement and improved technology, the complication of the effective data supplement and improved technology, the complication of the assimilation of non-synoptic data, among other factors, has still remained. This state of affairs has led Cane, et al. (1978) to suggest that scientists might fail to achieve the greatest impact with SEASAT data. Their opinion is that existing prediction boundary layer models had been unseccessful in showing the best way to utilize the data.

Methods for assimilating data in numerical models are becoming increasingly important as the search for ways to reduce the errors in meteorological analyses progresses. One method which has been in practice since the 1950's is called "intermittent" assimilation. This technique uses observations taken prior to analysis time. The information is extrapolated to present time via prediction equations and then mixed with the present data. Some of the early proponents of this method were Gilchrist and Cressman (1954), Bergthorsson and Döös(1955), Thompson (1961) (see Miyakoda and Talagrand, 1971). Other early techniques of data insertion were advanced by Cressman (1959), Gandin (1963), Sasaki (1969) and Tadjbakhsh (1969). Later, methods for the assimilation of past data in dynamical analysis were presented by Miyakoda and Talagrand (1971).

These works were followed by those of Talagrand and Miyakoda (1971) and Bengtsson and Gustavsson (1972) who proposed techniques for "continuous" data assimilation. In this method the data are inserted into the numerical prediction system at the times and places at which they are measured. In this way the data field is continuously updated.

More recently, methods derived for time-continuous assimilation of satellite data have been put forward by Ghil. et al. (1979). The insertion techniques (see Ghil, et al. (1979)) were implemented by a direct insertion method (DIM), a successive correction method (SCM) and a statistical assimilation method (SAM). Insertion of the data was accomplished using 10 minute time steps. Cane, et al. (1978) proposed an application to use SEASAT wind data. A possible technique for the assimilation of asynoptic data has been proposed also by Pierson (1979). This author has advanced three ways in which the SASS dealiased wind could be assimilated. They are:

1) Time step by time step,
2) Orbit segment by orbit segment, and
3) Three hour cycles that correct the SASS winds to given synoptic times.

The methods of time-continuous and intermittent assimilations are operational. But both methods have been in competition for some time. Talagrand and Miyakoda (1971) suggested that the continuous method has an advantage. They reasoned that the technique avoids the use of any kind of spatial "objective" analysis, which is intended to fill the spatial gaps in

the input data, and which inevitably introduces supplementary errors. Ghil, et al. (1979) reported that in a comparative experiment, the time-continuous assimilation of remote-sounding temperatures was superior to their intermittent assimilation.

Data Assimilation at NMC

An operational data assimilation method practised at NMC has been detailed by McPherson, et al. (1979). The system is based on updating a nine-level, and more recently, (see Yu and McPherson, 1981), a twelve-level spherical coordinate, primitive equation model by a local, multivariate, three dimensional, statistical interpolation method. This interpolation scheme is called optimal because it minimizes the mean-square error (observed minus predicted) of the observed field at points of measurements and the predicted values derived at the model's grid points. This optimal interpolation scheme, described by Bergman (1979), has its theoretical basis in the work of Gandin (1963).

The 9-level model serves as a "cradle" for the operational 7-level PE model. This model (9-LPE) accepts heterogeneous data by an intermittent assimilation process and updates them in 6-hour intervals, depositing them directly into the prediction model's vertical coordinates (McPherson, et al. (1979) rather than at mandatory pressure levels. For example, the 1800 GMT and 0600 GMT updates are integrated forward in time to 0000 GMT and 1200 GMT respectively. When the integration cycle reaches the initial time, an initial state is prescribed.

With respect to satellite data, the current practice is to treat them in the intermittent fashion with a ± 3 hour window (Ghil, et al. 1979). What is actually being done is that the model accepts all "good" satellite data made available in a 6-hour time interval. The model is therefore accepting asynoptic data collected anywhere in the time span 3 hours before to 3 hour after a main synoptic time and treating them (asynoptic data) as if they were at the synoptic time.

Impact of the SASS Wind Data on Weather Analysis and Prediction

SASS winds are products of a remote sensor and thus differ from anemometer winds in certain respect. The main differences are as follows: The SASS winds contain a directional ambiguity that has to be resolved; the winds require a model to infer wind velocity; and, the SASS measurements are averaged over relatively large areas. This averaging process qualifies the SASS winds to be a good candidate for objective analysis and numerical prediction.

According to a report by the Satellite Surface Stress Working Group (1982), for satellite observations to have a significant impact on numerical weather

prediction the following conditions must hold:

1) Substantial differences between the atmospheric state analyses produced with an without the data must occur:

2) The surface wind observations should not be inconsistent with the higher level analysis:

and 3) the forecast model should be sensitive to the low level wind modifications. Assimilation of scatterometer data can help to modify the analysis. Modification can result directly in the wind field and indirectly in the mass field through geostrophic adjustments. The resultant changes can impact the forecast and thus affect the initialization field at some future analysis time.

Studies of the effect of SASS data on operational numerical weather analysis and forecasting systems at NMC have been done. A global data assimilation experiment using SASS winds for two days in July 1978 has been conducted by Yu and McPherson (1979). To assess the impact of the SASS, two parallel experiments were run, one with SASS, the other without (NOSASS). For the SASS mode, global SASS winds together with other data sources conventionally available at NMC were assimilated at 6-hour intervals. For the NOSASS mode, the SASS data were excluded. The result of the experiments were then subjectively compared with satellite cloud imagery and streamline analyses. Their results gave the indication that, in general, the forecast from the analysis with SASS winds showed an improvement over that from analysis without SASS winds. It was also suggested that the SASS winds contributed real information to small-scale features. The authors also reported that in the Northern Hemisphere (during the summer) the impact of the SASS data was negligible. However, in the Southern Hemisphere (during the winter) significant differences in the analysis and prognostication resulted from the assimilation of SASS data. In the winter hemisphere initial state differences extended from 1000 to 250 mb and were as large as 120 m in geopotential height and 20 m/sec in the magnitude of the wind.

Another investigation of the effect of SASS wind data on the NMC surface pressure analysis was carried out by Yu and McPherson (1981). The study made use of Bergman's (1979) optimum interpolation technique. Comparison of a surface pressure analysis with SASS wind data against one without, showed a large pressure difference over the areas where ship reports were sparse. In areas where ship reports were plentiful, the addition of SASS data had a negligible effect.

The authors suggested that, for operational use, SASS winds may be desirable only in those areas where ship density falls below an assigned threshold value. It was further suggested that the use of the SASS data might be more beneficial in the modification of the lower troposphere winds rather than the pressure field.

A series of observing system simulation experiments conducted by Cane, et al. (1981) assessed the potential impact of marine wind data on numerical weather prediction. The authors made use of a coarse mesh, second-order version of the Goddard Laboratory for Atmospheric Sciences (GLAS) General Circulation Model (GCM) (Somerville, et al. 1974), with the additional feature of the split grid (Halem and Russel, 1973). This model was utilized to generate a nature run; it was also used for the assimilation and forecast

experiments. The nature run provided simulated conventional observations, satellite temperature profiles, and satellite scatterometer wind measurements.

An analysis-forecast cycle was performed in which only conventional data were assimilated; five 72-hour forecasts were made using the conventional analysis fields as initial conditions. In addition, analysis-forecast cycles for the same period, using simulated surface wind or temperature sounding data and conventional data as input were assimilated.

The scatterometer wind data were simulated with and without nominal SASS errors (± 2 m/sec in magnitude, ± 20° m direction) while the temperature soundings were simulated without error along actual Nimbus orbits. A time-continuous assimilation technique in 10-minute time steps was employed to prescribe the SASS data at the model's grid points. The data were inserted directly into the 9th level, the lowest active level of the model (∿ 945 mb) via the direct insertion method (DIM), and the successive correction method (SCM) (see Ghil, et al. 1979)). Temperatures were simulated at mandatory pressure levels at the sounder location, employing an interpolation scheme documented in Halem, et al. (1978). The simulated temperatures were assimilated by the (SCM) technique.

Forecasts were prepared from the resulting analysis field. The quality of the outcomes (when SASS data were utilized) was appraised by making comparisons of forecasts errors with those of the control forecast. Their results showed significant and consistent impacts in the level-9 wind fields and in the surface forecast over the North Pacific and North Atlantic. In addition, there was the striking improvement in the intensity, structure and placement of the intense extratropical cyclones over the ocean.

Other results from the analysis of the SEASAT-A wind data suggest that meteorological features over the ocean can be detected more accurately. Visual evidence of the SASS capabilities in locating features has been exhibited on the cover of Science (vol. 204, No. 4400). Ernst (1981) also displayed similar evidence of the SASS capabilities in locating synoptic features; NOAA VHRR cloud imagery was used for verifying his output. Figure 1 adapted from the Report of the Satellite Surface Stress Working Group (June 1982) shows a plot of dealiased surface wind vectors for the QE II wind field for a 50-km wind solution resolution. The plot superbly demonstrates the ability of the SASS to describe accurately the wind field and associated meteorological features. The storm center is shown here in the vicinity of 51° N latitude and it can be located within a radius of less than ½° of longitude of the smallest closed streamline.

Synopticians have also attested to some positive impacts of the SASS in their analyses. Atlas, et al. (1981) gave a report on a study in which dealiased SASS winds and conventional ship reports in the North Atlantic were mixed. These researchers found that the SASS winds were in good general agreement with most conventional ship reports. In fact, it was further stipulated (Atlas, et al. 1981) that the SASS served to define the synoptic and subsynoptic data scale flow with greater accuracy than is possible from the conventional data alone. Peteherych, et al. (1981) noted that the addition of SEASAT wind data in their analyses resulted in a more accurate placement of lows, highs, ridges and fronts. Cane and Cardone (1981) contended that the QE II storm could have been better defined by satellite wind measurements. They demonstrated, with the aid of a reanalysed surface pressure map, incorporating additional SEASAT data, that the boundaries of an available SASS swath was in excellent position to reveal the structure, intensity and location of the QE II storm.

Attention is drawn to yet another study, documented by Endlich, et al. (1981),

in which non-divergent SASS derived wind and GOES-2 satellite measurements of cloud motion direction were used to analyze the surface wind field over a part of the Northern Pacific. The resulting pressure field was found to be in "good" agreement with NMC's surface pressure field, transposed to the same grid, except in regard to the location of the low pressure center in the NW part of the field. It was noted that the NMC analysis was for 1800 GMT, whereas the SASS data in that part of the region was for approximately 2100 GMT. The asynoptic nature of the SASS data thus suggests a reason for the difference with respect to location.

Remarks

The foregoing studies have been cited mainly to give a somewhat brief accounting of partial results of various workers utilizing SASS data in numerical modeling and synoptic analysis. In these examples the sensitivity of numerical weather prediction to marine surface winds has been indicated.

It is no surprise that the results and conclusions of these researchers have been inconsistent with each other. And rightly so, since there appears to be an emergence of different "schools of thought" as relates the utilization of the remotely sensed information. A partitioning has come about not only on account of the findings, but also because of the divergent methodology that has been employed. In this paper, no attempt is made at a comparison of model physics. Nor is the author trying to mediate the so-called "differences" between the self-partitioned groups with their respective modus operandi. But there have been definitive positions (initiated by the results of their work) taken by various researchers. On the one hand, some investigators have demonstrated positive impacts when the SASS winds were utilized together with conventional data to produce forecasts in extratropical regions (mainly Northern Hemisphere). Cane, et al. (1981) have concluded that the surface wind alone might be as valuable as temperature soundings in numerical modeling. Endlich, et al. (1981) have suggested that the SASS winds, in combination with other remotely sensed data could be used to measure sea level winds and to compute the balanced-pressure field. Researchers at the Goddard Space Flight Center (GSFC) (see NASA Tech. Memorandum 83907) seem to be having some measure of success working with the SASS winds.

On the other hand, some scientists have had only limited success. This group of workers is associated with the National Meteorological Center. There is the claim that the inclusion of satellite over NOSAT data did not seem to be of any great meteorological consequence.

In summary, it is important to point out the following. The magnitude of the potential improvement revealed by the study of Cane, et al. (1981) is somewhat questionable. The use of the same model for the nature run and for forecasting overestimates the quality of the forecasts. The insertion of the simulated observation at the 9th level does not account for the errors made in assessing the free atmospheric flow nor for those that arise in the alias removal scheme. In the study of Yu and McPherson (1979, 1981) two points arouse immediate questioning. Firstly, data are stratified into six-hour time blocks and are treated as synoptic at the central time of the block. This suggests that the data base available for the update have information that are as much as three hours off time. To deal with this situation, they have assumed that the error introduced is not crucial for

large-scale or global applications. Secondly, the results of their research are based on a data set taken during the northern summer. During this period the Atlantic is rather inactive and gradients are not well defined. Thus their conclusions were made without taking the climatological situation into account. It is rather difficult for positive impacts to be realized under these conditions.

This assortment of diverse opinions and inconsistent results seems to mark the instability that the scientific community experiences at the brink of a major break-through. It just says that we have not yet fully solved the problem of using remotely sensed winds in numerical models.

At this stage, it is a matter of "blowing one's own horn". All evaluations of performance (output) must be viewed in relative terms, since the differences in numerical prediction results are judged by means of RMS errors, skill score and synoptic case studies. What yardstick is used to measure success and failure is clearly not standardized. The enigma, according to Ghil, et al. (1979) is that the assessment of the effect that sounding data and methods for their assimilation have on weather forecasting is complicated by the verification problem. We are without this standard since there exists no consensus on adequate measures for the accuracy and utility of a large-scale numerical forecast.

We have to admit that we are trying to solve a very difficult problem and, as is expected, approaches head out in several directions. Each contributing author sees room for improvement and expresses confidence in the future. Learning from others and from one's own mistakes will surely motivate the community in surging ahead to find the correct solutions.

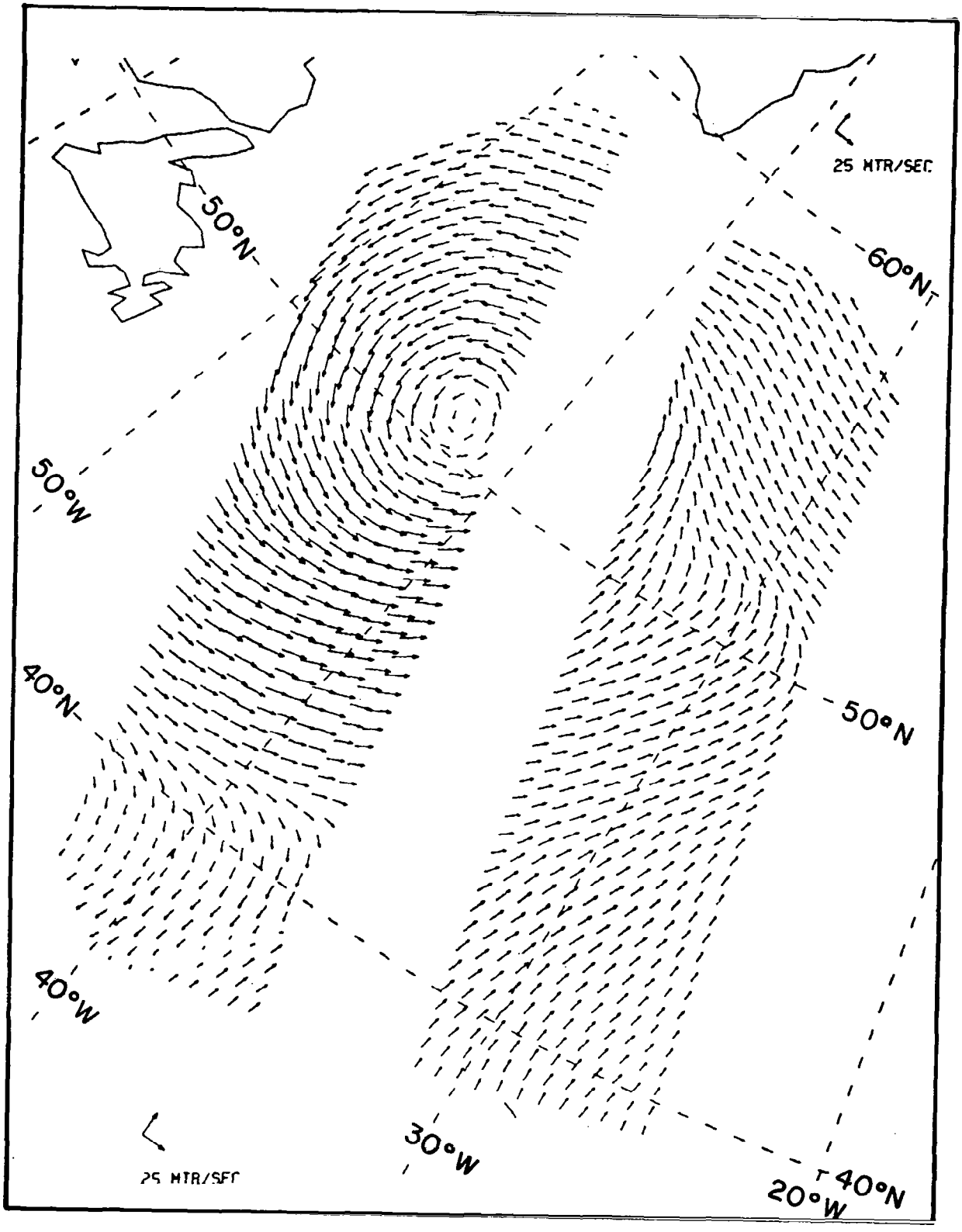

Figure 1 (Adapted from the Report of the Satellite Surface Stress Working Group) shows the true surface vector for the QE II wind field for a 50-km wind solution resolution. A well defined low center is shown in the vicinity of 51° N latitude.

D. STATING THE PROBLEM

The best synoptic analysis depends on the maximum amount of good available data. Meteorological satellites seem to offer an effective way to supplement the conventional synoptic data base. The recent experiment of SEASAT-A has helped marine and atmospheric scientists to focus in on an even more sought after prize - acquisition of global data. The task before them therefore, is to find the best way of utilizing this wealth of data.

Certain fundamental findings have helped to give researchers some impetus. The concept of retrieving marine surface wind by using a radar scatterometer to measure radar return signal from surface capillary waves has been successfully tested in the Skylab experiment (Cardone, et al. 1976). The scientific community has had substantial assurances (see JGR. April 1982) that scatterometer derived wind measurements are at least as accurate as the conventional reports by transient ships, weather ships and data buoys. The next phase is already being instituted in forecasting studies — the use of SASS winds for large-scale numerical analysis and prediction. The present state focuses partly on assessing and "debugging" the various outputs. This paper is, however, concerned with highlighting the problem of the systematic error (displacement error) that results from an intermittent assimilation scheme that utilizes a ± 3 hour window in the treatment of satellite wind data. This referenced procedure leads to errors in the initial value specification. An additional negative effect is realized as these errors are compounded with those made when conventional data are used. The author's aim is to determine the relative 12-hour displacement errors that are created when such an assumption is used.

It is reasonable to assert that these kinds of errors are found in the present initial value specification of forecast models. And they approximately double each day (Pierson 1983). Their manifestations are realized in the incorrect determination of pressure gradients, the value of central pressures and the locations of low centers. The particular errors can therefore be minimized by updating the quality of the first guess field.

It is also evident that there is no absolute measure of accuracy for estimating the location and strength of cyclones. This is not possible because, according to Gaby, et al. (1980), there is no absolute "ground truth", i.e., neither the exact locations nor the precise wind speeds of the cyclones are known. Especially over the oceans, the first guess field suffers from very serious errors. Pierson (1981)[+] has ascribed a probable error of ± 2 to ±3° of longitude to the location of low centers. These errors belong to the class of "systematic errors" as defined by Wallace and Woessner (1981), Colucci and Bossart (1979) and Leary (1971).

Some of the errors in operational prognoses at NMC have been studied in the past by Fawcett (1969), Leary (1971), Colucci and Bosart (1979), and Wallace and Woessner (1981). These studies have dealt with the different components of forecast errors with an aim of developing procedures for tracing errors that are related to the physics of the model. In this experiment the focus is to describe a form of the systematic error (12-hr DE) committed prior to the forecast cycle.

[+]Based on reported experience at FNOC

E. REPEAT ORBITS

Definition

During the final 26 days of the SEASAT-A mission, the satellite ground track repeated within a 2-km band at 3-day intervals. Klose (1979) prepared node tables for each orbit of the mission. The ascending and the descending nodes give the East longitude to four decimal places of the equatorial crossing north and south respectively. In the node tables a repeat orbit is detected when the ascending node (or descending node) East longitude of a particular orbit is practically equal to the ascending (or descending) node (i.e. 43 orbits) away. Repeat orbits are used in this study to simplify data analysis. The conclusions obtained are not critical to this choice.

Gordon and Barker (1980) used GOES-3 coincident orbits to study mesoscale transients in the Western Subtropical North Atlantic. Cheney and Marsh (1981) documented sea height variability by a similar method.

In this paper 3-day repeat orbits are used to study the surface movement of migratory cyclones in the North Atlantic and Pacific. It is suggested also that this method (to be described below) can be used to investigate other events that are important at the synoptic scale.

SEASAT Node Tables (see Klose 1979) provide the basic data for the repeat orbit model. Rev. No. "1351 to 1394" are selected as the "standard" 3-day repeat orbits. These are, however, relabelled as local orbit 1 to 43. The orbits were selected given the difference between, say, the ascending node of rev. no.1351 (356.4505° E. long) and that of rev. no. 1394 (356.4508° E. long). This very small difference of 0.0003° E. longitude represents the minimum difference for the orbits.

As can be seen from Table 1, starting times (GMT) at the Equator differ from those given by Klose (1979). The model suffers no drawbacks when the orbits are relabelled and local orbit no. 1 starts at the Equator at 0000z. The observation which is more important is the close agreement of the length of the period between each orbit as reported by Klose (1979) and that listed in Table 1 of this report. Small deviations arise only because of the simple averaging process utilized in this study. In this model, the period of each orbit is exactly 100.4651 minutes (1hr. 40min. 27.9sec.). This will account for the 43 orbits being completed in 3-days, or 14 1/3 orbits in one day. The repeat feature is realized when once again an orbit crosses the equator at ≈356.5° (E. long) at midnight. The model thus provides a simple tool for studying synoptic patterns without regard to precise orbit determination and complicated time sequences.

Seatrak Calculator

The "Seatrak" tracking calculator developed at the Jet Propulsion Laboratory (CALTECH 1977) is designed to provide the SEASAT user community with quick and accurate subsatellite position data for each minute of the day's orbits together with the corresponding sensor swath coverage. The Seatrak package comprises two transparent polar hemispheric maps plus sixteen overlays (8 for each hemisphere) which may be pivoted and aligned to indicate desired SEASAT orbit data.

The two hemispheric base maps (north and south) show latitude circles as concentric circles with the poles as centers. These circles form orthogonal sets with the longitude line that are the radii of these concentric circles. The longitude is measured in degrees east (from 0^{o} to 360^{o}). Of course, the latitutde is measured in degrees north or south from 0^{o} at the equator to 90^{o} at the poles.

For the present study only overlays 1 and 3 are of particular interest. Overlay 1 displays the relative orientations of SEASAT orbit passes (N.Hemisphere) for one day plus an indication of the first pass for the next day. The 25-degree shift in longitude between the successive orbit nodes is due to the earth's rotation during 1hr. 40min. 45sec. orbit period. Time marks are arranged along each ground track indicating 5-minute intervals, starting from time zero at the nodes (equatorial crossing). The time for a given node is found by adding the elapsed time (in terms of period) to the GMT time listed for the day's first orbit.

Overlay 3 also refers to the Northern Hemisphere. It displays the SEASAT ground track and the minute-by-minute progress for one orbit together with the corresponding swath coverage of the SASS. Relative locations for subsequent nodes are sequentially identified. Hemispheric base map for the Northern Hemisphere, Overlay 1 and Overlay 3 are displayed in the Appendix of this paper.

Setting up the Orbits

The Seatrak Satellite calculator provides accurate subsatellite positional data for each minute of each day's orbits together with the corresponding sensor swath coverage. For this study only the Northern Hemisphere Baseplate Map and Overlay 3 (SASS) are required. Notice that the orbital periods shown on overlay 1 are ignored. Instead, a constant period of 1hr. 40min. 27.9sec. (or 6027.9 sec.) is used. The first revolution is arbitrarily set up. The other 42 orbits follow in logical space-time sequence. So that forty—three orbits take 259199.7 sec. (3 days are 259200 sec.).

Table 1 provides a tabulation of local orbit data which includes orbit number, associated SEASAT orbit number, equatorial crossing times (GMT), ascending and descending nodes (^{o}E longitude), and the corresponding day for each 3-day cycle. Note that orbit No. 15 starts on day cycle 1 but ends on day cycle 2. Also, the first two-thirds of orbit 29 is during day 2. Figure 2a, a pattem of repeat orbits over the North Atlantic, is bounded southward by the Equator and northward by latitude 60^{o}. At the Equator the longitudinal distance spans from 280^{o}E to 350^{o}E. A similar layout (Fig.2b) is given for the North Pacific. In this case the latitudinal map area covers from the Equator to latitude 55^{o} N. The longitudinal extent along the Equator begins at 165^{o} E and ends at 260^{o} E.

The formula for identifying the orbits is as follows: The first day of the cyclone month* begins at 0000GMT. At that precise moment, the satellite is assumed to be over the Equator at 356.5^{o} E longitude. This represents the ascending node (Ω) for orbit No. 1 (corresponding to orbit No. 1351). Once overlay 3 is aligned over the baseplate map's East longitude (356.5^{o}), the sub-satellite track and the boundaries of the swath width can be easily duplicated. The sub-satellite tracks for consecutive orbits are laid out in similar fashion, except that the starting time for each additional crossing is successively 1hr. 40min. 27.9sec. later.

*Month in which cyclone is first detected.

TABLE 1 Description of simulated 3-day repeat local orbits of period 1 hr. 40 min. 27.9 sec., using basic information provided by Klose (1979).

LOCAL ORBIT No.	ASSOCIATED SEASAT ORBIT No.	STARTING TIME (GMT) AT EQUATOR	ASCENDING NODE (DEG.) E. LONG	DESCENDING NODE (DEG.) E. LONG	DAY CYCLE
1	1351	00:00	356.5	163.9	1
2	1352	01:40:27.9	331.3	138.8	1
3	1353	03:20:55.8	306.2	113.7	1
4	1354	05:10:23.7	281.1	88.6	1
5	1355	06:41:51.6	256.0	63.4	1
6	1356	08:22:19.5	230.9	38.3	1
7	1357	10:02:47.4	205.8	13.2	1
8	1358	11:43:15.3	180.6	348.1	1
9	1359	13:23:43.2	155.5	323.0	1
10	1360	15:04:11.1	130.4	297.9	1
11	1361	16:44:39.0	105.3	272.7	1
12	1362	18:25:06.9	080.2	247.6	1
13	1363	20:05:34.8	055.1	222.5	1
14	1364	21:46:02.7	030.0	197.4	1
15*	1365	23:26:30.6	004.8	172.3	1
	END OF DAY 1 (*First one-third of orbit is on day 1).				
16	1366	01:06:58.5	339.7	147.2	2
17	1367	02:47:26.4	314.6	122.0	2
18	1368	04:27:54.3	289.5	96.9	2
19	1369	06:08:22.2	264.4	71.8	2
20	1370	07:48:50.1	239.2	46.7	2
21	1371	09:29:18.0	214.1	21.6	2
22	1372	11:09:45.9	189.0	356.5	2
23	1373	12:50:13.8	163.9	331.3	2
24	1374	14:30:41.7	138.8	306.2	2
25	1375	16:11:09.6	113.7	281.1	2
26	1376	17:51:37.5	088.5	256.0	2
27	1377	19:32:05.4	063.5	230.9	2
28	1378	21:12:33.3	038.3	205.8	2
29Δ	1379	22:53:01.2	013.2	180.6	2
	END OF DAY 2 (Δ First two-thirds of orbit is on day 2).				
30	1380	00:33:29.1	348.1	155.5	3
31	1381	02:13:57.0	323.0	130.4	3
32	1382	03:54:24.9	297.8	105.3	3
33	1383	05:34:52.8	272.7	80.2	3
34	1384	07:15:20.7	247.6	55.1	3
35	1385	08:55:48.6	222.5	30.0	3
36	1386	10:36:16.5	197.4	4.8	3
37	1387	12:16:44.4	172.2	339.7	3
38	1388	13:57:12.3	147.1	314.6	3
39	1389	15:37:40.2	122.0	289.5	3
40	1390	17:18:08.1	096.9	264.4	3
41	1391	18:58:36.0	071.8	239.3	3
42	1392	20:39:03.9	046.7	214.1	3
43°	1393	22:19:31.8	021.6	189.0	3
	END OF DAY 3 (° Orbit ends on midnight of day 3).				

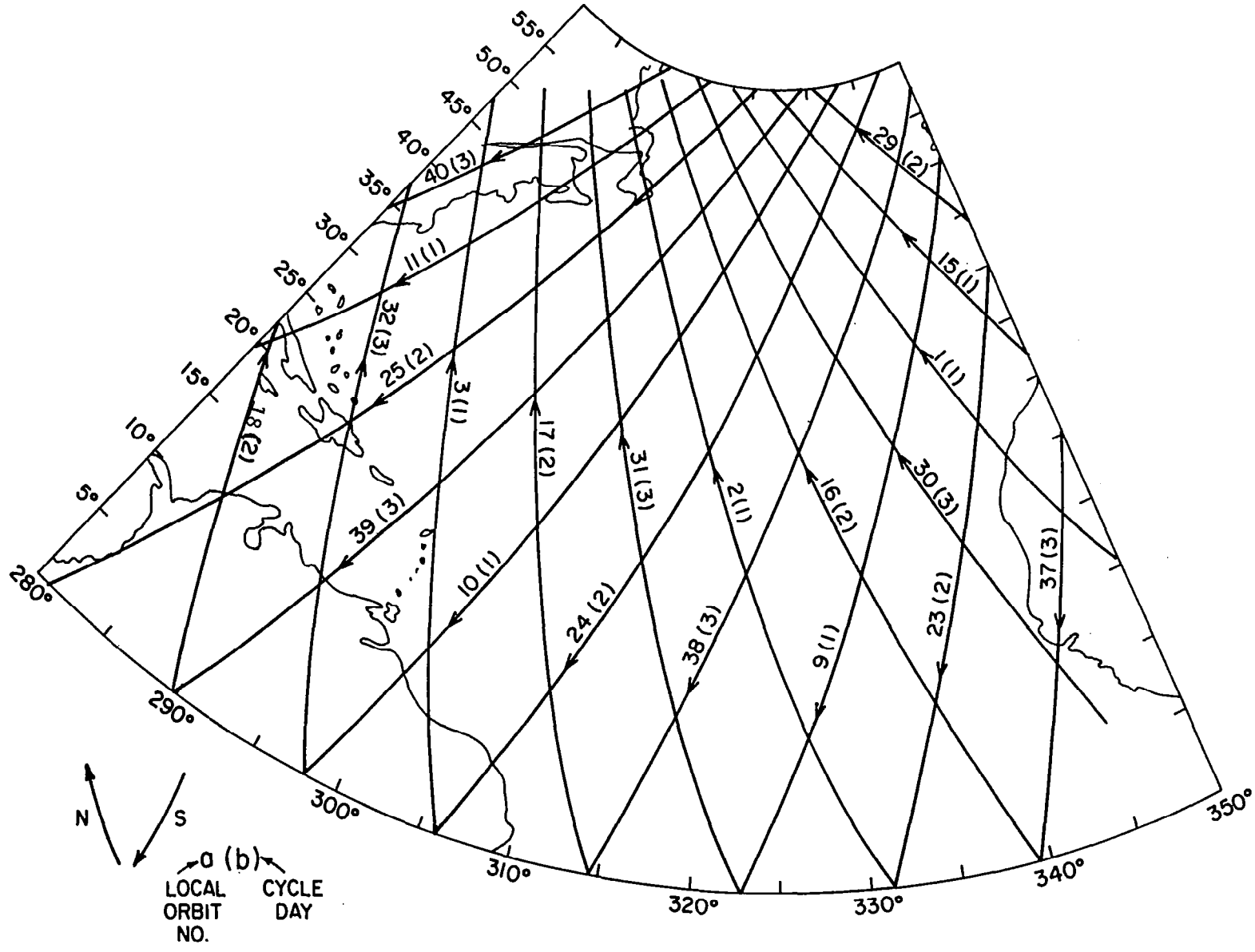

FIGURE 2(a) Pattern of Repeat Orbits Over the North Atlantic. Both North-and South-bound Orbits are Depicted with their Associated Local Orbit Number and Cycle Day.

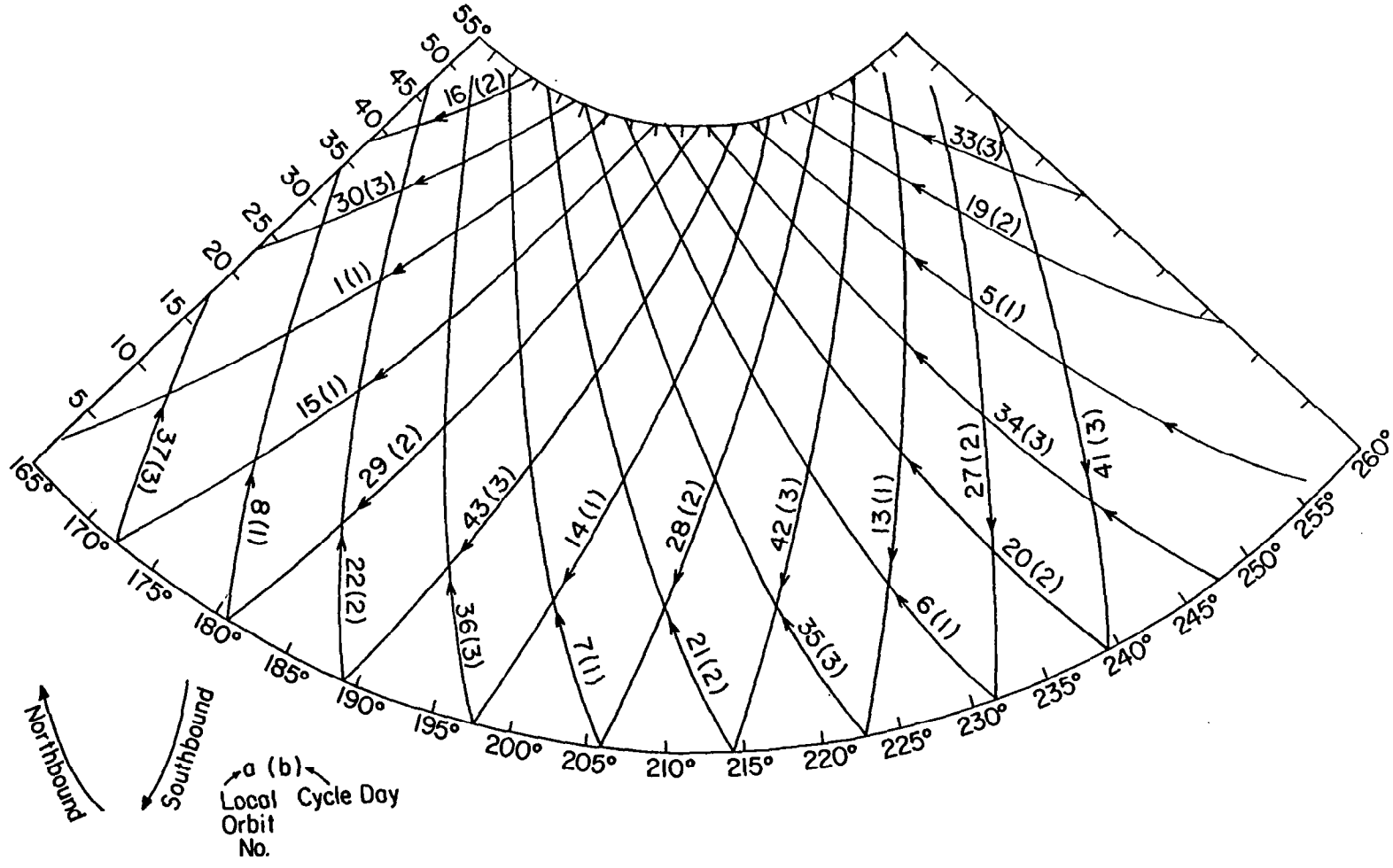

FIGURE 2(b) Pattern of Repeat Orbits Over the North Pacific. Both North-and South-bound Orbits are Depicted with their Associated Local Orbit Number and Cycle Day.

Transient cyclones that move across the oceans predominantly from west to east can therefore be studied by simulation using the model described above. Synoptic features for each month are studied independently. Cycle day 1 generally begins on the 1st day of each month at 0000z. There is, however, an exception to this rule.

When a cyclone that has had its beginning in a particular month continues into the following month, the cycle continues sequentially. The cycle day for a particular event is found by using the relationship: $D \equiv C \text{ Mod } 3$, where D is the total number of elapsed days, counting from the first day of the month in which the particular event commenced, up to, and including the date under consideration; C = 0, 1, 2, where the following holds:

C = 0 ---------- day 3
C = 1 ---------- day 1
C = 2 ---------- day 2

As an example, if the date of a cyclone under study is March 25 (knowing that the cyclone began in the month of March), it will belong to day 1 of the 3-day cycle. Now suppose that the same cyclone is still in existence in April. Its position as of April 4 will be credited to day 2 of the cycle.

Figures 2a and 2b illustrate features of successive orbits that aid in the interpretation of the results of the simulation experiment. Consider, for example, northbound orbit 34(3) in Figure 2b. Southbound orbit 41(3), seven orbits later, crosses this track at about 10° N some 12 hours 24 minutes later. A stationary meteorological feature at that point would be observed therefore at about a 12.5-hour interval. Southbound orbit 42(3), eight orbits later also crosses the same northbound orbit at about 37° N. A stationary meteorological pattern at this point would thus be observed some 13 hours 32 minutes later by the southbound pass. Orbit 43(3), nine orbits later also crosses the same northbound orbit at about 51.5° N some 15 hours 22 minutes later. From this we see that crossings at latitudes 10°, 38° and 51.5 N have respectively similar time separations all around the earth. In general, any two crossings that are composed of a particular orbit and another seven, eight and nine passes later are associated with revisit times of 12 hours 24 minutes, 13 hours 32 minutes and 15 hours 22 minutes respectively. The other crossings in Figures 2a and 2b do not correspond to crossings with separation times of less than 18 hours.

F. DATA

Ground Truth

The data used in this investigation are the principal tracks of centers of cyclones at sea level for the North Atlantic and North Pacific for December 1980 and January 1981. The data were selected from copies of the working charts for the smooth logs published each month in the Mariner's Weather Log. (NOAA, Eds.). Two original monthly charts were generously supplied by the editor.

The tracks are plotted on hemispheric maps; they represent the continuous paths of migratory cyclones over the oceans defined by their 12-hour positions. These paths represent the closest available to the truth since they are determined after the fact from careful post analyses of all pertinent data. This data will therefore serve as "ground truth". By means of the repeat orbit model, the centers of the cyclones can be defined in terms of position and time as spacecraft passes over them are simulated. With respect to a satellite like SEASAT, the cyclone's centers are identified and defined if they can be found somewhere within the swath of the SASS.

The data set comprises seventeen (17) cyclones of which ten are of the Pacific and seven are of the Atlantic. The study areas are found mainly between latitude 30^{o} N and 65^{o} N.

Pecularities of the Input Data and the SEASAT Observations

Figures 3(a) through 3(e) and 4(a) through 4(e) show the tracks of the low centers of seven extratropical cyclones that occurred over the North Atlantic and ten that occurred over the North Pacific during December 1980 and January 1981. The open circles show the 12-hourly locations of the low centers. If available, some of the intermediate 6 hourly position are shown by x's. The hourly movement of the low center is interpolated along the track. If the low center was within the two sided SEASAT swath for a simulated orbit, the position and time of the sighting is shown by an arrow emanating from that point along the track.

Although the tracks that are shown are assumed to be the true paths of the cyclone centers for the purposes of this study, the actual tracks illustrate some of the present difficulties of analyses of isobaric patterns and wind fields over the oceans. As examples, cyclone Atlantic 2 in Figure 3(b) shows a strange movement from 7/12 to 8/0 and Atlantic 5 in Figure 3(c) shows a perturbation from 19/12 to 20/0 to 20/12. Also Pacific 6 in Figure 4(d) has a "z" shaped track near the end of its existence. The spiraling motion of Pacific 1 in Figure 4(a) is also of interest.

Whether or not the present data density over the northern oceans actually permits the location of low centers to the accuracy needed to detect these kinds of movements accurately is difficult to determine. As shown by Pierson (1983), the errors in reported wind speed and direction for transient ships are sufficient to introduce errors in the location of a low center by amounts that would produce most of the small scale oscillations in the analysed cyclone tracks.

Another feature of these figures of importance in understanding SASS data is that the low centers are sighted less frequently in the southerly latitudes and more frequently in northerly latitudes. Although there are variations from one track to another, cyclone Atlantic 5 in Figure 3(c) is an illustration of this effect. During the first three days of its existence, from 15/12 to 18/12, this cyclone was sighted only 5 times whereas during the next three days from 18/12 to 21/12 it was sighted 15 times. During the last 6 hours from 21/12 to 22/0 it was sighted 5 times.

The more northerly portions of each cyclone track also illustrate the effect of dwell. The same area of the ocean can be within the swath of an instrument such as the SASS on a number of successive orbits, especially north of 55^{o} N for areas not shown in Figure 2a and 2b. When cylone Atlantic 5 reached 65^{o} N, it was sighted, at roughly 100 minutes intervals, six times from 13:56 to 22:05 on the 19th and 5 times from 15:01 to 21:34 on the 20th. Data such as these could be used to find out whether or not a given cyclone was deepening or filling as it moved along.

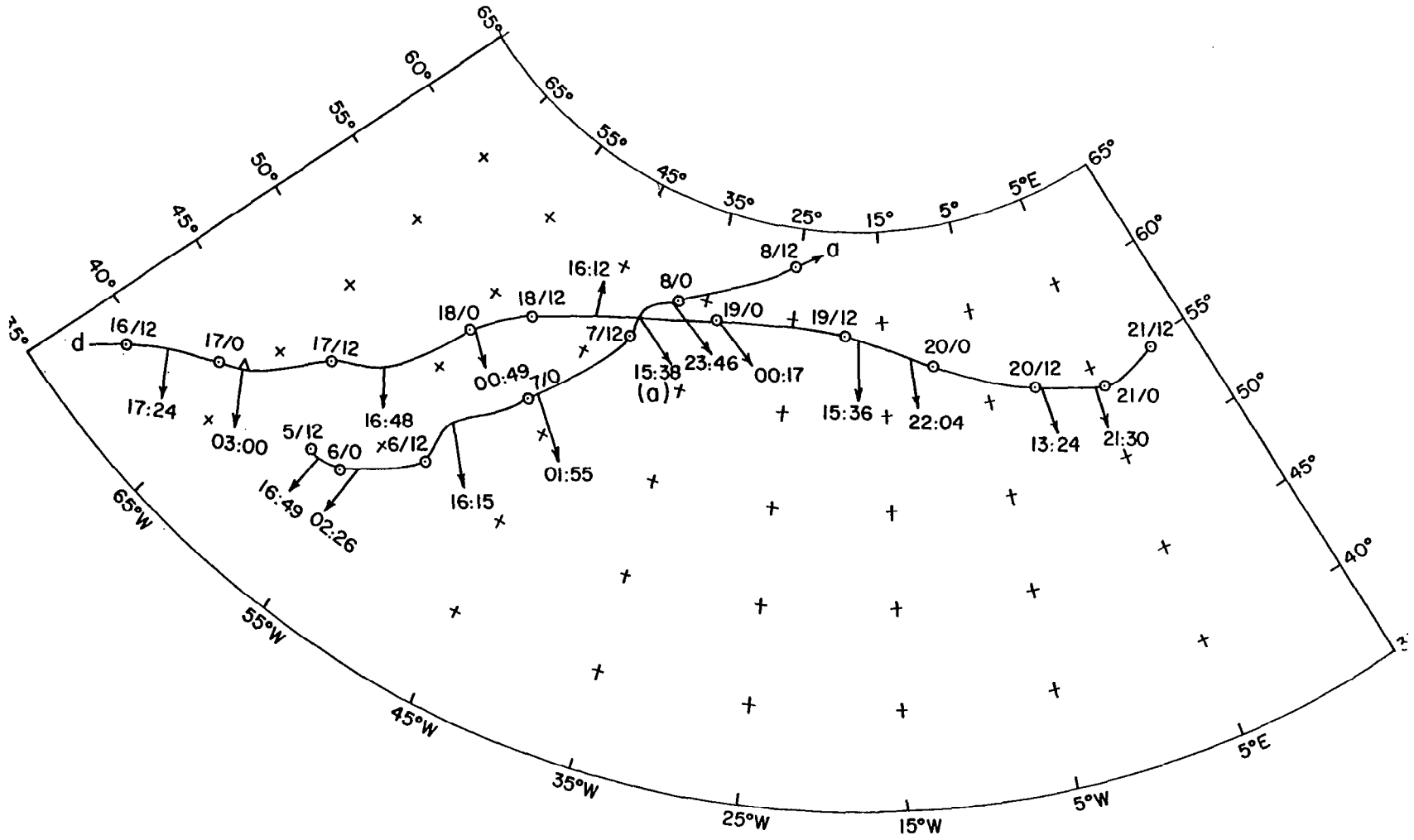

FIGURE 3 (a) Cyclone Tracks with 12-Hour Positions and SEASAT Sighting Times.
ID: a → Dec. 1980, Atlantic 1
d → Dec. 1980, Atlantic 4.

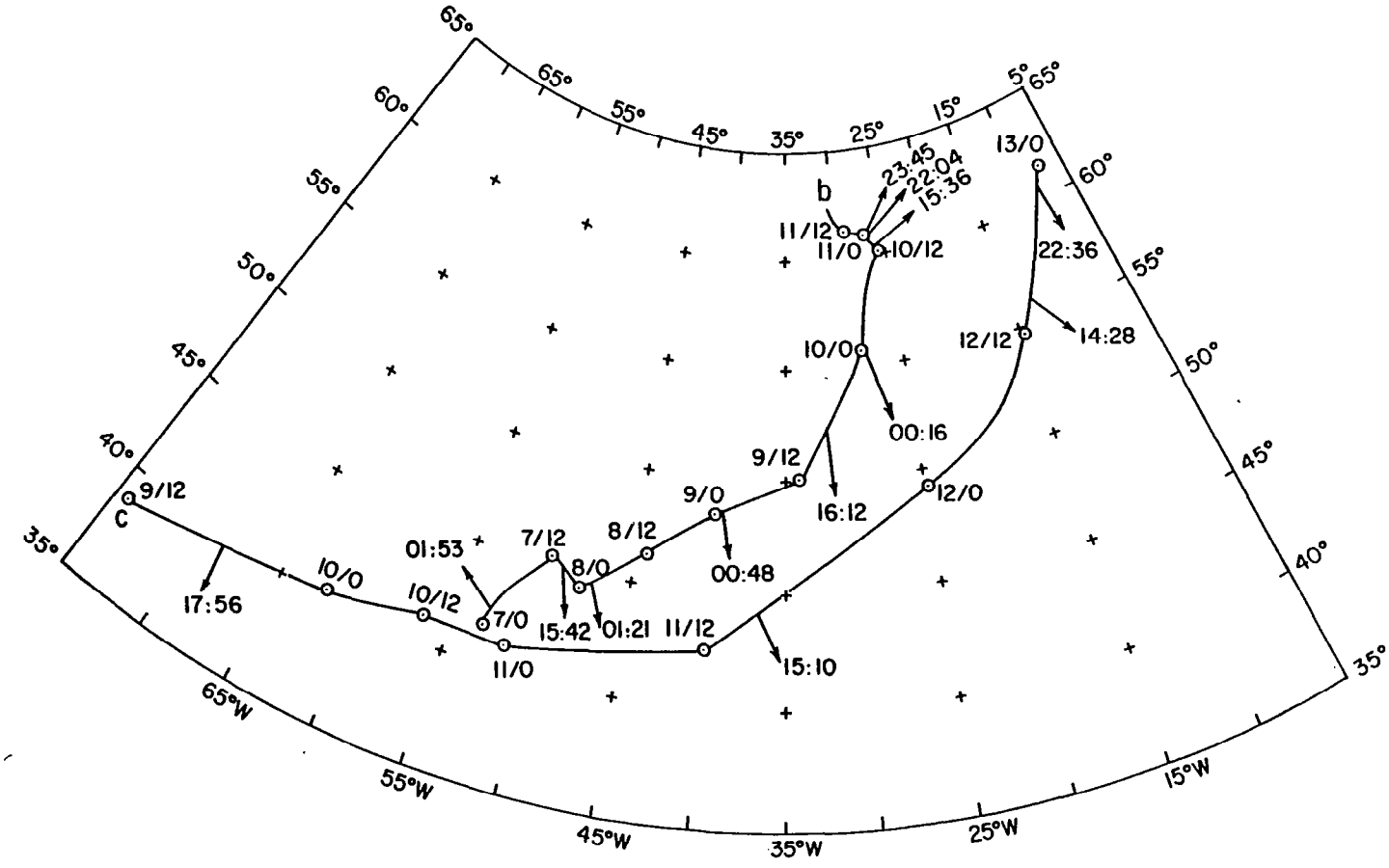

FIGURE 3 (b) Cyclone Tracks with 12-Hour Positions and SEASAT Sighting Times.
ID: b → Dec. 1980, Atlantic 2
c → Dec. 1980, Atlantic 3.

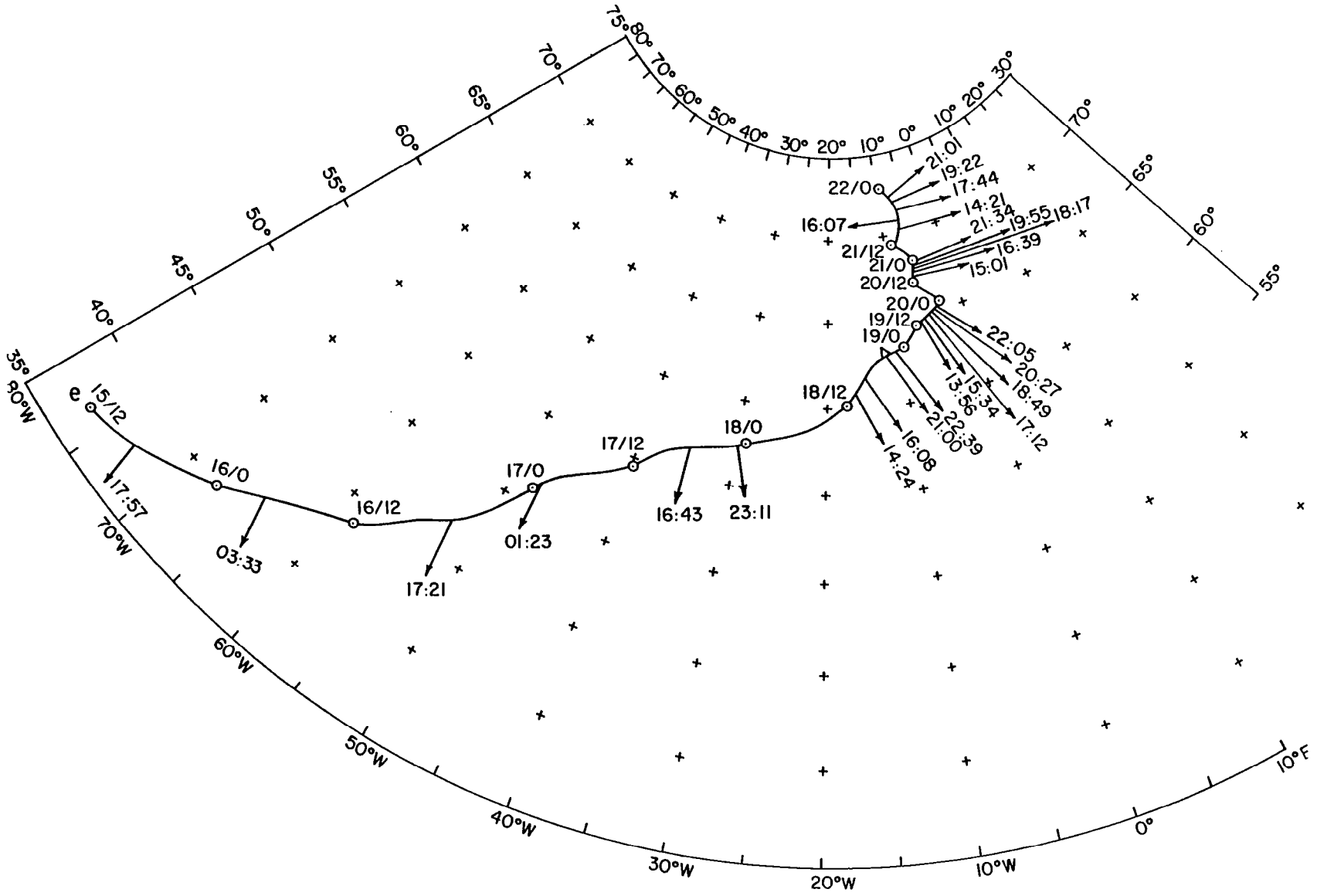

FIGURE 3 (c)
Cyclone Track with 12-Hour Positions and SEASAT Sighting Times.
ID: e → Jan. 1981, Atlantic 5.

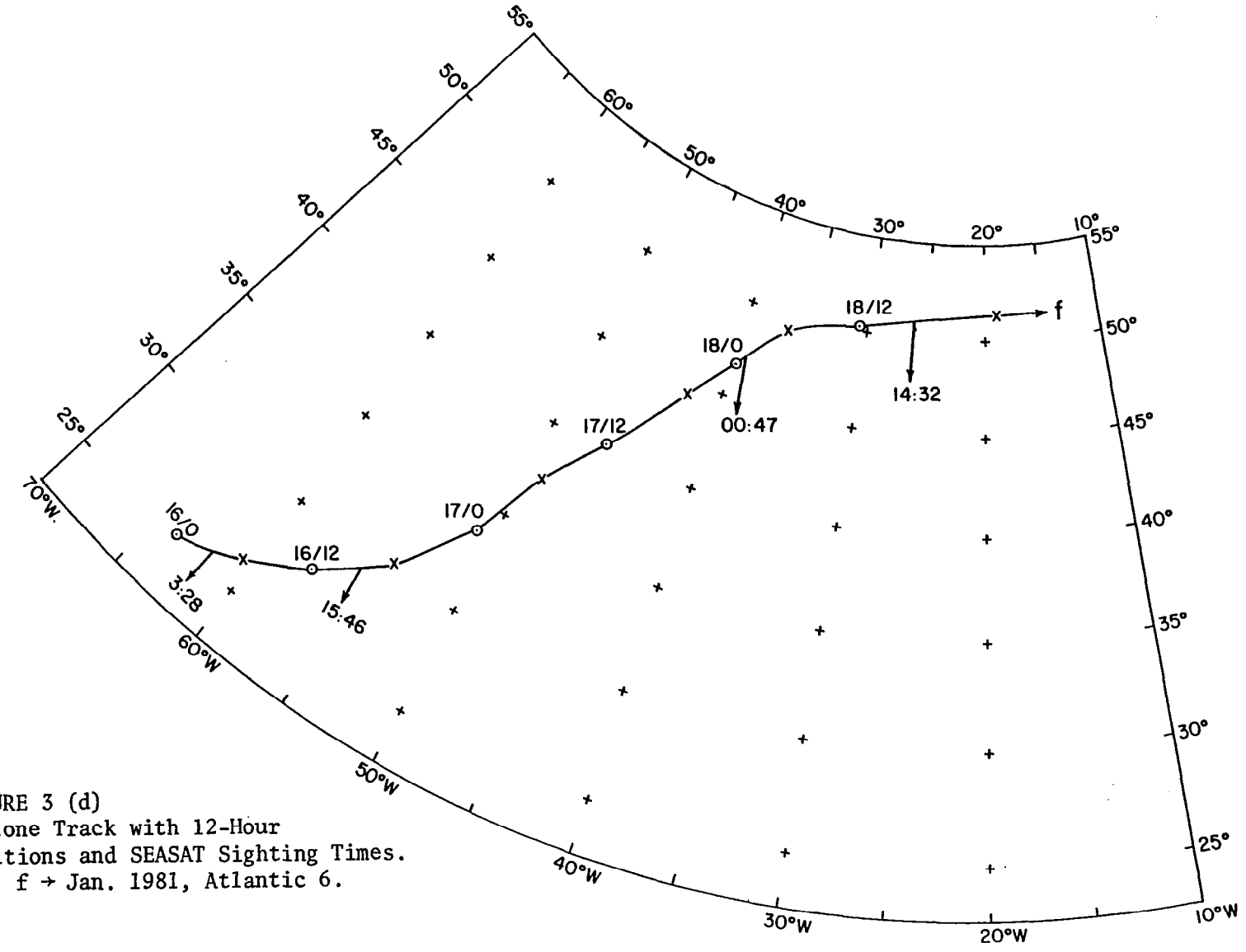

FIGURE 3 (d)
Cyclone Track with 12-Hour
Positions and SEASAT Sighting Times.
ID: f → Jan. 1981, Atlantic 6.

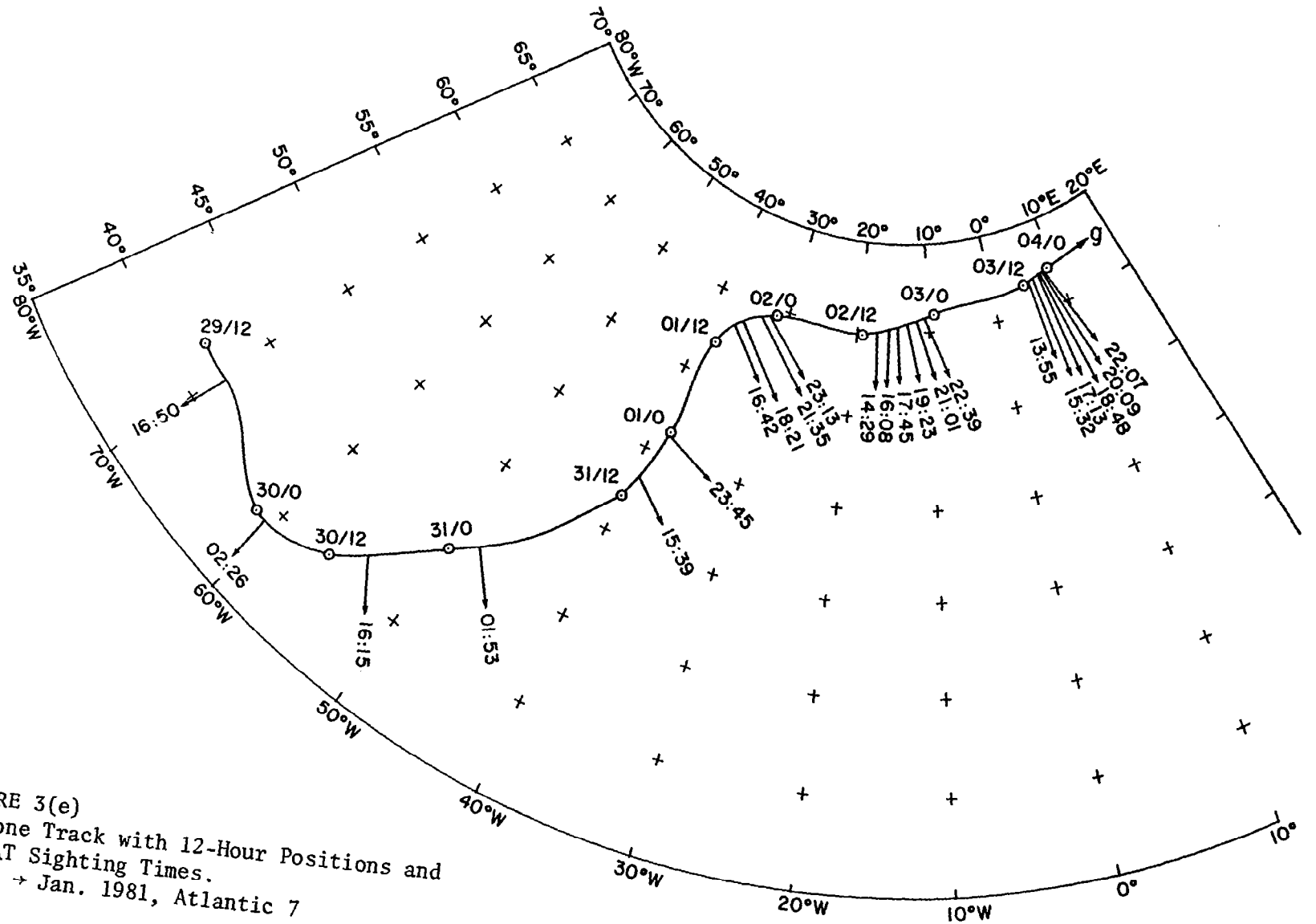

FIGURE 3(e)
Cyclone Track with 12-Hour Positions and SEASAT Sighting Times.
ID: g → Jan. 1981, Atlantic 7

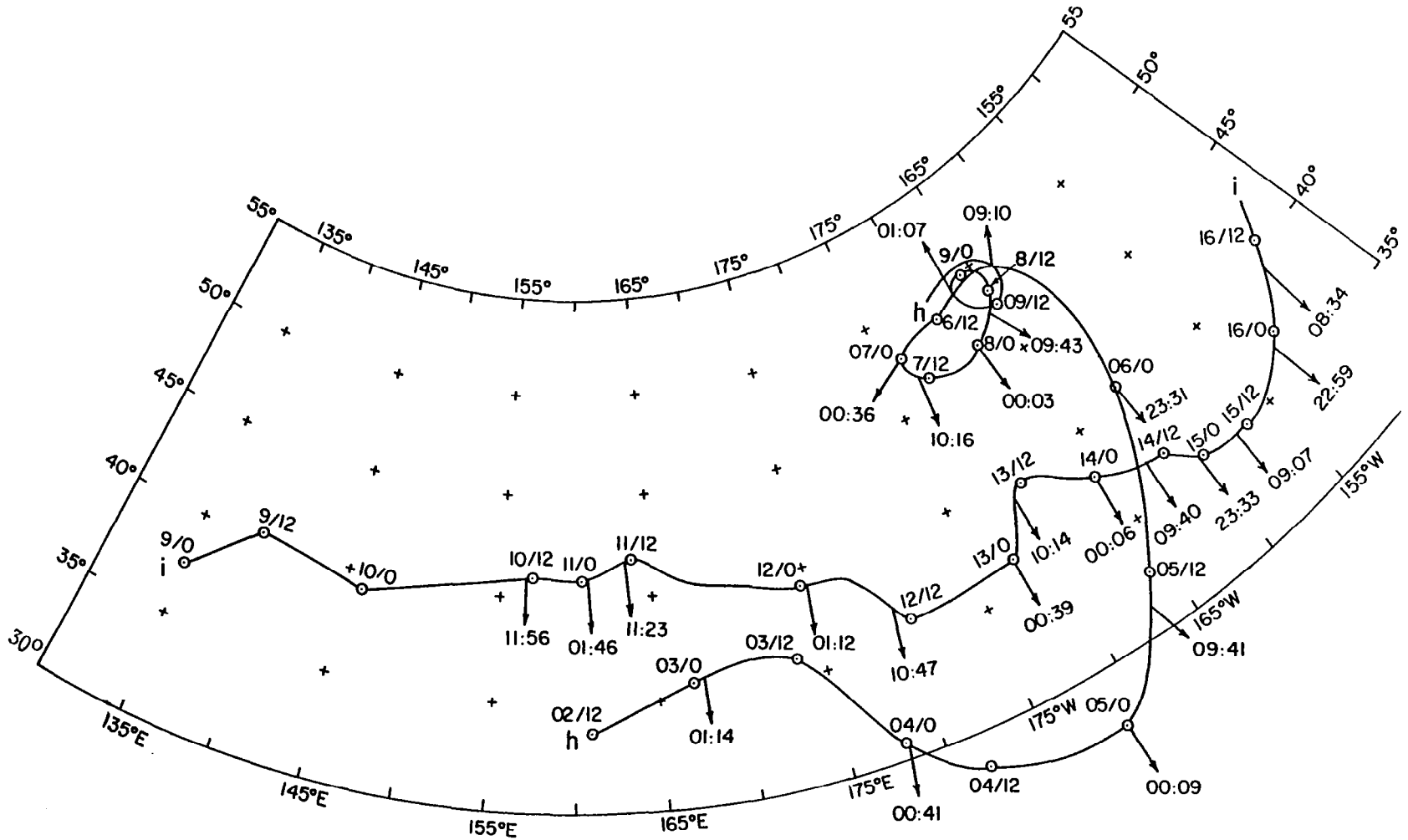

FIGURE 4(a) Cyclone Tracks Showing 12-Hour Positions and SEASAT Sightings Times
ID: h → Dec. 1980, Pacific 1
i → Dec. 1980, Pacific 2

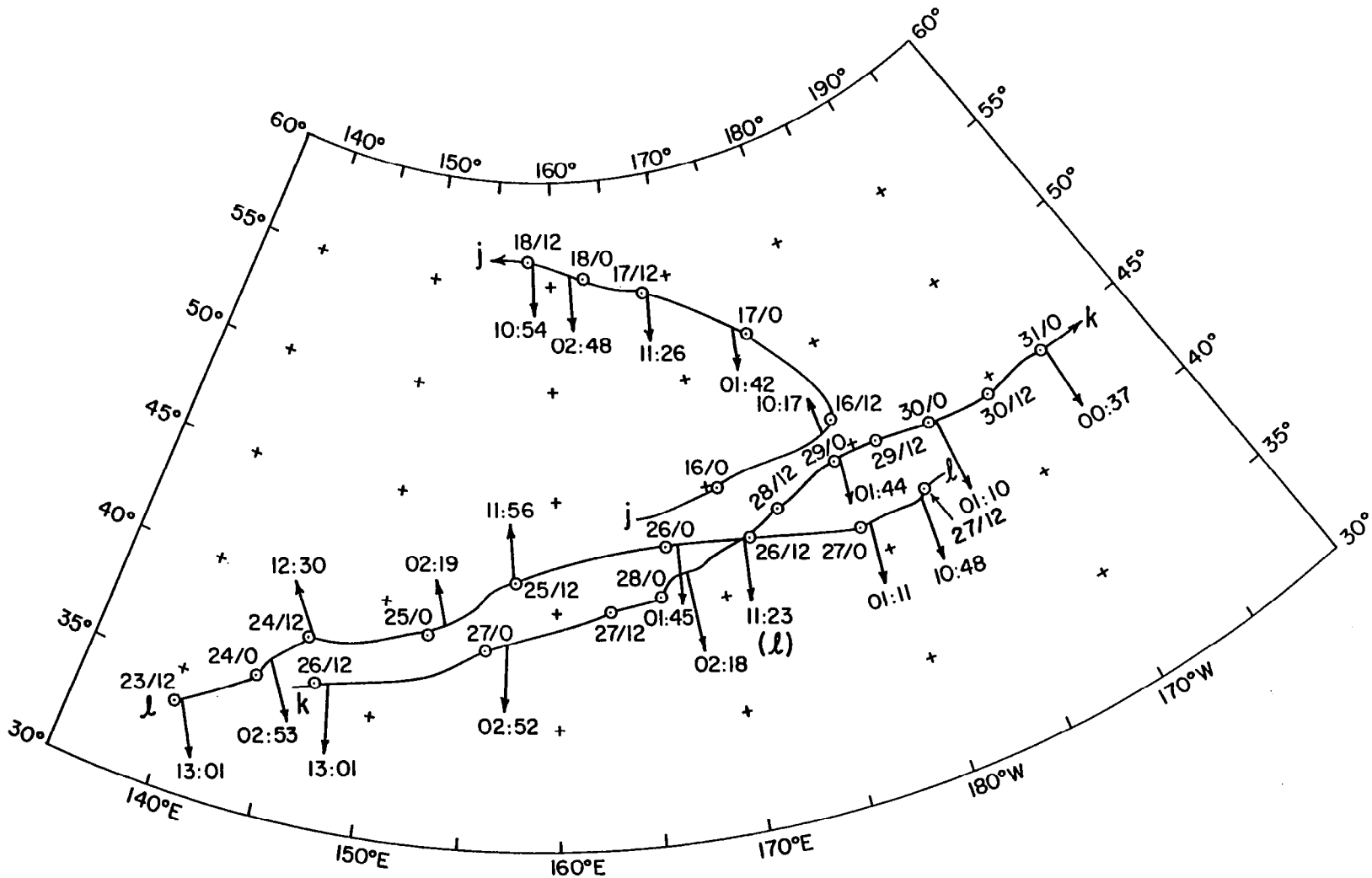

FIGURE 4(b) Cyclone Tracks Showing 12-Hour Positions and SEASAT Sighting Times.
ID: j → Dec. 1980, Pacific 3
k → Dec. 1980, Pacific 4
1 → Dec. 1980, Pacific 5.

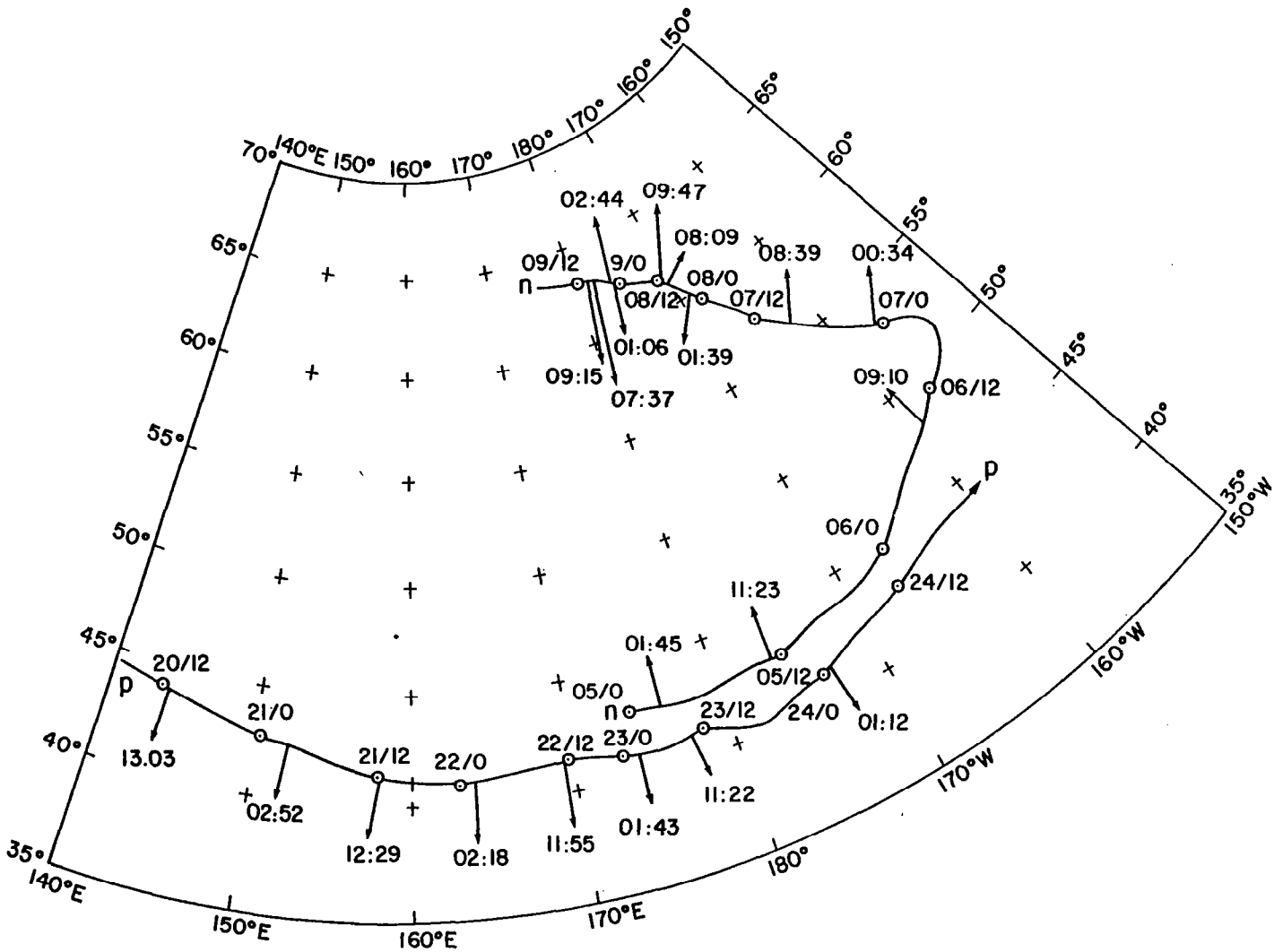

FIGURE 4(c) Cyclone Tracks Showing 12-Hour Positions and SEASAT Sighting Times.
ID: n → Jan. 1981, Pacific 7
p → Jan. 1981, Pacific 9.

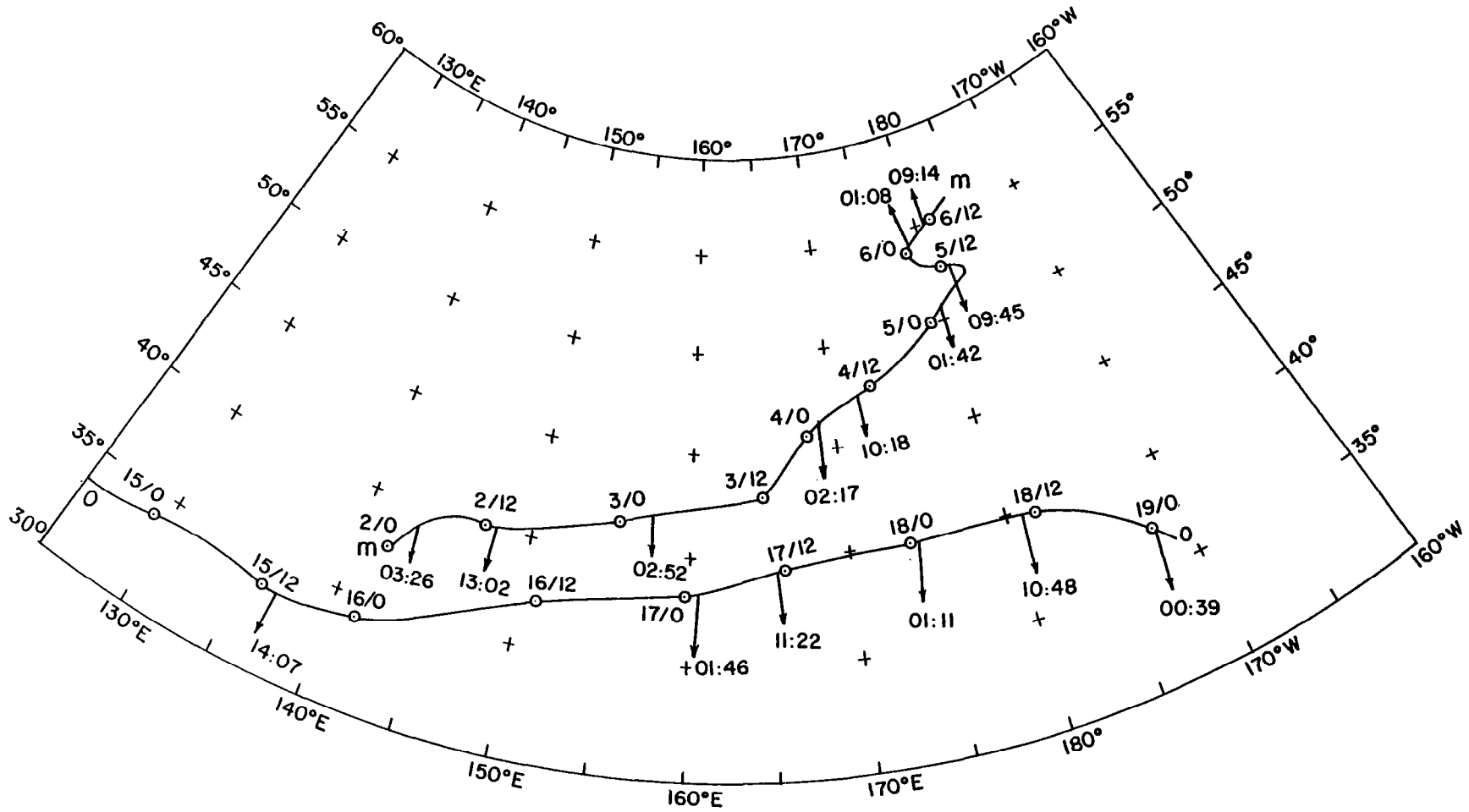

FIGURE 4(d) Cyclone Tracks Showing 12-Hour Positions and SEASAT Sighting Times.
ID: m → Jan. 1981, Pacific 6
o → Jan. 1981, Pacific 8.

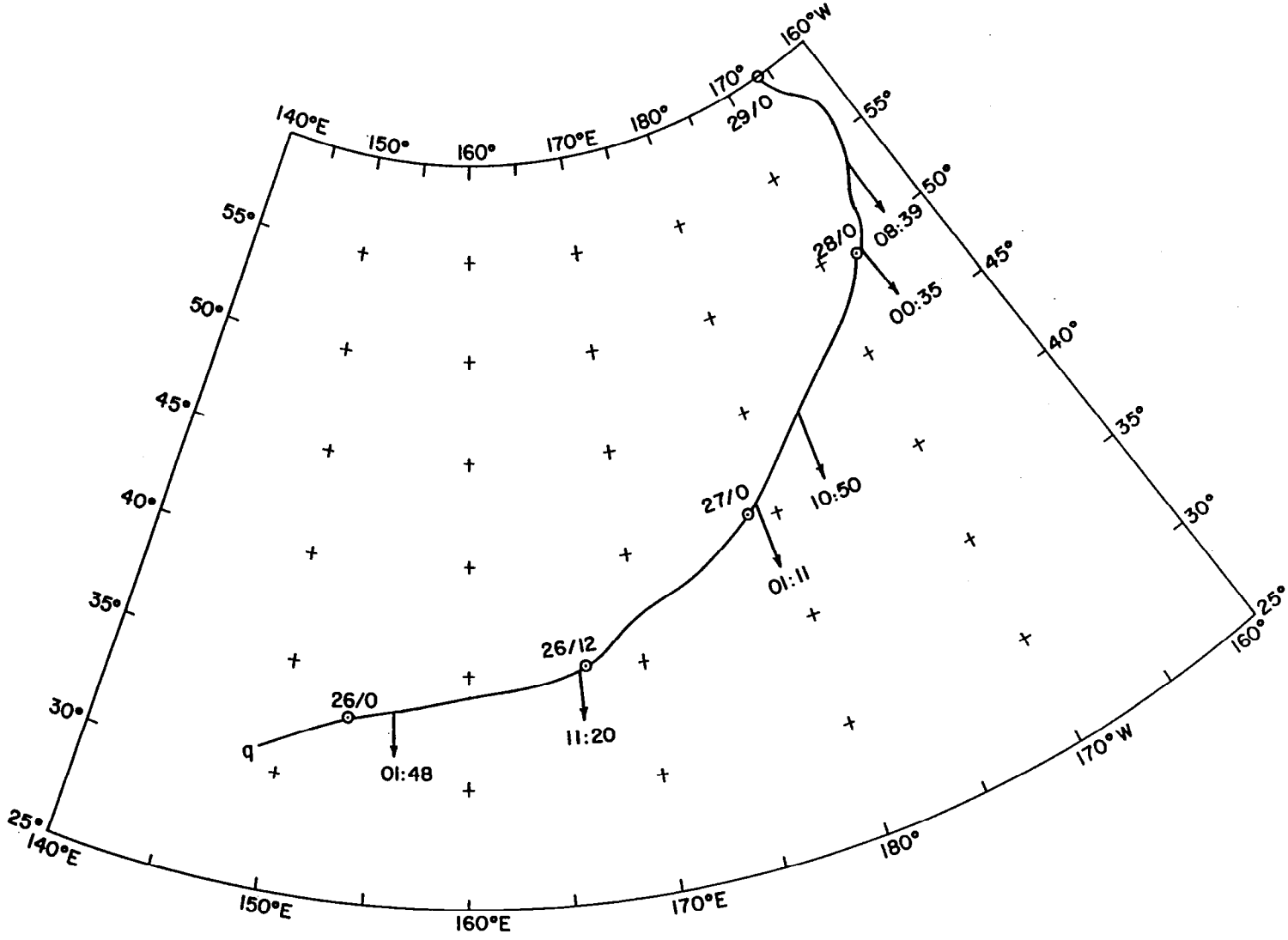

FIGURE 4(e) Cyclone Track Showing 12-Hour Positions and SEASAT Sighting Times.
ID: q → Jan. 1981, Pacific 10

G. ERROR CALCULATION

A quantitative goal of this investigation is to estimate the 12-hour linear displacement error that arises when the ± 3 hour window is used. Satellite data are asynoptic and as a consequence, a low center can be "detected" by the spacecraft at any position and time along its swath. The low's position may not be necessarily picked up by the satellite at the synoptic time. On occasions, the low is picked up well in advance of the synoptic map time and put in one position. At other instances, it is picked up at the last part of the six hour cycle and put in a second position. Especially in data-sparse areas, for example, over the ocean, the speed of the low along its track is therefore a strong function of when the spacecraft passed over the low. As long as a low comes under the swath of the SASS it is interpreted as belonging to the nearest synoptic time. When this information is used in this manner, gross errors will be produced from one synoptic update time to another. These errors would then propagate into very gross errors in a computer based numerical weather prediction forecast.

Figure 5 displays a segment, AB, of an idealized cyclone track with the dates and 12-hour positions indicated. They are marked X. The triangles (Δ) mark the positions and times when the low is found in the SASS swath. An example of the error created by using the ± 3-hour assumption is demonstrated. Two successive 12-hour low center positions, C and D, given in terms of position (lat. and long.) and time (date of month and GMT), furnish an example of the "mapping" procedure.

Because of the ± 3-hour assumption, the mapping is accomplished in the following manner. The time element of the cyclone event is mapped into the nearest 6-hour synoptic time. There is, however, no compensatory adjustment for the location. In this example, the time element (2230GMT), the time when the low is "picked" up, is mapped into 0000GMT, and that for 1445GMT is mapped into 1200GMT. Since CD represents the true displacement, MN represents the fictitious displacement. With respect to SASS obtained low center positions, erroneous speeds can therefore be calculated from one synoptic update and verification time to another. These lows are seen as if their true positions coincide with that given by the SEASAT observations. In this model, a fictitious speed is calculated by dividing the fictitious displacement by the difference of the two adjacent synoptic times.

In the study the following values are calculated:

True speed (V_1), i.e. the ratio of the displacement of true low positions and the difference of the synoptic times between them;

Fictitious speed (V_2), i.e. the ratio of the displacement of two successive SEASAT sightings and the difference of the mapped synoptic times.

Another value of the true speed can be derived by calculating the ratio (V_3) of the displacement of two consecutive sightings and the difference of their times of sightings. Since cyclone centers can either accelerate or decelerate over time intervals of twelve hours, V_3 needs not necessarily equal V_1. Either should be a better estimate than V_2.

$|V_1 - V_2|$ is thus an absolute hourly displacement error in the movements of these lows. The simulation experiment was performed for 12-hour intervals so as to have a more appropriate comparison with the control data set which shows 12-hourly positions of low centers.

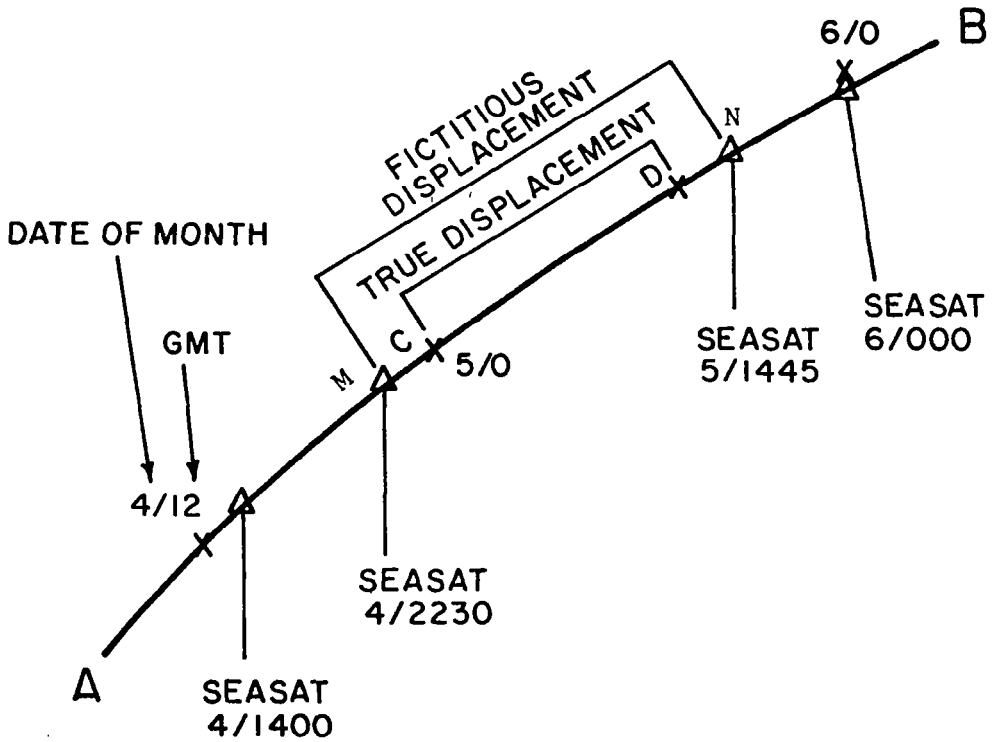

FIGURE 5 Segment of an idealized cyclone track showing "true positions" of low centers (marked X). The Δs are the SEASAT positions (subsatellite positions for closest approach abeam) when the low is somewhere in the swath. The dates and times of the occurrences are given.

H. DATA ASSIMILATION USING THE MODEL OF REPEAT ORBITS

The winds obtained by a scatterometer become available at different times during the orbits of the spacecraft. If the current practice, to group the data into 6-hour synoptic time blocks, is adhered to, discontinuities in the analysed meteorological fields can result. The following discussion explains this observation. The model of the repeat orbits (Figure 2b) over the Pacific displays at least four successive northbound or southbound orbits. Each of these orbits that begins at about 55° N and moves southward to the Equator (or starts at the Equator and moves northward) lasts for about 16 minutes. The four successive northbound orbits are about 100 minutes apart as they cross the Equator. A time interval of about 416 minutes (almost 7 hours) is required to receive a full data set for these four orbits. This data set thus belongs to at least two different synoptic blocks. The actual times of the observations, nothwithstanding, this data set must be partitioned into two different synoptic time zones. At the partitioning point it is observed that data that were once closely related in time (even as close as minutes) are now separated by a six-hour time gap. The partitioning thus creates a "time discontinuity" with respect to synoptic features. In all cases, except for a stationary meteorological pattern, the phenomenon of time discontinuity introduces an additional problem — the distortion of the "true" meteorological pattern.

This rearrangement of the data with respect to a time sequence allows the matching of data that are related in terms of position but are quite a mismatch in terms of time. Data at one particular point can be representative of the synoptic situation at time t_o while a neighboring point could be representative of another time t_1. t_o and t_1 can be as much as 6 hours apart. Especially for migratory cyclones, the synoptic pattern changes. A wind that was measured at a particular point many hours ago (up to six hours) is different from one that is measured at a much later time. A distortion of the meteorological feature must result. This effect is not only felt at the surface but also at the higher levels. Such diagrammatic representations of curvature, gradients and placement of low centers both at the surface and aloft are therefore not properly dealt with. When the analysed field of the wind, for example, is misrepresented, other associated fields, which depend upon it, are therefore erroneous. The fields of divergence and curl of the vector wind thus lose validity. We can also think of what can result when we try to infer vertical motion under the above described conditions.

The paths and low center positions shown in Figures 3 and 4 comprise the data set. In this study they are considered as ground "truths". As a low center can be picked up at any time along the known track, the highlights of the maps are the successively marked positions and times of the SEASAT sightings. These simulated positions are arrived at by using the graphs of the frozen orbits of Figures 2a and 2b. A simple linear interpolation scheme is applied as most sightings do not occur at 12-hour positions. The distance between two consecutive sightings is measured along the path rather than along the displacement from one point to another. When the path deviates from a straight line it is subdivided into smaller segments that approximate straight lines. In a west to east direction the distance can be found from the angular

difference $\Delta\lambda$ between two point on specifying the latitude. For example, the distance along a latitude circle can be measured by the following formula:

$$D = \kappa(\cos\psi)\Delta\lambda \quad \text{where}$$

$\kappa = 2\pi a/360$; a is the radius of the Earth. When the radius has an average value of 6370 km., κ = 111 km.

As the paths of these cyclones are rather erratic and their true speeds are not constant, an irregular pattern of sighting develops. Due to "dwell" the cyclones in the vicinity of latitude 60° N in both oceans are sampled more frequently on an areal basis. The drawn arrows (shown in Fig. 3 and 4) intersect the cyclones paths where the satellite observations are made. The sighting times are marked at the end of each arrow. Table (2) is a tabulation of sighting statistics. There are 84 sightings for the Atlantic as opposed to 81 for the Pacific. The greater number of sightings for the Atlantic is a result of dwell. In the Atlantic, the dwell phenomenon accounts for the greatly increased number of sightings for cyclones e and g. Respectively 26 and 22 sightings are recorded for the two cyclones. In the Pacific the highest number of sightings recorded is twelve and this is associated with cyclone n. The cyclone duration refers to the number of days and hours for which 12-hour positions are reported. Pertinent to this discussion is the duration of the cyclone over ocean areas. The duration time ends (a) when the cyclone fills and becomes nonexistent, (b) when the cyclone reaches a land area, and (c) when in most cases, the path goes beyond the northern extent of the study maps (see Figures 3 and 4).

For this data set an average duration time for the Atlantic cyclones is 4.4 days with a standard deviation of 1.4 days. That for the Pacific is 4.6 days with standard deviation of 1.6 days. The average durations for both ocean are, more or less, equal. For the Pacific, where the absence of dwell is observed, there is an average of 8.5 sightings per cyclone. The relatively small standard deviation of 2.8 sightings for the Pacific is compared with a standard deviation of 8.9 sightings for the Atlantic (average = 11.6 sightings). The average for the Atlantic is rather unstable. A more representative average for that area is masked by the occurences of dwell.

TABLE 2: A TABULATION OF CYCLONE DURATION AND THE FREQUENCY OF SEASAT SIGHTINGS FOR BOTH OCEANS.

OCEAN AREA	CYCLONE ID	CYCLONE DURATION (DAYS AND HOURS)		No. OF SIGHTINGS
Atlantic	a	3		6
Atlantic	b	4	12	9
Atlantic	c	3	12	4
Atlantic	d	5		10
Atlantic	e	6	12	26*
Atlantic	f	2	18	4
Atlantic	g	5	12	22*
Pacific	h	7		11
Pacific	i	7	12	13
Pacific	j	2	12	5
Pacific	k	4	12	6
Pacific	l	4		9
Pacific	m	4	12	9
Pacific	n	4	12	12
Pacific	o	4		6
Pacific	p	4		8
Pacific	q	3		6

* High number of sightings is due to dwell.

TABLES 3(a) THROUGH 3(q):

Cyclone analysis data showing times and positions of low centers of surface "truth" with associated simulated SEASAT "sightings" (time, position, orbit No.). The true speed (V_1), fictitious speed (V_2), and (V_3), the speed as a function of two consecutive sightings, are also tabulated.

Note: Cyclones are identified according to the month, year and geographical position.

TABLE 3(a): Dec. 1980; Atlantic 1.

DATE	TRUE			SEASAT				SYNOPTIC GROUPING (GMT)	V_1		V_2		V_3	$\lvert V_1-V_2 \rvert$	12hr-DE
	TIME	LAT	LONG	LAT	LONG	ORBIT No.	TIME		(Km/hr)	(Mi/hr)	(Km/hr)	(Mi/hr)	(Km/hr)	(Km/hr)	(Km)
05(2)	1200	42.8N	58.9W	42.8N	58.0W	25	16:49	1800							
							(09:37)		19.1	10.3	36.9	19.9	23.0	17.8	213.5
06(3)	0000	42.8N	56.4N	43.2N	55.5W	31	02:26	0000							
							(13:49)		48.0	25.9	38.2	20.6	49.7	9.8	117.9
	1200	45.7N	52.0W	48.0N	51.8W	39	16:15	1800							
							(09:40)		63.0	34.0	87.1	47.0	54.1	24.1	289.1
07(1)	0000	51.5N	47.6W	51.6N	46.9W	2	01:55	0000							
							(13:43)		48.4	26.1	43.9	23.7	57.6	4.4	53.4
	1200	56.9N	42.0W	57.9N	41.0W	10	15:38	1800							
							(08:08)		43.7	23.6	47.3	25.5	34.8	3.4	42.3
08(2)	0000	59.5N	38.0W	59.4N	38.2W	15	23:46	0000							

TABLE 3 (b): Dec. 1980; Atlantic 2.

DATE	TRUE			SEASAT				SYNOPTIC GROUPING (GMT)	V_1		V_2		V_3	$\lvert V_1-V_2 \rvert$	12hr-DE
	TIME	LAT	LONG	LAT	LONG	ORBIT No.	TIME		(Km/hr)	(Mi/hr)	(Km/hr)	(Mi/hr)	(Km/hr)	(Km/hr)	(Km)
7 (1)	0000	41.3N	53.0W	42.0N	53.0W	2	01:53	0000							
							(13:49)		33.4	18.0	26.7	14.4	34.8	6.7	80.1
	1200	45.3N	50.3W	45.1N	49.2W	10	15:42	1800							
							(09:39)		15.9	8.6	31.9	17.2	19.8	15.9	191.3
8 (2)	0000	44.1N	48.2W	44.4N	47,3W	16	01:21	0000							
							(23:27)		32.8	17.7	31.5	17.0	32.2	1.3	15.6
9 (3)	0000	48.2N	39.7W	48.3N	39.5W	30	00:48	0000							
							(15:24)		45.6	24.6	34.7	18.7	40.6	10.9	131.2
	1800	53.3N	30.3W	52.2N	32.0W	39	16:12	1800							
							(08:04)		44.5	24.0	77.8	42.0	57.8	33.4	400.3
10 (1)	0000	55.5N	28.5W	55.8N	28.4W	1	00:16	0000							
							(15:20)		31.5	17.0	29.7	16.0	34.8	1.9	22.2
	1200	60.0N	26.0W	60.4N	26.1W	10	15:36	1800							
							(06:31)		10.0	5.4	10.0	5.4	9.3	0.0	0.0
11 (2)	0000	61.0N	27.0W	61.0N	26.5W	14	22.07	0000							
							(08:09)		10.0	5.4	13.9	7.5	10.0	3.9	46.7
				61.1N	27.0W	15	23:45	0000							

TABLE 3(c): Dec. 1980; Atlantic 3.

DATE	TRUE			SEASAT				SYNOPTIC GROUPING (GMT)	V_1		V_2		V_3	$\lvert V_1-V_2 \rvert$	12hr-DE
	TIME	LAT	LONG	LAT	LONG	ORBIT No.	TIME		(Km/hr)	(Mi/hr)	(Km/hr)	(Mi/hr)	(Km/hr)	(Km/hr)	(Km)
9 (3)	1800	39.6N	68.3W	39.6N	68.4W	40	17:56	1800							
							(45:14)		63.2	34.1	57.6	31.1	61.3	5.6	66.7
11 (2)	1200	42.3N	40.0W	44.0N	36.7W	24	15:10	1800							
							(23:18)		96.6	52.1	119.5	64.5	92.5	23.0	275.8
12 (3)	1200	54.7N	14.6W	56.0N	13.1W	38	14:28	1200							
							(08:08)		72.3	39.0	48.2	26.0	71.2	23.1	289.1
13 (1)	0000	61.3N	7.5W	60.5N	8.7W	43	22:36	0000							

TABLE 3(d): Dec. 1980; Atlantic 4.

DATE	TRUE			SEASAT				SYNOPTIC GROUPING (GMT)	V_1		V_2		V_3	$\lvert V_1-V_2 \rvert$	12hr-DE
	TIME	LAT	LONG	LAT	LONG	ORBIT No.	TIME		(Km/hr)	(Mi/hr)	(Km/hr)	(Mi/hr)	(Km/hr)	(Km/hr)	(Km)
16(1)	1200	39.1N	72.1W	40.8N	70.0W	11	17:24	1800							
							(09:36)	0000	41.7	22.5	71.5	38.6	44.8	29.8	358.0
17(2)	0000	42.4N	67.5W	43.0N	65.9W	17	03:00	0600	48.2	26.0	35.8	19.3	44.8	12.4	149.0
							(13:48)		61.7	33.3	70.1	37.8	60.8	8.3	100.0
	1200	46.7N	62.0W	48.3N	58.4W	25	16:48	1800							
							(08:01)		74.1	40.0	95.6	51.6	71.5	21.5	258.0
18(3)	0000	52.5N	55.0W	52.6N	55.0W	30	00:49	0000							
							(15:23)		52.4	28.3	41.9	22.6	48.9	10.6	126.8
	1200	55.0N	51.0W	57.0N	46.0W	39	16:12	1800							
							(08:05)		96.7	52.2	126.8	68.4	94.0	30.0	360.3
19(1)	0000	59.3N	33.6W	59.3N	33.2W	1	00:17	0000							
							(15:19)		55.6	30.0	50.2	27.1	58.9	5.4	64.5
	1200	59.3N	19.0W	59.2N	17.3W	10	15:36	1800							
							(06:28)		66.2	35.7	59.1	31.9	54.9	7.0	84.5
20(2)	0000	57.5N	10.0W	58.0N	12.0W	14	22:04	0000							
							(15:20)		52.8	28.5	67.5	36.4	52.8	14.6	175.7
	1200	55.1N	0.5W	55.0N	0.4E	23	13:24	1200							
							(08:06)		36.0	19.4	26.9	14.5	39.8	9.1	109.0
21(3)	0000	54.0N	5.7E	54.1N	4.9E	28	21:30	0000							

TABLE 3(e): JAN. 1981, Atlantic 5.

DATE	TRUE			SEASAT				SYNOPTIC GROUPING (GMT)	V_1		V_2		V_3	$\lvert V_1-V_2 \rvert$	12hr-DE
	TIME	LAT	LONG	LAT	LONG	ORBIT No.	TIME		(Km/hr)	(Mi/hr)	(Km/hr)	(Mi/hr)	(Km/hr)	(Km/hr)	(Km)
15(3)	1800	38.0N	73.1W	38.0N	73.1W	40	17:57	1800							
							(09:36)		84.3	45.5	67.8	36.6	84.7	16.5	197.9
16(1)	0000	39.9N	67.8W	41.5N	65.0W	3	03:33	0600							
							(13:48)		86.4	46.6	96.7	52.2	84.1	10.4	124.5
	1200	43.6N	58.9W	47.0N	53.0N	11	17:21	1800							
							(08:02)		79.7	43.0	103.8	56.0	77.5	24.1	289.1
17(2)	0000	50.8N	48.4W	51.5N	47.7W	16	01:23	0000							
							(15:20)		64.1	34.6	54.3	29.3	63.8	9.8	117.9
	1200	54.4N	40.0W	56.5N	35.0W	25	16:43	1800							
							(06:28)		45.4	24.5	52.8	28.5	48.9	7.4	89.0
18(3)	0000	57.4N	29.4W	57.3N	30.0W	29	23:11	0000							
							(15:13)		60.0	32.4	68.6	37.0	54.1	8.5	102.3
	1200	60.0N	17.7W	60.5N	17.0W	38	14:24	1200							
							(01:44)		54.3	29.3	18.9	10.2	65.2	35.4	424.8
	1800	62.2N	14.3W	61.6N	15.4W	39	16:08	1800							
							(06:36)		54.3	29.3	55.2	29.8	50.2	0.9	11.1
				62.8N	12.7W	42	21:00	1800							
							(06:36)		46.9	25.3	27.6	14.9	50.2	19.3	231.3
				62.8N	12.7W	42	21:00	0000							
							(1:39)		14.3	7.7	27.2	14.7	19.3	13.0	155.7
19(1)	0000	63.0N	10.0W	63.1N	11.3W	43	22.39	0000							
							(15:17)		14.3	7.7	20.9	11.3	16.5	6.7	80.1
	1200	64.3N	8.0W	64.4N	7.4W	9	13:56	1200							
							(08:09)		18.0	9.7	13.3	7.2	19.8	4.6	55.6
							22:05	0000							

TABLE 3 (f): Jan. 1981; ATLANTIC 6

DATE	TRUE			SEASAT				SYNOPTIC GROUPING (GMT)	V_1		V_2		V_3	$\lvert V_1-V_2 \rvert$	12hr-DE
	TIME	LAT	LONG	LAT	LONG	ORBIT No.	TIME		(Km/hr)	(Mi/hr)	(Km/hr)	(Mi/hr)	(Km/hr)	(Km/hr)	(Km)
16(1)	0000	25.1N	63.9W	25.8N	62.0W	3	03:28	0600							
							(12:18)		64.5	34.8	63.2	34.1	61.7	1.3	15.6
	1200	28.0N	57.5W	29.4N	55.3W	10	15:46	1800							
							(33:01)		74.1	40.0	81.4	43.9	73.9	7.2	86.7
18(3)	0000	46.6N	39.8W	47.1W	39.3W	30	00:47	0000							
							(13:45)		68.6	37.0	92.1	49.7	80.2	23.5	282.4
	1200	50.1N	30.3W	51.0N	25.4W	38	14:32	1200							

TABLE 3 (g): JAN. 1981; Atlantic 7.

DATE	TRUE			SEASAT				SYNOPTIC GROUPING (GMT)	V_1		V_2		V_3	$\lvert V_1-V_2 \rvert$	12hr-DE
	TIME	LAT	LONG	LAT	LONG	ORBIT No.	TIME		(Km/hr)	(Mi/hr)	(Km/hr)	(Mi/hr)	(Km/hr)	(Km/hr)	(Km)
29(2)	1800	41.9N	68.4W	42.0N	65.5W	25	16:50	1800							
							(09:36)		114.0	61.5	139.2	75.1	87.3	25.2	302.4
30(3)	0000	39.3N	61.8W	39.3N	60.8W	31	02:26	0000							
							(13:49)		45.8	24.7	35.4	19.1	46.1	10.4	124.5
	1200	40.3N	56.1W	41.6N	53.9W	39	16:15	1800							
							(09:38)		61.9	33.4	109.5	59.1	68.2	47.6	571.5
31(1)	0000	44.5N	49.8W	45.6N	48.0W	2	01:53	0000							
							(13:46)		74.9	40.4	58.7	31.7	76.7	16.1	193.5
	1200	52.0N	40.0W	53.1N	39.4W	10	15:39	1800							
							(08:06)		40.8	22.0	51.9	28.0	38.4	11.1	133.4
01(2)	0000	56.3N	38.3W	56.1N	38.3W	15	23:45	0000							
							(16:57)		47.6	25.7	45.8	24.7	48.6	1.9	22.2
	1200	62.0N	38.0W	63.2N	36.3W	25	16:42	1800							
							(1:39)		47.6	25.7	48.7	26.3	47.3	1.1	13.3
		62.0N	38.0W	63.7N	36.0W	26	18:21	1800							
02(3)	0000	64.7N	32.0W	64.4N	33.4W	28	21:35	0000							
							(04:52)		41.9	22.6	32.1	17.3	39.5	9.8	117.9
		64.7N	32.0W	64.5N	32.2W	29	23:13	0000							
							(15:16)		48.9	26.4	61.5	33.2	48.4	12.6	151.2
	1200	64.7N	19.5W	64.9N	17.3W	38	14:29	1200							
				65.0N	15.7W	39	16:08	1800							

TABLE 3 (g): JAN. 1981; Atlantic 7. (Cont'd).

DATE	TRUE			SEASAT				SYNOPTIC GROUPING (GMT)	V_1		V_2		V_3	$\lvert V_1-V_2 \rvert$	12hr-DE
	TIME	LAT	LONG	LAT	LONG	ORBIT No.	TIME		(Km/hr)	(Mi/hr)	(Km/hr)	(Mi/hr)	(Km/hr)	(Km/hr)	(Km)
02	1200	64.7N	19.5W	64.9N	17.3W	38	14:29	1200							
				65.0N	15.7W	39	16:08	1800							
	1800	65.1N	14.2W	65.0W	14.3	40	17:45	1800							
				65.3N	13.0W	41	19:23	1800							
				65.7N	11.6W	42	21:01	1800							
							(08:10)		41.0	22.1	27.2	14.7	40.0	13.7	164.6
				65.7N	10.4W	43	22.39	0000							
							(15:16)		54.1	29.2	63.0	34.0	49.5	8.9	106.7
03(1)	1200	66.5N	4.7E	66.6N	5.8E	9	13:55	1200							
						10	15:32	1800							
						11	17:13	1800							
						12	18:48	1800							
						13	20:29	1800							
							(08:12)		16.7	9.0	11.1	6.0	16.3	5.6	66.7
04(2)	0000	66.9N	8.6E			14	22:07	0000							

TABLE 3(h): Dec. 1980; Pacific 1.

DATE	TRUE			SEASAT				SYNOPTIC GROUPING (GMT)	V_1		V_2		V_3	$\lvert V_1-V_2 \rvert$	12hr-DE
	TIME	LAT	LONG	LAT	LONG	ORBIT No.	TIME		(Km/hr)	(Mi/hr)	(Km/hr)	(Mi/hr)	(Km/hr)	(Km/hr)	(Km)
3 (3)	0000	35.8N	166.8E	36.0N	167.5E	30	01:14	0000							
							(23:27)		53.9	29.1	52.1	28.1	53.4	1.9	22.2
4 (1)	0000	31.0N	177.6E	30.9N	177.8E	1	00:41	0000							
							(23:28)		48.9	26.4	48.4	26.1	49.5	0.6	6.7
5 (2)	0000	27.6N	171.2W	27.6N	171.2W	15	00:09	0000							
							(09:32)		65.0	35.1	50.0	27.0	63.0	15.0	180.1
	0600	30.0N	168.5W	31.7N	166.8W	21	09:41	1200							
							(13:50)		83.4	45.0	84.3	45.5	79.5	0.9	11.1
6 (3)	0000	40.7N	161.1W	40.3N	161.4W	29	23:31	0000							
							(09:39)		124.0	66.9	90.8	49.0	112.9	33.2	398.1
	1200	48.8N	169.8W	49.6N	162.4W	35	09:10	1200							
							(15:26)								
7 (1)	0000	48.0N	173.6W	48.0N	174.0W	1	00:36	0000							
							(9:40)		20.8	11.2	13.9	7.5	17.2	6.9	82.3
	1200	46.5N	172.0W	46.8N	173.0W	7	10:16	1200							
							(13:47)		31.3	16.9	36.0	19.4	31.9	4.6	55.6
8 (2)	0000	49.9N	168.1W	49.1N	168.1W	15	00:03	0000							
							(9:40)		28.9	15.6	23.4	12.6	29.1	5.6	66.7
	1200	49.0N	165.0W	48.2N	165.4W	21	09:43	1200							
							(15:24)		18.2	9.8	27.8	15.0	21.7	9.6	115.6
9 (3)	0000	50.2N	166.5W	50.0N	167.5W	30	01:07	0000							

TABLE 3(i): Dec. 1980; PACIFIC 2.

DATE	TRUE			SEASAT				SYNOPTIC GROUPING (GMT)	V_1		V_2		V_3	$\lvert V_1-V_2 \rvert$	12hr-DE
	TIME	LAT	LONG	LAT	LONG	ORBIT No.	TIME		(Km/hr)	(Mi/hr)	(Km/hr)	(Mi/hr)	(Km/hr)	(Km/hr)	(Km)
10 (1)	1200	41.0N	156.8E	41.0N	156.7E	8	11:56	1200							
							(13:50)		22.4	12.1	25.2	13.6	21.9	2.8	33.4
11 (2)	0000	41.0N	160.0E	41.1N	160.5E	16	01:46	0000							
							(09:37)		26.1	14.1	18.5	10.0	23.2	7.6	91.2
	1200	42.0N	163.4E	42.0N	163.0E	22	11:23	1200							
							(13:49)		80.4	43.4	86.7	46.8	75.2	6.3	75.6
12 (3)	0000	39.5N	174.0E	39.4N	174.7E	30	01:12	0000							
							(09:35)		55.2	29.8	46.0	24.8	57.6	9.3	111.2
	1200	36.4N	179.8W	36.9N	179.7W	36	10:47	1200							
							(13:52)		52.8	28.5	60.0	32.4	52.1	7.2	86.7
13 (1)	0000	36.9N	172.6W	37.0N	172.4W	1	00:39	0000							
							(09:35)		34.3	18.5	28.7	15.5	36.0	5.6	66.7
	1200	39.7N	170.0W	39.5W	170.7W	7	10:14	1200							
							(13:52)		34.5	18.6	40.8	22.0	35.2	6.3	75.6
14 (2)	0000	37.9N	166.0W	37.9N	166.0W	15	00:06	0000							
							(09:34)		30.9	16.7	22.8	12.3	28.5	8.2	97.8
	1200	37.0N	161.5W	37.0N	162.8W	21	09:40	1200							
							(13:52)		18.5	10.0	24.8	13.4	21.5	6.3	75.8
15 (3)	0000	35.7N	159.7W	35.7N	159.9W	29	23:33	0000							
							(09:34)		26.3	14.2	20.4	11.0	25.6	5.9	71.2
	1200	35.2N	156.5W	35.2N	157.3W	35	09:07	1200							
							(13:52)		39.8	21.5	40.6	21.9	35.2	0.7	8.9
16 (1)	0000	37.1N	151.9W	36.9N	152.0W	43	22:59	0000							
							(09:35)		43.6	23.5	35.2	19.0	44.1	8.3	100.1
	1200	41.0N	148.0W	39.5N	149.0W	6	08:34	1200							

TABLE 3(j): Dec. 1980; Pacific 3.

DATE	TRUE			SEASAT				SYNOPTIC	V_1		V_2		V_3	$\lvert V_1-V_2 \rvert$	12hr-DE
	TIME	LAT	LONG	LAT	LONG	ORBIT No.	TIME	GROUPING (GMT)	(Km/hr)	(Mi/hr)	(Km/hr)	(Mi/hr)	(Km/hr)	(Km/hr)	(Km)
16 (1)	1200	46.4N	179.0E	46.0N	178.2E	7	10:17	1200							
							(15:25)		56.7	30.6	69.5	37.5	54.1	12.8	153.4
17 (2)	0000	51.4N	175.0E	52.0N	174.1E	16	01:42	0000							
							(09:44)		51.9	28.0	40.8	22.0	50.2	11.1	133.4
	1200	54.4N	167.5E	54.4N	167.9E	22	11:26	1200							
							(15:22)		26.5	14.3	37.2	20.1	29.1	10.7	129.0
18 (3)	0000	55.5N	162.5E	55.7N	161.4E	31	02:48	0000							
							(08:06)		25.6	13.8	17.8	9.6	26.3	7.8	93.4
	1200	56.3N	158.1E	56.2N	158.5E	36	10:54	1200							

TABLE 3(k): Dec. 1980; Pacific 4.

DATE	TRUE			SEASAT				SYNOPTIC GROUPING (GMT)	V_1		V_2		V_3	$\lvert V_1-V_2 \rvert$	12hr-DE
	TIME	LAT	LONG	LAT	LONG	ORBIT No.	TIME		(Km/hr)	(Mi/hr)	(Km/hr)	(Mi/hr)	(Km/hr)	(Km/hr)	(Km)
26 (2)	1200	36.0N	146.7E	36.1N	147.6E	23	13:01	1200							
							(13:51)		71.0	38.3	75.2	40.6	65.2	4.2	51.0
27 (3)	0000	38.5N	155.7E	38.6N	157.0E	31	02:52	0000							
							(23:26)		40.4	21.8	41.7	22.5	42.6	1.3	15.6
28 (1)	0000	40.6N	166.0E	40.6N	167.4E	2	02:18	0000							
							(23:26)		48.9	26.4	41.0	22.1	41.9	8.0	95.6
29 (2)	0000	44.8N	178.3E	44.8N	178.5E	16	01:44	0000							
							(23:26)		21.7	11.7	22.1	11.9	22.6	0.4	4.4
30 (3)	0000	44.3N	174.9W	44.4N	174.6W	30	01:10	0000							
							(23:27)		27.6	14.9	28.0	15.1	28.7	0.4	4.4
31 (1)	0000	44.7N	166.3W	44.7N	166.2W	1	00:37	0000							

TABLE 3(1): Dec. 1980; Pacific 5.

DATE	TRUE			SEASAT				SYNOPTIC GROUPING (GMT)	V_1		V_2		V_3	$\lvert V_1-V_2 \rvert$	12hr-DE
	TIME	LAT	LONG	LAT	LONG	ORBIT No.	TIME		(Km/hr)	(Mi/hr)	(Km/hr)	(Mi/hr)	(Km/hr)	(Km/hr)	(Km)
23 (2)	1200	34.0N	140.0E	34.0N	140.3E	23	13:01	1200							
							(13:52)		34.3	18.5	41.5	22.4	36.0	7.2	86.7
24 (3)	0000	35.8N	143.5E	36.7N	144.2E	31	02:53	0000							
							(09:37)		27.8	15.0	18.5	10.0	23.1	9.3	111.2
	1200	38.0N	146.0E	38.0N	146.2E	37	12:30	1200							
							(13:49)		51.0	27.5	55.2	29.8	48.0	4.3	51.1
25 (1)	0000	39.0N	152.5E	39.4N	153.4E	2	02:19	0000							
							(09:37)		42.6	23.0	34.7	18.7	43.4	8.0	95.6
	1200	41.6N	157.1E	41.6N	157.1E	8	11:56	1200							
							(13:49)		77.1	41.6	84.5	45.6	73.4	7.4	89.0
26 (2)	0000	42.8N	166.6E	42.8N	167.4E	16	01:45	0000							
							(09:38)		30.6	16.5	28.0	15.1	34.8	2.6	31.1
	1200	42.5N	172.0E	42.5N	171.7E	22	11:23	1200							
							(13:48)		48.2	26.0	55.2	29.8	48.0	7.0	84.5
27 (3)	0000	41.4N	179.0E	41.4N	179.4E	30	01:11	0000							
							(09:37)		29.8	16.1	22.8	12.3	28.5	7.0	84.5
	1200	42.0N	176.9W	41.9N	177.2W	36	10:48	1200							

TABLE 3(m): Jan. 1981; Pacific 6.

DATE	TRUE			SEASAT				SYNOPTIC GROUPING (GMT)	V_1		V_2		V_3	$\lvert V_1-V_2 \rvert$	12hr-DE
	TIME	LAT	LONG	LAT	LONG	ORBIT No.	TIME		(Km/hr)	(Mi/hr)	(Km/hr)	(Mi/hr)	(Km/hr)	(Km/hr)	(Km)
2 (2)	0000	37.5N	142.0E	39.0N	143.0E	17	03:26	0600							
							(09:36)		41.1	22.2	76.9	41.5	48.0	35.8	429.2
	1200	40.0N	147.1E	40.0N	147.7E	23	13:02	1200							
							(13:50)		60.6	32.7	71.5	38.6	62.1	10.9	131.2
3 (3)	0000	41.4N	155.3E	42.0N	157.3E	31	02:52	0000							
							(23:25)		51.3	27.7	46.5	25.1	47.6	4.8	57.8
4 (1)	0000	45.6N	168.0E	46.2N	168.2E	2	02:17	0000							
							(08:01)		39.7	21.4	14.4	26.7	39.8	13.0	155.7
	0600	46.9N	170.0E	47.4N	172.4E	7	10:18	1200							
							(15:24)		41.5	22.4	59.7	32.2	46.5	18.2	217.9
5 (2)	0000	49.9N	178.9E	51.0N	180.0E	16	01:42	0000							
							(08:03)		44.3	23.9	29.1	15.7	43.4	15.2	182.4
	0600	52.0N	176.5W	52.5N	178.0W	21	09:45	1200							
							(15:23)		22.6	12.2	30.9	16.7	24.1	8.3	100.1
6 (3)	0000	53.7N	178.3E	54.0N	178.8E	30	01:08	0000							
							(08:06)		21.7	11.7	13.2	7.1	19.3	8.5	102.3
	0600	54.1N	179.3E	55.0N	178.1W	35	09:14	1200							

TABLE 3(n): JAN. 1981; Pacific 7.

DATE	TRUE			SEASAT				SYNOPTIC	V_1		V_2		V_3	$\lvert V_1-V_2 \rvert$	12hr-DE
	TIME	LAT	LONG	LAT	LONG	ORBIT No.	TIME	GROUPING (GMT)	(Km/hr)	(Mi/hr)	(Km/hr)	(Mi/hr)	(Km/hr)	(Km/hr)	(Km)
5 (2)	0000	42.8N	173.7E	42.6N	175.7E	16	01:45	0000							
							(09:38)		67.6	36.5	53.4	28.8	66.3	14.3	171.2
	1200	42.7N	176.0W	42.9N	176.3W	22	11:23	1200							
							(21:47)		67.8	36.6	62.5	33.7	68.9	5.4	64.5
6 (3)	0600	47.0N	161.9W	48.0N	159.7W	35	09:10	1200							
							(15:24)		54.5	29.4	72.5	39.1	56.5	18.0	215.7
7 (1)	0000	52.7N	157.0W	53.0N	157.5W	1	00:34	0000							
							(08:05)		57.1	30.8	79.7	43.0	59.1	22.6	271.3
	0600	54.8N	160.9W	56.0W	163.6W	6	08:39	0600							
							(17:00)		39.5	21.3	31.7	17.1	33.5	7.8	93.4
8 (2)	0000	59.3N	169.0W	59.7N	169.6W	16	01:39	0000							
							(06:30)		29.7	16.0	30.0	16.2	27.8	0.4	4.4
	0600	60.7N	170.5W	61.0N	171.4W	20	08:09	0600							
							(01:38)		16.7	9.0	4.6	2.5	17.0	12.0	144.5
				61.4N	171.5W	21	09:47	1200							
							(15:19)		17.4	9.4	21.7	11.7	17.0	4.3	51.1
9 (3)	0000	62.5N	176.0W	62.1N	176.0W	30	01:06	0000							
				62.2N	176.5W	31	02:44	0000							
							(04:53)		17.0	9.2	15.2	8.2	18.7	1.9	22.2
	0600	62.5N	177.5W	62.7N	178.0W	34	07:37	0600							
							(08:09)		19.8	10.7	13.9	7.5	20.4	5.9	71.2
				62.9N	178.7W	35	09:15	1200							

TABLE 3(o): Jan. 1981; Pacific 8.

DATE	TRUE			SEASAT				SYNOPTIC	V_1		V_2		V_3	$\lvert V_1-V_2 \rvert$	12hr-DE
	TIME	LAT	LONG	LAT	LONG	ORBIT No.	TIME	GROUPING (GMT)	(Km/hr)	(Mi/hr)	(Km/hr)	(Mi/hr)	(Km/hr)	(Km/hr)	(Km)
15 (3)	1200	33.8N	135.7E	33.7N	136.3E	38	14:07	1200							
							(35:39)		62.3	33.6	62.6	33.8	63.2	0.4	4.5
17 (2)	0000	38.3N	159.6E	38.4N	160.8E	16	01:46	0000							
							(09:36)		44.7	24.1	36.0	19.4	45.0	8.7	104.5
	1200	39.1N	165.9E	39.3N	165.7E	22	11:22	1200							
							(13:49)		57.6	31.1	61.9	33.4	56.9	4.3	51.1
18 (3)	0000	39.9N	173.8E	40.0N	174.5E	30	01:11	0000							
							(09:37)		58.2	31.4	47.6	25.7	59.3	10.6	126.7
	1200	39.8N	178.0W	39.9N	178.6W	36	10:48	1200							
							(13:51)		53.6	28.9	58.6	31.6	50.8	5.0	60.0
19 (1)	0000	36.9N	172.0W	36.6N	171.8W	11	00:39	0000							

TABLE 3(p): Jan. 1981; Pacific 9.

DATE	TRUE			SEASAT				SYNOPTIC GROUPING (GMT)	V_1		V_2		V_3	$\lvert V_1-V_2 \rvert$	12hr-DE
	TIME	LAT	LONG	LAT	LONG	ORBIT No.	TIME		(Km/hr)	(Mi/hr)	(Km/hr)	(Mi/hr)	(Km/hr)	(Km/hr)	(Km)
20 (2)	1200	43.9N	143.1E	43.6N	144.0E	23	13:03	1200							
							(13:49)		47.4	25.6	55.6	30.0	48.2	8.2	97.8
21 (3)	0000	42.5N	150.1E.	42.4N	152.0E	31	02:52	0000							
							(09:37)		53.0	28.6	41.3	22.3	51.5	11.7	140.1
	1200	41.3N	158.6E	41.0N	158.0E	37	12:29	1200							
							(13:49)		35.0	18.9	41.3	22.3	35.8	6.3	75.6
22 (1)	0000	41.9N	162.5E	41.0N	164.0E	2	02:18	0000							
							(09:37)		48.2	26.0	38.5	20.8	48.0	9.6	115.6
	1200	41.4N	169.6E	41.4N	169.6E	8	11:55	1200							
							(13:48)		22.4	12.1	28.0	15.1	24.3	5.6	66.7
23 (2)	0000	40.8N	172.7E	40.9N	173.2E	16	01:43	0000							
							(09:39)		33.5	18.1	25.9	14.0	32.2	7.6	91.2
	1200	41.0N	177.4E	40.9N	177.3E	22	11:22	1200							
							(13:50)		57.8	31.2	68.4	36.9	59.3	10.6	126.8
24 (3)	0000	41.0N	174.0W	41.4N	173.4W	30	01:12	0000							

TABLE 3(q): Jan. 1981; Pacific 10.

DATE	TRUE			SEASAT				SYNOPTIC GROUPING (GMT)	V_1		V_2		V_3	$\lvert V_1-V_2 \rvert$	12hr-DE
	TIME	LAT	LONG	LAT	LONG	ORBIT No.	TIME		(Km/hr)	(Mi/hr)	(Km/hr)	(Mi/hr)	(Km/hr)	(Km/hr)	(Km)
26 (2)	0000	32.9N	153.4E	33.4N	156.3E	16	01:48	0000							
							(09:32)		105.3	56.8	79.1	42.7	99.7	26.1	313.6
	1200	35.0N	166.8E	35.0N	166.4E	22	11:20	1200							
							(13:51)		91.0	49.1	99.9	53.9	86.5	8.9	106.7
27 (3)	0000	40.2N	178,1E	40.5N	179.0E	30	01:11	0000							
							(09:39)		57.1	30.9	46.5	25.1	57.6	10.6	126.8
	1200	44.3N	175.7W	44.1N	176.2W	36	10:50	1200							
							(13:45)		72.5	39.1	81.0	43.7	70.6	8.5	102.3
28 (1)	0000	49.5N	167.2W	49.6N	166.8W	1	00:35	0000							
							(08:04)		60.0	32.4	84.5	45.6	62.8	24.5	293.5
	0600	52.2N	165.4W	53.6N	163.9W	6	08:39	0600							

I. A QUANTITATIVE DISCUSSION OF THE OUTCOME OF THE SIMULATION EXPERIMENT

Tables 3 (a) through 3 (q) give a detailed summary of the input data utilized in the simulation experiment, along with derived quantities that are measures of the error related to the use of the ± 3 hour window. The relevant input data are the conventional synoptic hours and the geographical position (lat. and long.) for the center of the cyclone, referred to as "TRUE". With the aid of Table 1, Figures 2a and 2b, the positions and times of SEASAT sightings are computed. The local orbit number and the synoptic grouping (the main synoptic time nearest the time of the SEASAT sighting) are also listed. In the other columns are shown derived quantities (already discussed) which relate to the displacement error. Since the input data comprise 12-hour positions of the cyclones, the error is calculated as a 12-hour displacement error (12-hr DE). The output data are then tabulated. Some elementary statistical properties of the data are investigated so that relevant conclusion can be drawn from the study.

The calculated errors are first classified in Table (4) to show a distribution of the 12-hr DE. A class interval of 50 km. ($\sim 1\frac{1}{2}^{o}$ of long.) is chosen. As a result, the data fall conveniently into 9 continuous classes with 0.05 km as the lowest class boundary. The one event of zero, a perfect correlation between V_1 and V_2, is not treated. At the other end, an extreme data point (571.5 km. $\sim 5^{o}$ of long.) is also left out as it is located in an interval 3 classes away from the upper boundary of the 9th.

In reality, 124 12-hour DEs with maximum error in the vicinity of 4^{o} of long. are considered. Column 6 (% CF^{*}) shows an "inverted" cumulative frequency. This representation, in addition to the accompanying ogive (see Fig. 6), is adopted so that the errors can be described in terms of "greater than" rather than "less than".

The grouped data are highlighted by a set of histograms (see Fig. 7) showing the distribution of the errors in both oceans and in each ocean. The mid points of the classes are shown on the horizontal axis while the % relative frequency is described on the vertical. The data are then subdivided into two categories. One classification is used to investigate errors for which V_1 is greater than V_2, i.e., for which the true speed of the cyclone is greater than the fictitious speed. The other category is the reversed condition ($V_1 < V_2$). A further condition is stipulated —— errors belong to classes 2 through 9. Statistics of the simulation experiment are summarized in Table 5.

A glance at Table (4) and Fig. (7 a), reveal clearly that while Class 2 (50.05 km to 100.05 km) contains the modal frequency for the total sample, the median and the mean are located in class 3, (100.05 km to 150.05 km). For the total sample, the average 12-hr DE is 123.5 km ($\sim 1.1^{o}$ of long.) and the standard deviation is 95.5 km. ($\sim .9^{o}$ of long.). A hump which comprises 6.5% of the data appears in the interval 250.05 to 300.05 km. Then an interesting observation is noted. While 16.1% of the data are of magnitude 50 km. or less, the same percentage accounts for all errors above 200 km ($\sim 2^{o}$ of long.). Thus about 68% of the errors have magnitudes between 50 and 200 km.

The individual ocean (see Fig. 7 b and 7 c) displays some characteristic differences. Considering the data (taken as a whole) for the Pacific Ocean, it is found that while the modal class remains unchanged, the frequency is

elevated (> 40%). The median shifts downwards to class 2. The mean which has a magnitude of 104.6 km. ($\sim 1^{o}$ of long.) is also shifted to the left. The standard deviation for this subset is 82 km ($\sim .7^{o}$ of long.). In terms of the Atlantic Ocean, class No. 3 remains the modal class but the median is shifted also to class 3, to the right. The average error of 150.6 km. ($\sim 1.4^{o}$ of long.) is also upshifted and falls just outside the upper boundary of class 3. The hump which appeared in the total data reappears in the Atlantic but this time the frequency is elevated. This signifies that the main contribution of the class-6 error (350.05 to 300.05 km) in the total data comes from the Atlantic. The standard deviation of the Atlantic data is 107.1 km ($\sim 1^{o}$ of long.).

Twenty events have errors $\leq$ 50 km. This subset has a mean of 20.0 km and a standard deviation of 13.5 km. For synoptic purposes, the data greater than 50 km. are investigated more fully. In this range, as is expected, all averages are shifted upwards and standard deviations moved downwards (see Table 5). In this category there are 104 data points (magnitude > 50 km). The overall average for these events is 143.5 km ($\sim 1.3^{o}$ of long.) and the standard deviation is 91.0 ($\sim 0.8^{o}$ of long.). With respect to the individual ocean, the average for the Atlantic is 174.2 km ($\sim 1.6^{o}$ of long.), and that for the Pacific is 122.4 km ($\sim 1.1^{o}$ of long.). The analyzed errors with their stipulated conditions (see Table 5) are presented in graphical form in Fig. (8) for easier scrutiny and comparison.

Results of the analysis of cyclone movement for both the Atlantic and the Pacific oceans disclose that Atlantic cyclones (within latitudes 30^{o} and 65^{o} N) move, on the average, about 14% faster than those in the Pacific. However, the variability of these average speeds is in general smaller for the Pacific (Std. Dev. = 21.2 km). This picture is duplicated in the case of 12-hr displacement errors. Whereas the average for the Atlantic is 150.6 km ($\sim 1.4^{o}$ of long.), it is only 104.6 km ($\sim 0.9^{o}$ of long.) for the Pacific. In this sample, the average error for the Atlantic is about 40% larger than that for the Pacific. Again, the Pacific displays errors that have smaller variability (Std. Dev. = 82.0 km $\sim 0.7^{o}$ of long.). When the smaller errors ($\leq$ 50 km) are excluded, the average Pacific error is increased by 17%. For the Atlantic this increase measures 15.6%. Thus when the larger errors of both oceans are compared, the magnitudes of those in the Atlantic are still 40% larger than those in the Pacific. This is again explained by the observation which shows that the Atlantic has a higher frequency of errors at its upper class intervals.

Comments are in order for the various conditions that have been applied to the data. The data points seem to be divided evenly between the $V_1 > V_2$ ($\sim$ 48.4%) and the $V_1 < V_2$ (51.6%) and also when the additional restriction (excluding errors $\leq$ 50 km.) is placed on these 2 categories. In this case the division is 51.0% and 49.0% respectively.

Considering the entire data set the average 12-hr DE is found to be 10% larger when $V_1 < V_2$. This number increases to 21% when the smaller errors are excluded (error $\leq$ 50 km.). When the data are partitioned on an oceanic basis, this trend continues in the Atlantic. The average errors are respectively 22% and 31% greater for $V_1 < V_2$. In the Pacific ocean the pattern is somewhat slightly reversed. When $V_1 > V_2$ (true speed > fictitious speed), the average 12-hr DE is 8% larger than its counterpart. But this dominance is reduced when only the bigger errors ($\geq$ 50 km) are considered. Another noticeable feature is that there exists less variability in the error data, even when the smaller errors are excluded, for the condition $V_1 > V_2$. This

is true both when the total data-set and also when subset of each ocean are considered.

CLASS No.	CLASS BOUNDARY	CLASS MIDPOINT	FREQUENCY	RF	% CF*
1	0.05 - 50.05	25.05	20	.161	100
2	50.05 - 100.05	75.05	41	.331	83.9
3	100.05 - 150.05	125.05	31	.250	50.8
4	150.05 - 200.05	175.05	12	.097	25.8
5	200.05 - 250.05	225.05	4	.032	16.1
6	250.05 - 300.05	275.05	8	.065	12.9
7	300.05 - 350.05	325.05	2	.016	6.4
8	350.05 - 400.05	375.05	3	.024	4.8
9	400.05 - 450.05	425.05	3	.024	2.4

TABLE 4 DISTRIBUTION OF 12HR- DISPLACEMENT ERRORS (KM).

TABLE 5 SUMMARY STATISTICS OF 12 HR-DE

AREA	CONDITION	No. OF EVENTS	V_1		12 HR-DE	
			MEAN	STD. DEV.	MEAN	STD. DEV.
Both Oceans		124	48.1	22.1	123.5	95.5
(Atlantic and	Excluding errors $\leq$ 50Km	104			143.8	91.0
Pacific)	$V_1 > V_2$	60			117.2	81.7
	$V_1 > V_2$ (errors $\geq$ 50Km)	53			130.3	78.0
	$V_1 < V_2$	64			129.5	107.0
	$V_1 < V_2$ (errors $\geq$ 50Km)	51			157.9	101.6
		51	51.7	23.0	150.6	107.1
Atlantic	Excluding errors $\leq$ 50KM	43			174.2	99.9
	$V_1 > V_2$	23	48.8	17.0	130.6	92.1
	$V_1 > V_2$ (errors $\geq$ 50 Km)	21			141.3	89.2
	$V_1 < V_2$	28	54.9	25.9	167.	117.1
	$V_1 < V_2$ (errors $\geq$ 50Km)	22			205.7	101.3
		73	45.5	21.2	104.6	82.0
Pacific	Excluding errors $\leq$ 50Km	61			122.4	78.0
	$V_1 > V_2$	37	47.1	20.2	108.9	74.9
	$V_1 > V_2$ (errors $\geq$ 50Km)	32			123.2	70.3
	$V_1 < V_2$	36	44.0	22.5	100.2	89.5
	$V_1 < V_2$ (errors $\geq$ 50 Km)	29			121.6	87.0

FIGURE 6 Ogive of 12-hr Displacement Errors (km).

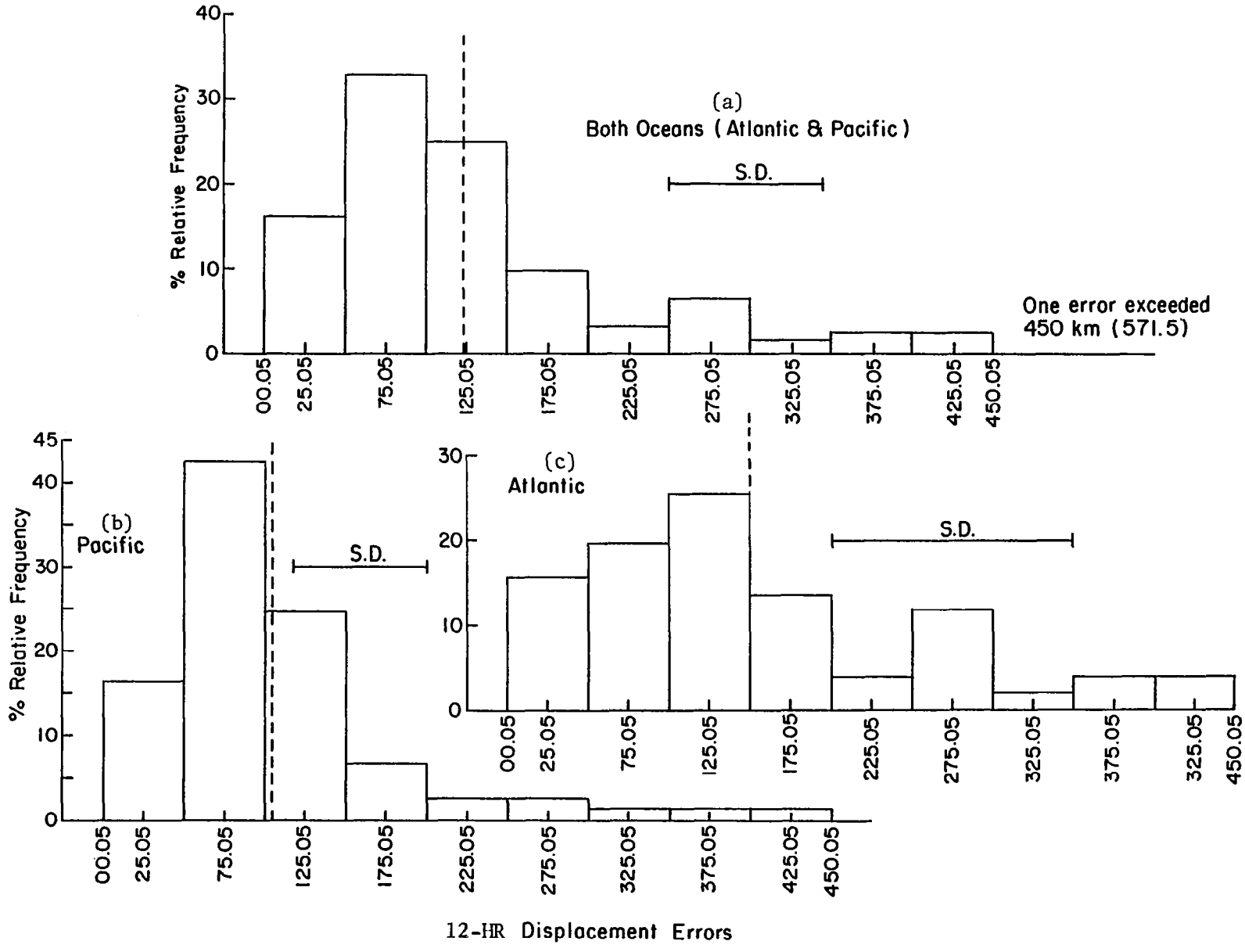

FIGURE 7 Hiatograms of 12-Hr Displacement Errors Showing Mean and Standard Deviation: (a) Both Oceans (Atlantic and Pacific), (b) Pacific Ocean and (c) Atlantic Ocean.

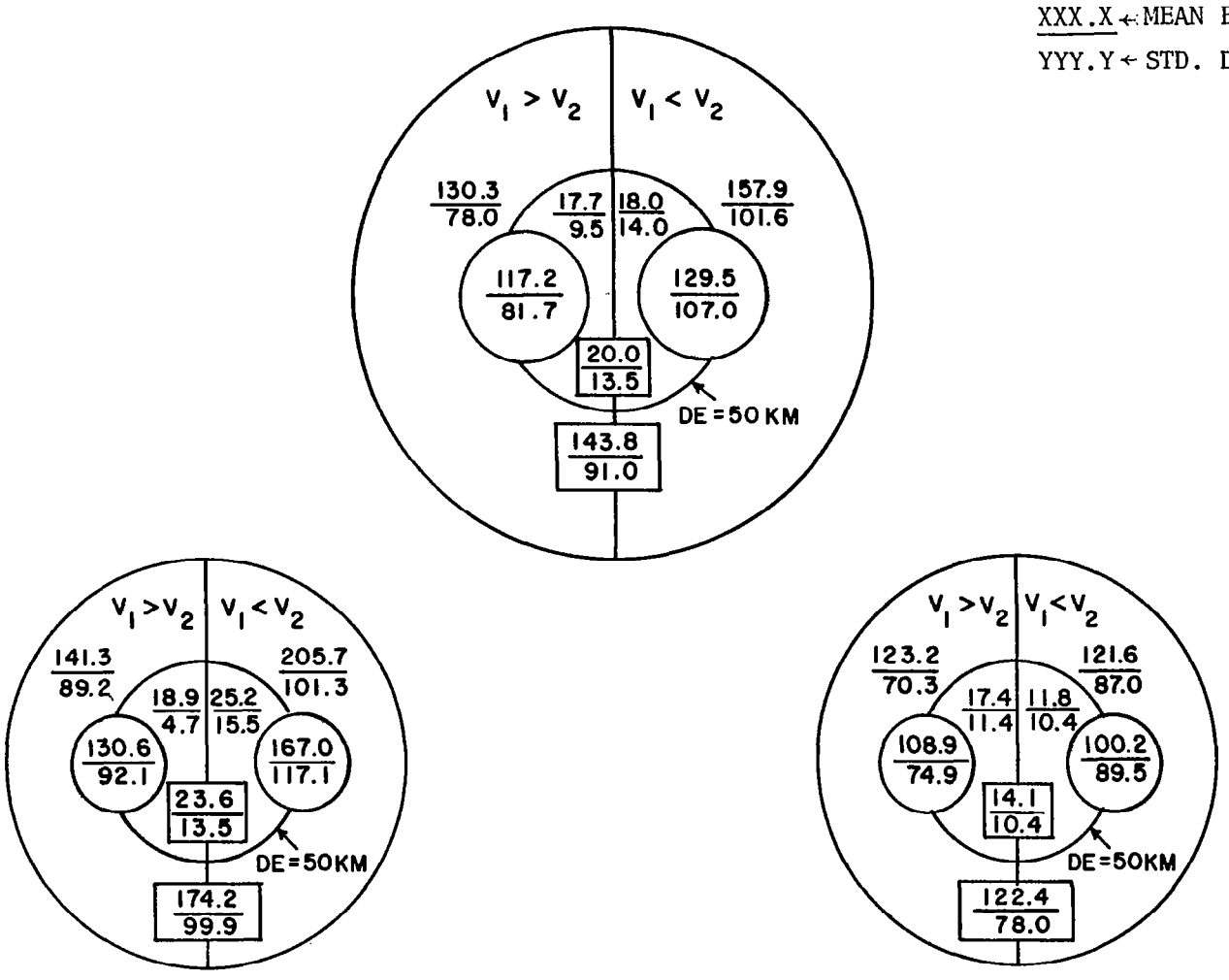

FIGURE 8 A Compact Graphical Form of Summary Statistics of Errors Given in Table 5.

J. THE SPECIAL ERROR PROBLEMS

Researchers who use the ± 3-hour window run the risk of compounding the problem even further when certain conditions exist. The areas of complication are seen in the following two cases.

1) The SEASAT sampling time is at an intermediate synoptic hour (i.e. at 0300, 0900, 1500, 2100z), and

2) the dwell situation is operative.

CASE 1 (Sampling at intermediate synoptic times)

This special case is highlighted in Figures (3a) and (3c). A triangle (Δ) marks the position of these occurrences. The data show samplings at 0300z (Atlantic, 4 d) and 2100z (Atlantic, 5e). The examples that follow are extracted from Table 3c and 3d. These errors are associated with SEASAT observations taken at an intermediate synoptic hour.

ID	SEASAT TIME	SYNOPTIC GROUPING	12-hr DE
Atlantic 4d	0300	0000	358.0
	0300	0600	149.0
Atlantic 5e	2100	1800	11.1
	2100	0000	231.3

They highlight the differences between the choices of the associated synoptic time. For cyclone Atlantic 4d, the difference between the two 12 hr-DEs is 209 km (∿ 2° long.). This represents a relative difference of 140%. The situation for Atlantic 5e is even more astonishing. Although the difference between the two quantities are 220 km (∿ 2° long.), the relative difference is almost 2000%. In the one case, the smaller error is associated with the later synoptic time (0300z mapped into 0600z) while in the other case, the smaller error is associated with the earlier synoptic time (2100z mapped into 1800z). These two examples point out that which ever choice of synoptic time is made for the mapping, the associated error is in the order of 2° of longitude. Superficially, one might think that an appropriate way to overcome this obstacle is to generate data fields for the intermediate hours (0300, 0900, 1500 and 2100). Certainly, the errors will be smaller. However, the economic feasibility aside, the problem of partitioning will still remain. This problem could be irradicated by utilizing a scheme that inserts the incoming data on a continuous real-time basis as discussed earlier.

CASE 2 (Increased number of samplings due to "dwell").

Good examples of the dwell phenomenon are furnished in Figs. 3c and 3e. Above about 58° N latitude, cyclones are sampled more frequently on an areal basis. In this area the cyclone can be picked up on as many as six consecutive passes of SEASAT. This situation ought to be a "blessing" rather than a "curse", since the best analysis relies on the maximum amount of good data. For example (see Fig. 2e), observations at 16:42z and 18:21z are associated with the 1800z synoptic hour of the first of the month; observations at 16:08z, 17:45z and 19:23z are associated with 1800z of the 2nd; and observations at 15:32z, 17:13z, 18:48z and 20:09z are also associated with 1800z of the 3rd. Logically the largest displacement errors will be associated with those sighting times that are farthest away from the main synoptic hour. Thus if the present criterion (± 3 hour window) is adhered to, the minimum error will be committed by selecting the observation nearest the synoptic hour. But all other observations are vital and should not be discarded. Locating the center of a cyclone every 100 minutes for synoptic purposes is a most desirable practice. As in the former case, the adoption of the continuous insertion technique to circumvent this dilemma is again suggested.

K. OTHER PERTINENT RESULTS OF THE SIMULATION EXPERIMENT

A difference may arise between the derived quantity V_3 and the true speed (V_1). Apart from the random errors accrued in measuring displacements, the added complexity of calculating distances traversed by a low center without a known pattern of acceleration and deceleration must be taken into consideration. The relative differences of V_1 and V_3 are, however, small. In any event, compared to V_2, these quantities are much better estimates of the true speed of the cyclone.

As was pointed out before, there is variability of the speed from event to event and the sighting times for these events also change. Thus V_1 and V_3 may not be the same. A distribution of the relative differences are shown in Fig. 9. The mean relative departure of V_3 from V_1 is 6.5% with a standard deviation of 5.8%. Fifty-seven percent of the sample has an average relative departure of less than 5% while seventy-seven percent of the total has an average of less than 10%.

Figure 10 depicts a 3-degree smoothed average of the speeds of low centers and the 12-hr DE plotted against a common horizontal axis of latitude between 35° N and 65° N. As is expected, the graph for speed shows an oscillation about the average (48.1 km/hr) for the whole sample. Peaks are located in the vicinity of 38° N, 47° N, 52° N and 58° N. A maximum of about 58.5 km/hr is found at 58° N. Valleys are found near 42° N, 50° N, 54° N and 62° N. The deepest valley (minimum) with a value of 30 km/hr is situated near 60° N. There is thus the suggestion that the greatest variability in cyclone speed is found in the region above 50° N.

In the case of the 12-hr DE, the graph shows ridges near 40° N, 44° N and 48° N. The largest of these averages (200 km) is located about 48° N. Two pronounced minima of magnitude (80 km) are situated near 46° N and 62° N. A third relative minimum is located at 42° N. A plateau is also found between 50° N and 56° N. The strong correlation between the pronounced minimum for the average cyclone speed and the average 12-hr DE near 62° N is easily seen.

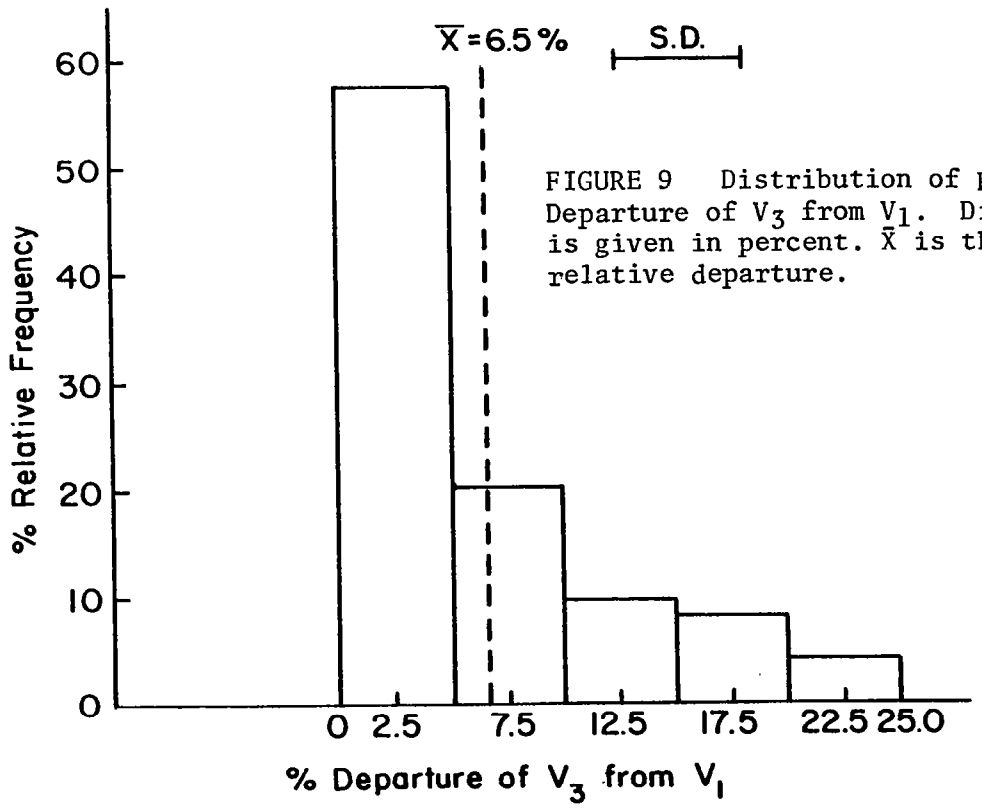

FIGURE 9 Distribution of Relative Departure of V_3 from V_1. Difference is given in percent. $\bar{X}$ is the mean relative departure.

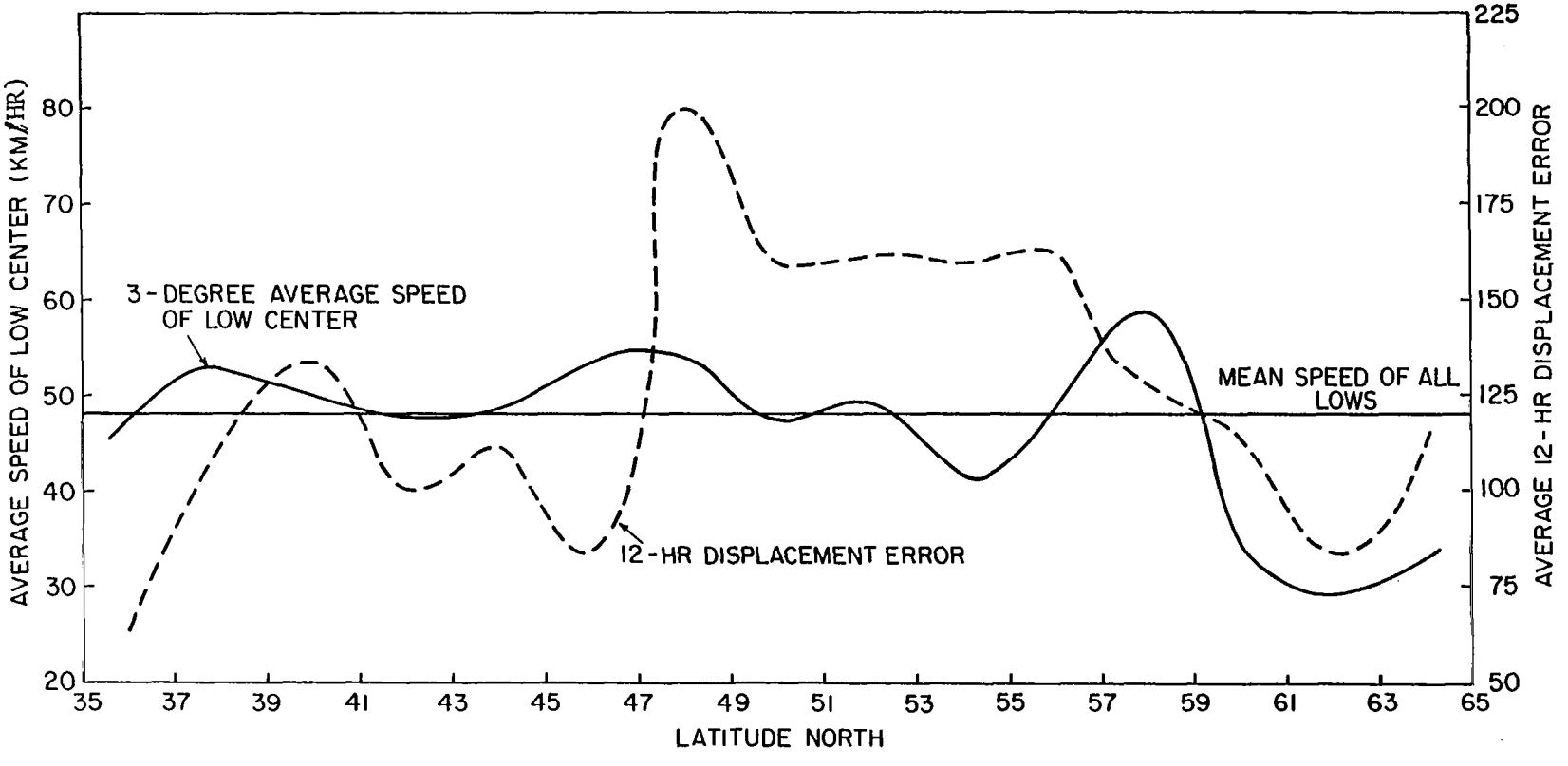

FIGURE 10 12-hr Displacement Error and 3-Degree Smoothed Average Speed (km/hr) Versus Latitude.

L. SOME ASPECTS OF MULTIPLE SIGHTINGS OF THE SAME CYCLONE AND OTHER METEOROLOGICAL FEATURES

The bracketed numbers in Table 2 represent the revisit times between two consecutive sightings of the same cyclone. These times seem to fall into groups that relate to specific features of the orbit's geometry, the sighting location (lat. and long.) and the velocity of the particular cyclone. All the permutations of revisit events are present in the data set. Consecutive sightings can be composed of northbound orbits followed by southbound orbits, southbound by southbound, southbound followed by northbound and northbound followed by southbound. Fig. 11 is a plot of the revisit times and the frequencies of their occurrences.

The elapsed times (to the nearest hour) of two consecutive sightings by SEASAT for the data set are illustrated below:

S → S	N → N	N → S	S → N
2	2	12	6
5	22	14	7
23	24	15	8
24		16	9
45		17	10
		36	33

The small numbers (2 and 5 hours) associated with a S→S or N→N event are indicative of the dwell phenomenon. A slowly moving cyclone located north of 55° N can be sighted on successive orbits or on every other orbit. These orbits are either consecutively northbound or southbound. Elapsed times of 22, 23 and 24 hours are those occasions when a cyclone is picked up at most twice in a 24-hour period. Thirteen or fourteen orbits elapse before the cyclone is revisited. If it is first seen by a northbound orbit, the next sighting is also by a northbound; else a southbound by a southbound. An elapsed time of 45 hours (nearly two days) is also observed for a southbound followed by a southbound orbit. These observations reveal that there are some features of the wind field over the ocean that will be missed during the course of a day or more if a single scatterometer is utilized. Revisit scenarios can be extended over the course of three different days.

Cyclones confined to latitude north of 25° N and south of 60° N have revisit times orchestrated by northbound followed by southbound orbits, or vice-versa. The elapsed times for N→S are larger than those for S→N (6-10 hours for S→N as opposed to 12-17 hours for N→S). Sightings related to those revisit times generally follow a sequence of S→N→S or N→S→N. There are few cases of occurrences of S→N and N→S when the elapsed time has been in the order of 33 and 36 hours respectively. This shows that the particular meteorological event has not been sampled for an entire day.

As is expected, 18 and 30 hours are not good candidates for revisit times since the spacecraft is located, at the end of these times, 90° away from the location of the last sighting with respect to a particular event. This can be explained by noting that the ground track shifts westward 25° at the equator for each successive orbit. As was pointed out before, the revisit times for stationary meteorological features at the intersections of two orbits at locations displaced respectively northward are 12 hr. 24 min, 13 hr. 32 min. and 15 hr. 22 min. These times relate to northbound followed by southbound orbits.

For southbound followed by northbound passages, the elapsed times for two consecutive sightings of a stationary meteorological event are respectively 11 hr. 55 min., 9 hr. 38 min., 8 hr. 6 min. and 6 hr. 31 min. as the cyclones are displaced northward.

The revisit times for moving cyclones therefore cluster around those of the stationary systems. The general west to east direction of motion coupled with the variable speeds (sometimes accelerating, sometimes decelerating) of the low centers account for sighting times that are generally about 100 minutes before or after these constant times.

FIGURE 11 A Plot of SEASAT Revisit Times for Cyclones in Total Data Set Studied.

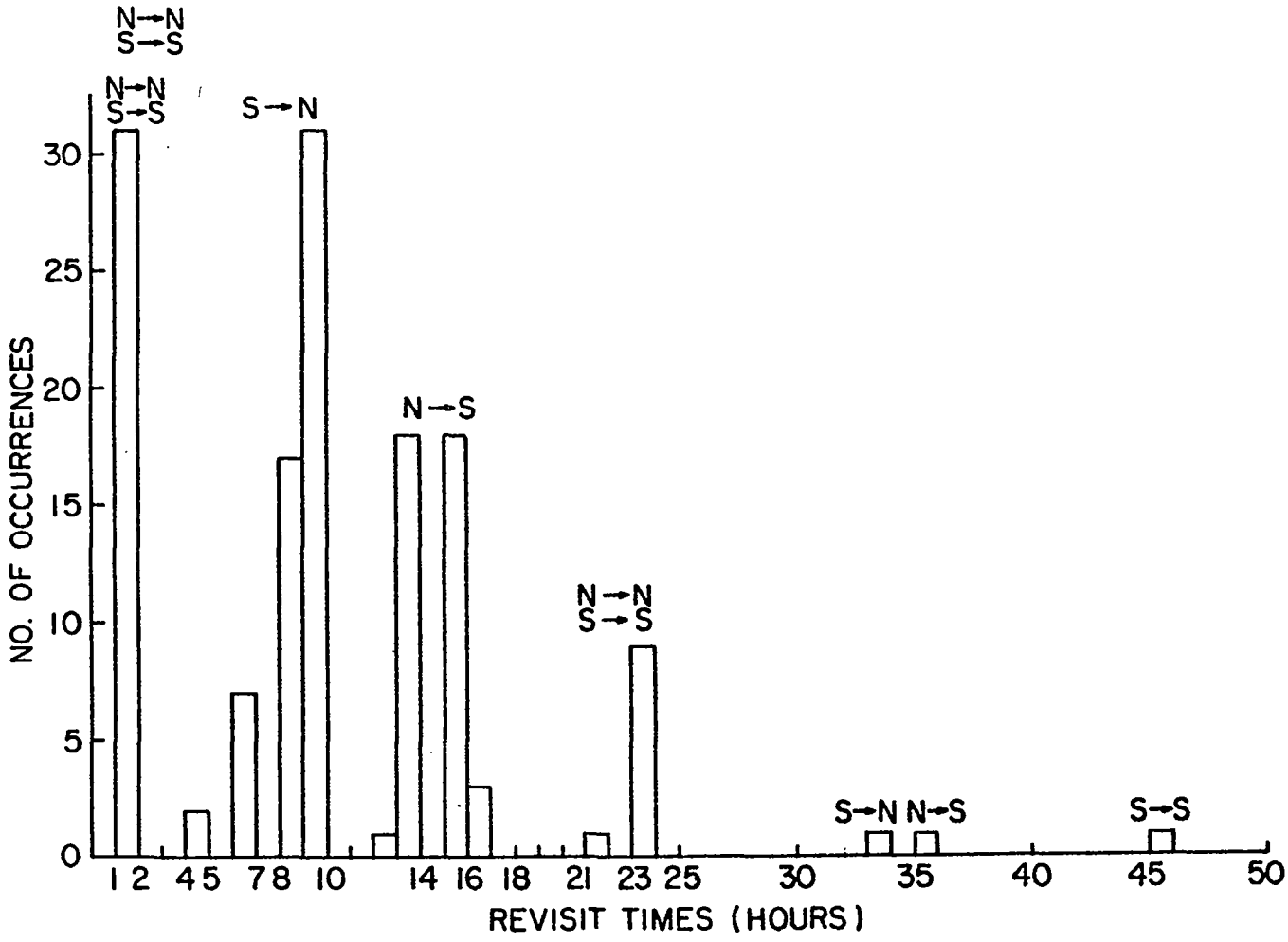

Evidence has already been shown that the SASS produces detailed wind field patterns for areas over the ocean that are within the swath. This amount of detail enables wind circulation to be readily observed. Cyclonic wind shear associated with frontal systems can therefore be detected (Brown 1983). The deformation of isobaric patterns and the wrong placement of low centers associated with the ± 3 hour window assimilation technique have already been discussed. Most often, in temperate latitudes, lows are accompanied by frontal systems. The effect of this assimilation method proves equally problematic for the placement of fronts on weather maps.

To illustrate this problem, a simple simulation experiment is carried out. Figure 12 shows five successive six-hourly "true" positions of a frontal systems during a 24 -hour period. The feature is characterized by an occlusion, cold front and warm front system. The example is taken from the Northern Hemispheric Surface Charts for Jan. - Mar. 1977. The synoptic times are Jan. 24, 0000z, 0600z, 1200z, 1800z and Jan. 25, 0000z. During the 24-hour period the system is observed four times by SEASAT. Portions of the subsatellite track of the four orbits are also drawn and labelled. In considering the portions that are observed the SASS swath must be taken into consideration.

The sightings of portions of the frontal system are as follows:

At 0220z orbit No. 2 (1352) going southward observes a considerable portion of the meteorological feature. For a duration of about 5 minutes, the center of the cyclone, the occlusion, cold front and warm portions are observed in the latitudes between about 36^{o} N to 20^{o} N.

At 1152z orbit No. 8 (traveling north) observes the occlusion, warm front and the extreme right portion of the cold front for about two minutes. One hundred minutes, or so, later (1130z), orbit No. 9 moving northward looks down on the left edge of the cold front. And again at 2408z southbound orbit No. 15 sights a portion of the warm front.

Thus is the 24-hour period a very large portion of the frontal system has been observed by the SASS. The sighting pattern for this example has been S→N→N→S. In the majority of the cases, different areas of the system are sighted. It can generally be concluded that frontal types with this configuration cannot be located in its entirety by one SEASAT pass. In this illustration two out of four of these observations give information of distinctly different portions of the system. Pass No. 9 observes the cold front while pass No. 15 observes only the warm front portion.

An analysis of how this data are assimilated with respect to the (± 3-hour window) is described in Table (6) that follows.

TABLE 6 Analysis of an Example of Frontal Mapping

ORBIT No.	DIR	SEASAT TIME	SYNOPTIC MAPPING TIME	FRONTAL SYSTEM	RELATIVE RATE OF MOTION
2	S	0220 (9:32)	0000 (12:00)	OC CF WF	
8	N	1152	1200	OC {right edge} CF WF	SLOW
9	N	1330 (12:16)	1200 (12:00)	CF {left edge}	SLOW
15	S	2408	0000	WF {right half}	SLOW

OC = Occlusion
CF = Cold front
WF = Warm front

From the above Table 6 some remarks are in order. On occasions different portions of the system are observed. Adhering to the mapping procedure of the intermittent assimilation scheme will obviously lead to some similar problems as outlined before with regard to cyclone centers. When the speeds of the various portions of the system are inferred, it will be found that there is a lack of synchronization between them. Sometimes cold front portions will move too slowly or too quickly. At other times warm front portions will act in a similar manner. The elapsed time (bracketed number in the SEASAT time column) between two consecutive observations of the same portions of the front can be compared with the fictitious time (bracketed numbers under SYNOPTIC MAPPING Time). After the second observation in this example, the use of the current mapping procedure will cause the frontal system to move at a different rate than what is stipulated by observation.

If frontal systems that extend over larger areas of the ocean are considered, similar outcomes of inferred movement can be expected. In such cases, many more orbits will be involved and the result will show a worsening effect. Many different portions of the same front will be constrained to travel at varying speeds. The lopsided motion of the system will result in the deformation of the true configuration of the meteorological front plus the creation of displacement errors similar to those of cyclone centers that have already been discussed.

FIGURE 12 Successive Six-Hourly Positions of a Frontal System Showing the Subsatellite Tracks of Orbits that would Observe Them. The orbit Number is Given at the Head of the Arrows. The GMT Times are the Starting Times of the Observation. The Duration for Each Observation is Also Given.

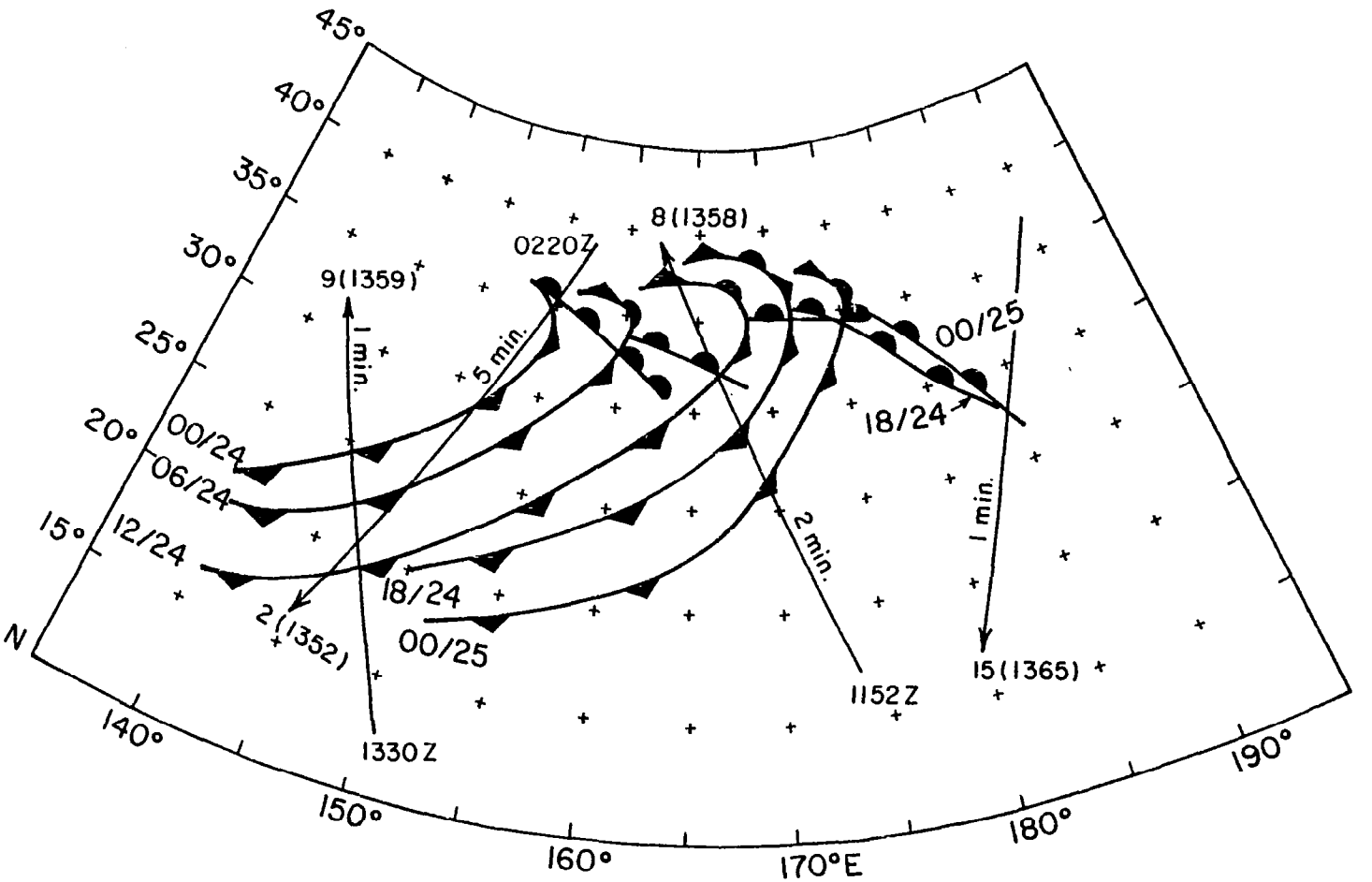

SUMMARY AND CONCLUSION

Evidence exists as to the applicability and the potency of the SASS data. A recent paper by Pierson, et al. (1983) demonstrates useful synoptic properties of the data. The addition of high-quality real-time global wind information to the existing background meteorological field should have positive effects on our computer based weather forecasts. If some notable improvement is not effected, it is because we fail to utilize the data efficiently.

In the search for the best ways of incorporating the new data, scientists have embarked upon divergent paths and have arrived at different results. Phillips (1976), Tracton (1981), Ghil, et al. (1979) and Atlas, et al. (1982) have all, in part, agreed that the disparate results are an implication that satellite impact is highly dependent on the particular analyses and forecast system used to incorporate the data. Two dominant schools of thought have emerged in this competitive arena. One main difference in their methodology is grounded in the format for inserting asynoptic satellite data in their models. The two methods in competition are the intermittent and the time-continuous assimilation techniques.

The researchers who practise the time-continuous technique claim to have enjoyed a great measure of success. Those who use the intermittent method have reported relatively marginal success, or in a few cases, practically none at all (see Tracton (1981)). In actual fact, workers associated with the NMC have registered beneficial impacts mainly in areas where there is a paucity of background conventional data, as for example, in the Southern Hemisphere.

The omission of any noticeable impact in the Northern Hemisphere experiment can be easily explained. These researchers collected data from that area during the summer. In this season the North Atlantic is relatively inactive with respect to meteorological events. There are scarcely any organized features that could produce well-defined gradients in the wind field. Weak or non-existing gradients would not therefore have any tangible effect on the existing conditions. Impact was registered when Southern Hemisphere data were assimilated because of the reverse situation — meteorological activity is heightened in the winter hemisphere.

The main investigation has been centered around the ± 3-hour assimilation window that has been adhered to by certain groups of investigators. The scheme has been adjudged to be questionable on account of the unsound mapping procedure relating to the time element of asynoptic observations. Asynoptic data are treated as if they belong to the nearest main synoptic hour, for example, information of 0910z and 0845z are treated at 1200z and 0600z respectively.

A series of best low center positions from the Atlantic and Pacific oceans have been simulated incorporating a method of repeat or frozen orbit, aided by the Seatrak Satellite calculator. These low centers are located at various times during the passage of SEASAT. Given the asynoptic nature of satellite observation, the sighting of a low center by the SASS can occur at any time. These times are not necessarily at main synoptic hours. The result of this study shows that there is a low incidence of occurrence of the coincidence of SEASAT sightings times and synoptic hours. Within ± 30 minutes of main synoptic times, the data shows 12% of coincidence. When the time elements of asynoptic observations are mapped into these main synoptic times, errors are created in the inferred speeds of low centers from one map update time to

another. These are the errors that multiply in the forecast cycle and contribute to the gross errors that are present in the output (forecast).

Analysis of the a sample chosen from the Atlantic and Pacific oceans has revealed an average absolute 12-hour linear displacement error of 1.1^{o} of longitude and a standard deviation of 0.9^{o} of longitude. About 84% of the sample has errors in excess of 0.5^{o} of longitude; sixteen percent has errors larger than 2^{o}.

If the results of the sample studied are considered indicative of the general wrong placements of low centers, then they are suggesting that these errors have levels comparable to those (about 2^{o} of longitude) presently realized in the conventional data. The results may further help to provide a simple explanation for the low skill score that relates to forecasts that are products of the ± 3-hour intermittent assimilation when SASS data are included in a background with conventional data. In this context, inclusion of satellite winds could, at best, create no added positive impact on the forecast, but could on occasions, cause a degrading of the background field as the magnitude of the 12-hour DEs are sometimes twice as large as those found in the conventional field.

Recalling that the input data are the best low center positions after careful reanalyses, the derived errors represent a lower bound condition. With the known inaccuracies and the paucity of conventional data relating to the placement of low center, a larger average error is therefore descriptive of "operational" analyses performed, for example, at NMC. Thus a mean error in excess of 2^{o} of longitude can be expected when the intermittent assimilation technique is utilized.

Not only is the wrong placement of lows problematic but also the many effects that are rather concommitant with it. For the one thing, the meteorologist will receive the wrong signals with reference to the life cycle of the cyclone. Whether or not the cyclone is filling or deepening cannot be known with any measure of certainty. Added to all this is the fact that the instantaneous discontinuity of time that results from the ± 3-hour mapping procedure creates blurred surface winds fields, deformed isobaric patterns and frontal systems. In general, poor analyses will result. Other problems must also be considered. The special cases of dwell and sampling at intermediate synoptic hours help to confound the situation even more. To use only data that are nearest a synoptic time would signify the loss of valid information.

The errors that have been studied have come about on account of the intermittent assimilation method utilized. It thus seems logical that a hard look should be given to this method with the aim of revising it. Inserting real-time SASS data by the continuous scheme will certainly help to irradicate some, if not most, of the existing problems that have been discussed. At least the continuous assimilation techique should be tested so that the maximum amount of good data can be used with the aim of making better weather forecasts.

REFERENCES

Atlas, R. (1981): The Effects of Varying Amounts of Satellite Data, Orography and Diabatic Processes on the Numerical Prediction of an Intense Cyclones, Research Review - 1980-81, NASA Tech. Memo. 83907. GSFC. Greenbelt, Maryland.

Atlas, R., G. Cole, A. Pursch, and C. Long, (1981): Interactive Processing of Seasat Scatterometer Data, Research Review 1980-81, NASA Tech. Memo. 83907, GSFC. Greenbelt, Maryland,

Barrick, D. E., J. C. Wilkerson, P. M. Voiceshym, G. B. Born, and D. B. Lame, (1979): Seasat Gulf of Alaska Worshop II Report, Rep. 622-107. Jet Propul. Lab., Pasadena Calif.

Bengtsson, L. and N. Gustavsson, (1972): Assimilation of Non-Synoptic Observations. Tellus 24, 5, 383-399.

Bergman, K. H., (1979): Multivariate Analysis of Temperatures and Winds Using Optimum Interpolation. Mon. Wea. Rev., 107, 1423-1444.

Born, G. H., J. C. Wilkerson, and D. B. Lame, (1979): Seasat Gulf of Alaska Workshop Report, Vol. 1 and 2, Rep. 622-101. Jet Propul. Lab., Pasadena, Calif.

Brown, R. A., V. J. Cardone, T. Guymer, J. Hawkins, J. E. Overland, W. J. Pierson, S. Peteherych, J. C. Wilkerson, P. M. Voiceshyn, and M. Wurtele (1982): Jour. of Geophy. Res. Vol. 87, No. C5. 3355-3364.

Businger, J., R. Stewart, T. Guymer, D. B. Lame, and G. H. Born, (1980): Seasat-JASIN Workshop Report, Rep. 80-62, Jet Propul. Lab., Pasadena, Calif.

Cane, M. A., V. J. Cardone, M. Halem, I. Halberstam and J. Ulrich, (1978): Realistic Simulations of the Global Observation System of Seasat-A Marine Wind Data. NASA GSFC. Unpublished Manuscript.

Cane, M. A. and V. J. Cardone, (1981): The Potential Impact of Scatterometry on Oceanography: A Wave Forecasting Case. Oceanography from Space, J.F.R. Gower. Ed. Plenum Press. New York and London; 587-595.

Cane, M. A., V. J. Cardone, M. Halem, and I. Halberstam, (1981): On the Sensitivity of Numerical Weather Prediction to Remotely Sensed Marine Surface Wind Data: A Simulation Study. J. of Geophy. Res., Vol. 86, No. C9. 8093-8106.

Cardone, V. J., J. D. Young, W. J. Pierson, R. K. Moore, J. A. Greenwood, C. Greenwood, A. K. Fung, R. Salfi, H. L. Chan, M. Afarani, and M. Komen, (1976): The Measurement of the Winds near the Ocean Surface with a Radiometer-Scatterometer on Skylab, A Joint Meteorological, Oceanographic, and Sensor Evaluation Program for Experiment S193 on Skylab, NASA CR-147478.

Cheney, R. E. and J. G. Marsh, (1981): Oceanic Eddy Variability Measured by GOES-3 Altimeter Crossover Differences. EOS, Vol. 62, No. 45,. 743-752.

Colucci, S, J. and L. F. Bosart, (1979): Surface Anticyclone Behavior in NMC Prediction Models. Mon. Wea. Rev., 107, 377-394.

Cressman, G. P., (1959): An Operational Objective System. Mon. Wea. Rev., 85, 367-374.

Dey, C. H., (1978): Noise Suppression in a Primitive Equation Prediction Model. Mon. Wea. Rev. 106, No, 2, 159-173.

Endlich, R. M., D. W. Wolf, C. T. Carlson , and J. W. Maresca, Jr. (1981): Oceanic Wind Balance and Pressure-Height Fields Derived from Satellite Measurements, Mon. Wea. Rev., 1981, 109, 2009-2016.

Ernst, J. A., (1981): Scatterometer-Derived Winds over the QE II Storm. Oceanography from Space , J. F. R. Gower, Ed. Plenum Press, New York and London; 573-579.

Fawcett, E. B., (1969): Systematic Errors in Operational Barroclinic Prognoses at the National Meteorological Center. Mon. Wea. Rev., 97, 670-682.

Gaby, D. C., J. B. Lushine, B. M. Mayfield, S. C. Pearce and F. E. Torres, (1980): Satellite Classification of Atlantic Tropical and Subtropical Cyclones: A Review of Eight Years of Classifications at Miami. Mon. Wea. Rev., 108 587-595.

Gandin, L. S., (1963): Objective Analysis of Meteorological Fields Gidrometeorologicheskow Izdatel'-stvd. Leningrad, 1960. Translated from Russian in English, Israel Program for Scientific Translations, Jerusalem, 1965.

Ghil, H., M. Halem and R. Atlas. (1979): Time-Continuous Assimilation of Remote-Sounding Data and Its Effect on Weather Forecasting. Mon. Wea. Rev. 107. 140-171.

Gordon, A. L., and T. N. Baker, (1980): Ocean Transients as Observed by GOES-3 Coincident Orbits. J. Geophys. Res. 85, 502-506.

Halem, M., M. Ghil, R. Atlas, J. Susskind and W. J. Quirk, (1978): The GISS Sounding Temperature Impact Test. NASA Tech. Memo. 78063. Goddard Space Flight Center.

Halem, M. and G. Russell, (1973): A Splitgrid Differencing Scheme for the GISS Model. Inst. Space Stud. Res. Rev., 194-201.

Herman, G. F., and W. T. Johnson, (1978): The Sensitivity of the General Circulation to Arctic Sea-Ice Boundaries: A Numerical Experiment. Mon. Wea. Rev., 106, 1649-1664.

Jones, W. L., L. C. Schroeder, D. H. Boggs, E. M. Bracalente, R. A. Brown, G. J. Dome, W. J. Pierson and F. J. Wentz, (1982): The SEASAT-A Satellite Scatterometer: The Geophysical Evaluation of Remotely Sensed Wind Vectors over the Ocean. J. Geophy. Res. Vol. 87, No. C5, 3297-3317.

Klose, J. C., (1979): SEASAT Node Tables and Osculating Orbital Elements, 622-215; NASA, Jet Propul. Lab.

Leary, C., (1971): Systematic Errors in Operational National Meteorological Center Primitive-Equation Surface Prognoses. Mon. Wea. Rev., 99, 409-413.

Lorenz. E. N., (1963): The Predictability of Hydrodynamic Flow. Trans. New York Acad. Sci. Ser. 2, 25. 409-432.

McPherson, R. D., K. H. Bergman, R. E. Kistler, G. E. Rasch and D. S. Gordon, (1979): The NMC Operational Global Data Assimilation System. Mon. Wea. Rev. 107, 1445-1461.

Miyakoda, K. and O. Talagrand, (1971): Assimilation of Past Data in Dynamical Analysis I. Tellus 23, No. 4-5, 310-317.

Moore, R. K., and A. K. Fung, (1979): Radar Determination of Wind at Sea. Proc. IEEE, 67, 1504-1521.

Peteherych, S., P. M. Woiceshyn, W. Appleby, L. Chu, J. Spagnol, and J. E. Overland, (1981): High Resolution Marine Meteorological Analysis Utilizing Seasat Data. Oceanography from Space. J. F. R. Gower Ed. Plenum Press, New York and London. 581-586.

Phillips, N. A., (1976): The Impact of Synoptic Observing and Analysis Systems on Flow-Pattern Forecasts. Bull. Amer. Meteor. Soc., 57, 1225-1240.

Pierson, W. J., L. J. Tick, and L. Baer, (1966): Computer-Based Procedures for Preparing Global Wave Forecasts and Wind Field Analysis Capable of Using Wave Data Obtained by a Spacecraft. 6th Symposium. Naval Hydrodynamics. ACR-136. Office of Naval Research, Dept. of the Navy.

Pierson, W. J., (1979): A Suggested Technique for the Assimilation of the SASS Winds from Seasat into National Meteorological Center Operational Numerical Weather Prediction Models. CUNY IMAS, Prepared for Spacecraft Oceanography Group of the NESS, NASA under Grant #04-6-158-44049 Contract 7-35355.

Pierson, W. J., (1981): The Variability of Winds over the Ocean in Beal, R., P. S. DeLeonibus and I. Katz,Eds. Spaceborne Synthetic Aperture Radar for Oceanography. John Hopkins University Press. Oceanographic Studies No. 7.

Pierson, W. J., (1983): The Measurement of the Synoptic Scale Wind over the Ocean. Special Journal of Geophysical Research, Vol. 88, No. C3, February 28, 1983, Paper 2C1518.

Ross, D. B., (1981): The wind speed Dependency of Ocean Microwave Backscatter, in Spaceborne Synthetic Aperture Radar for Oceanography, Eds. R. C. Beal, P. DeLeonibus and I. Katz, John Hopkins Press, Baltimore, Md., 75-86.

Sasaki, Y. (1969): Proposed Inclusion of Time Variation Terms, Observational and Theoretical, in Numerical Variational Objective Analysis. Jour. Meteor. Soc. of Japan. 47, 115 - 124.

Schroeder, L. C., D. H. Boggs, G. Dome, I. M. Halberstam, W. L. Jones, W. J. Pierson, F. J. Wentz, (1982): The Relationship Between Wind Vector and Normalized Radar Cross-Section Used to Derive SEASAT-A Satellite Scatterometer Winds. J. Geophys. Res., Vol. 87, No. C5, 3318-3336.

Sherman, J. W., (1981): General SEASAT and Nimbus 7 Capabilities and Description in Working Draft for a Report on the NOAA SEASAT and Nimbus-7 Experience. Section 2.

Somerville, R. C. J., P. H. Stone, M. Halem, J. E. Hensen, J. S. Hogan, L. M. Druyan, G. Russell, A. S. Lacis, W. J. Quirk and J. Tenenbaum, (1974): The GISS Model of the Global Atmosphere, J. Atmos. Sci., 31, 84-117.

Sylvester, W. B., (1978): A SOWM Swell Verification Study: Extratropical Winter Storm Forcing of the Wave Climate in the East of the Southern Caribbean Chain. Ph.D. Thesis, New York University.

Tadjdakhsh, I. G. (1969): Utilization of Time-Dependent Data in Running Solution of Initial Value Problems. Jour. Appl. Meteor. 8, 389-391.

Talagrand, O. and K. Miyakoda, (1971): The Assimilation of Past Data in Dynamical Analysis II. Tellus 23, 4-5, 381-327.

Tracton, M. S., A. J. Desmarais, R. J. Van Haaren, and R. D. McPherson, (1980): The Impact of Satellite Soundings on the National Meteorological Center's Analysis and Forecast System. The Data System Test Results. Mon. Wea. Rev., 108, 543-586.

Tracton, M. S., A. J. Desmarais, R. J. Van Haaren, and R. D. McPherson, (1981): On the System Dependency of Satellite Sounding Impact - Comments on Recent Impact Test Results. Mon. Wea. Rev., 109, 197-200.

Wallace, J. M., and J. K. Woessner, (1981): An Analysis of Forecast Error in the NMC Hemispheric Primitive Equation Model. Mon. Wea. Rev. 109, 244-2449.

Yu Tsann-Wang and R. D. McPherson (1979): Surface Pressure Analysis Using Scatterometer-Derived Wind Data from the SEASAT-A Satellite. Preprint Paper, 4th Conference on Numerical Weather Prediction, Oct. 29-Nov. 1, 1979. Silver Spring, MD. 351-355.

Yu Tsann-Wang and R. D. McPherson, (1981): Global Data Assimilation Experiments with Scatterometer Winds from SEASAT-A in Working Draft for A Report on the NOAA SEASAT and NIMBUS 7 Experience.

ADDITIONAL REFERENCES

Atlas, R., M. Ghil, and M. Halem (1982): The Effect of Model Resolution and Satellite Sounding Data on GLAS Model Forecasts. Mon. Wea. Rev., 110, No. 7, 662-682.

Brown, R. A. (1983): On a Satellite Scatterometer as an Anemometer. Seasat Special Issue II: Scientific Results. Reprinted from Journal of Geophysical Research, Vol. 88, Number C3, February 28, 1983.

Druyan, L. M. (1974): Short-range Forecast with the GISS Model of the Global Atmosphere. Mon. Wea. Rev., 102, 269-279.

Pierson, W. J., W. B. Sylvester, and R. E. Salfi (1983): Synoptic Scale Wind Field Properties from the SEASAT SASS. Technical to be Submitted to NASA under Contract NAGW-266.

Sanders, F. and J. R. Gyakum (1980): Synoptic - Dynamic Climatology of the "Bomb". Mon. Wea. Rev., Vol. 108, 1589-1606.

Report of the Satellite Surface Stress Working Group; Scientific Opportunities Using Satellite Stress Measurements over the Ocean. Prepared for NASA (June 1982).

APPENDIX

The diagrams that follow are representations of components of the JPL SEATRAK CALCULATOR used in this study.

Figure a: Northern Hemispheric Base Map

Figure b: Overlay 1 (Orbits/Day).

Figure c: Overlay 3 (SASS).

Note: Refer to section E for a fuller description of the calculator.

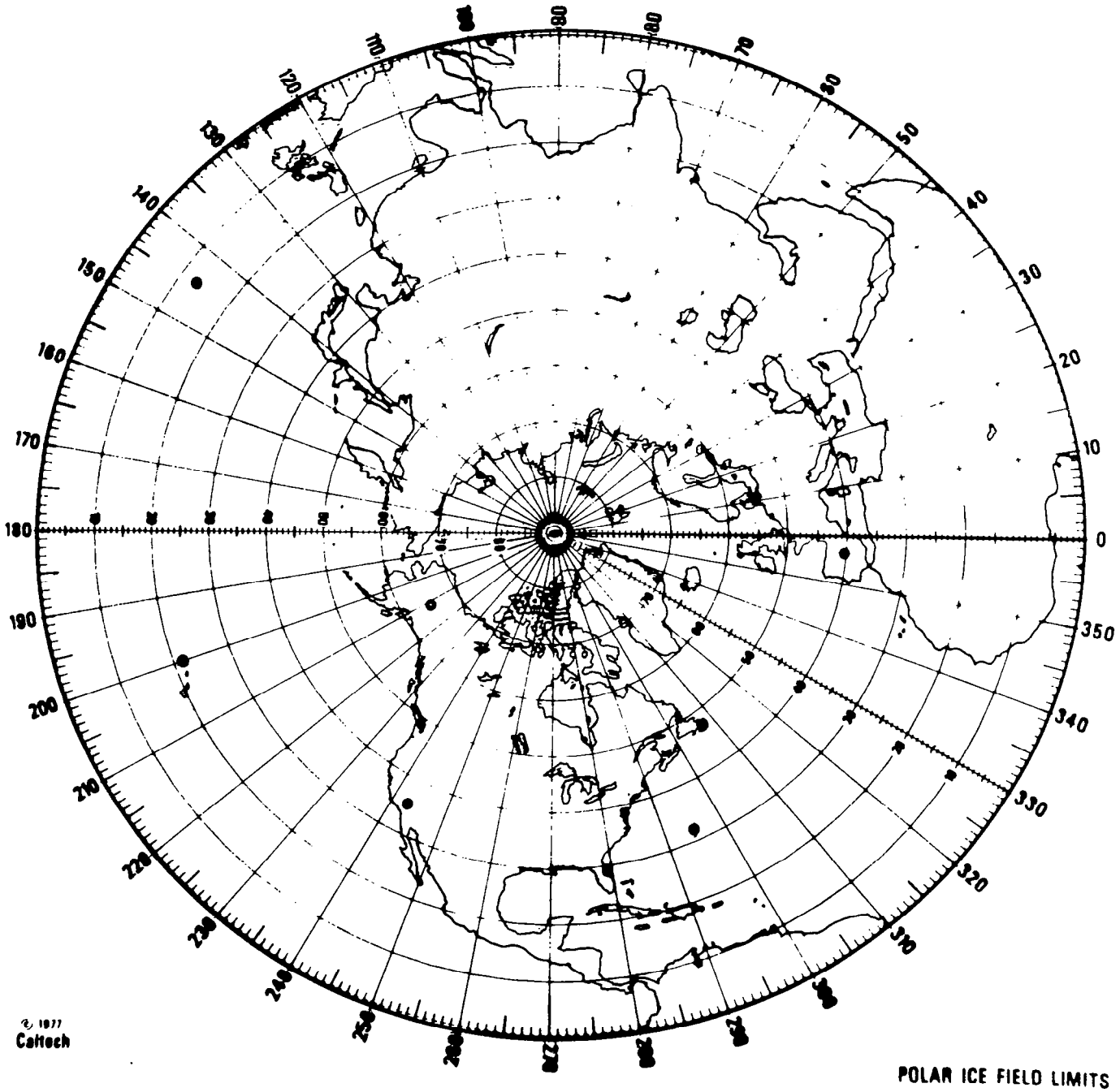
90
80
70
60
50
40
30
20
10
0
350
340
330
320
310
300
290
280
270
260
250
240
230
220
210
200
190
180
170
160
150
140
130
120
110
100
© 1977
Caltech
POLAR ICE FIELD LIMITS

FIGURE a

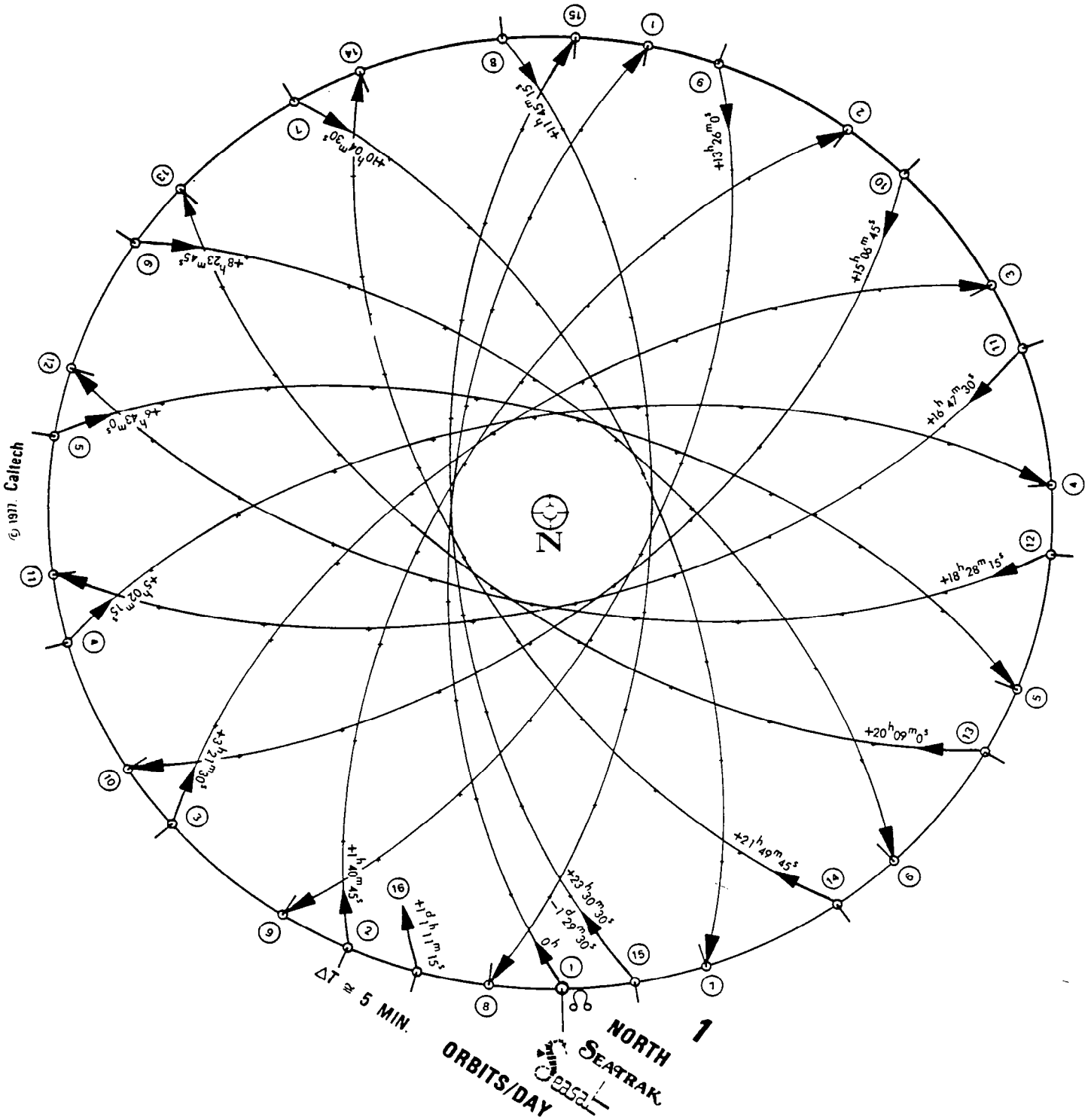
© 1971 Caltech
N
+11h45m15s
+13h26m0s
+15h08m45s
+16h47m30s
+18h28m15s
+20h09m0s
+21h49m45s
+23h30m30s
-1d29m30s
0h
+1h40m45s
+3h21m30s
+5h02m15s
+6h43m0s
+8h23m45s
+10h04m30s
ΔT ≈ 5 MIN.
ORBITS/DAY
NORTH
SEATRAK
1

FIGURE b

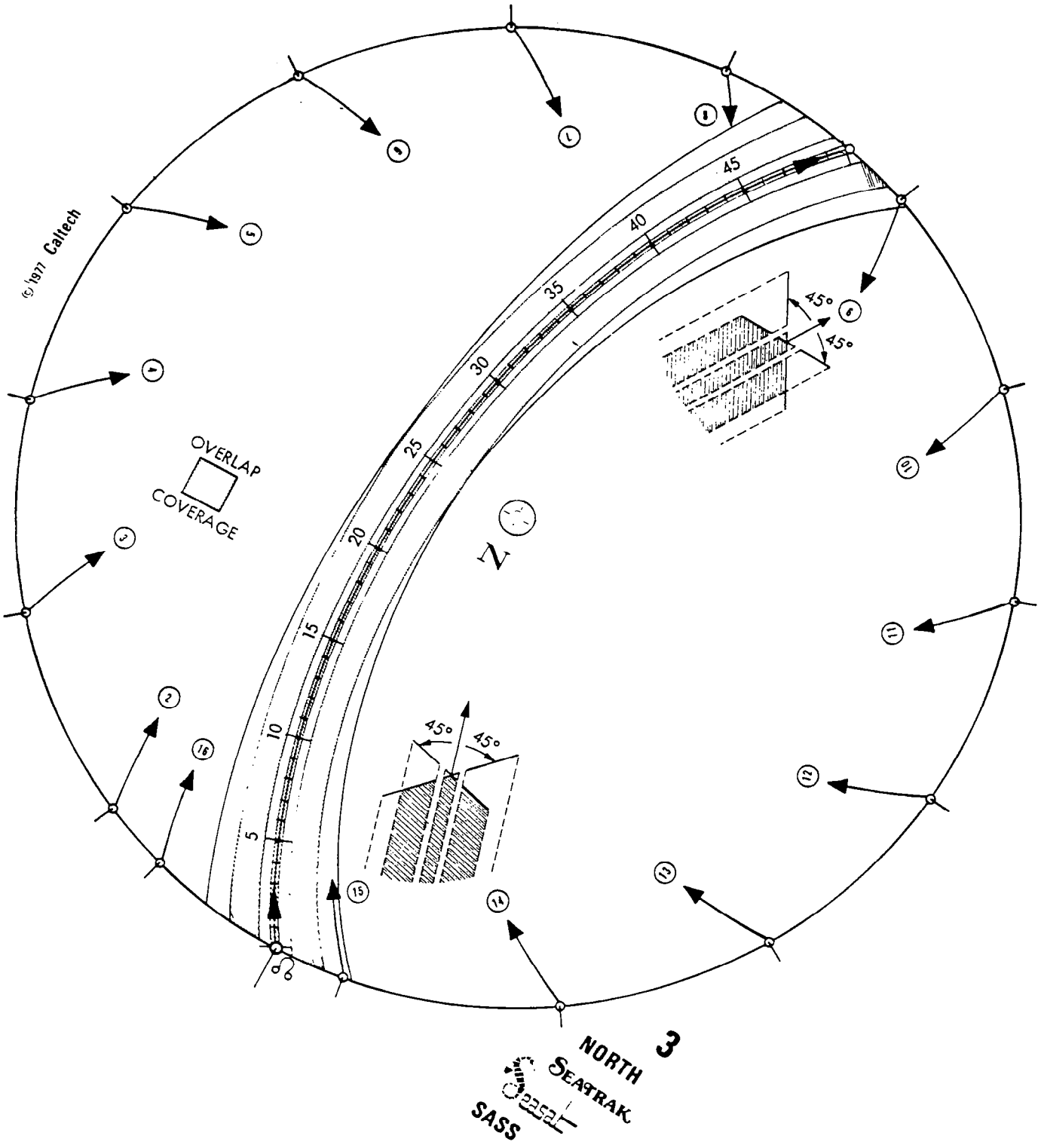
(c) 1977 Caltech
OVERLAP
COVERAGE
N
45
40
35
30
25
20
15
10
5
45°
45°
45°
45°
NORTH
SEASAT
SASS
3

FIGURE c

ACKNOWLEDGEMENTS

The production of this paper is a demonstration of an exercise in "praxis". An idea is formulated in one's mind; it is then verbalized and quickly put into action. Professor Willard J. Pierson participated in the early part of this exercise. His criticisms were of vital importance to me. I wish to thank him sincerely. My thanks are also extended to the sponsors of this research, the National Aeronautics and Space Administration. Mrs. Gertrude Fisher, who did the drawings, and Mrs. Candida Jimenez, our typist, have contributed vitally.

1. Report No.	2. Government Accession No.	3. Recipient's Catalog No.
NASA CR-3799		

4. Title and Subtitle	5. Report Date
A SEASAT SASS SIMULATION EXPERIMENT TO QUANTIFY THE ERRORS RELATED TO A ±3-HOUR INTERMITTENT ASSIMILATION TECHNIQUE	May 1984
	6. Performing Organization Code
7. Author(s)	8. Performing Organization Report No.
WINFIELD B. SYLVESTER	
	10. Work Unit No.
9. Performing Organization Name and Address	11. Contract or Grant No.
CUNY INSTITUTE OF MARINE AND ATMOSPHERIC SCIENCES AT THE CITY COLLEGE CONVENT AVENUE AT 138th STREET NEW YORK, NY 10031	NAGW-266
	13. Type of Report and Period Covered
12. Sponsoring Agency Name and Address	Contractor Report
NATIONAL AERONAUTICS AND SPACE ADMINISTRATION OCEANIC PROCESSES BRANCH/OSSA WASHINGTON, DC 20546	14. Sponsoring Agency Code

15. Supplementary Notes

TECHNICAL MONITOR: William C. Patzert, Code EE

16. Abstract

The scientific community has been given great assurances of the usefulness and the validity of the SASS data. Notwithstanding, an area of uncertainty exists in the current techniques for the insertion of real-time information from spacecraft in computer based numerical predictions.

This study examines the operational aspect of an intermittent assimilation scheme currently utilized for the specification of the initial value field. The main focus here is to quantify the absolute 12-hour linear displacement error of the movement of low centers. This error is attributable to the ± 3-hour window used in the assimilation cycle when asynoptic data are inserted in computer models. A series of SEASAT repeat orbits over a sequence of "best" low center positions are simulated by using the Seatrak satellite calculator provided by the Jet Propulsion Laboratory. These low centers are, upon appropriate interpolation to hourly positions, located at various times during the ± 3-hour assimilation cycle.

Error analysis for a sample of best cyclone center positions taken from the Atlantic and Pacific oceans reveals a minimum average error of 1.1° of longitude and a standard deviation of 0.9° of longitude. The magnitude of the average error seems to suggest that by utilizing the ± 3-hour window in the assimilation cycle, the quality of the SASS data is degraded to the level of the background since the errors that result from the assimilation technique have comparable magnitudes to those realized in conventional data.

A further consequence of this assimilation scheme is the effect which is manifested as a result of the blending of two or more juxtaposed vector winds, generally possessing different properties (vector quantity and time). The outcome of this is to reduce gradients in the wind field and to deform isobaric and frontal patterns of the initial field.

17. Key Words (Suggested by Author(s))	18. Distribution Statement
SEASAT Scatterometry Model data assimilation SASS	Unclassified-unlimited Subject Category 43

19. Security Classif. (of this report)	20. Security Classif. (of this page)	21. No. of Pages	22. Price
Unclassified	Unclassified	85	A05

For sale by the National Technical Information Service, Springfield, Virginia 22161

NASA-Langley, 1984